Sea-level changes, coastal evolution and paleoceanography of coastal waters in SE - Vietnam since the mid - Holocene

Dissertation zur Erlangung des Doktorgrades

der Mathematisch-Naturwissenschaftlichen Fakultät

der Christian-Albrechts-Universität zu Kiel

vorgelegt von

Maximiliano Michelli

Kiel

2008

Referent/in.....

Korreferent/in.....

Tag der mündlichen Prüfung:.....

Zum Druck genehmigt: Kiel,.....

Der Dekan

Abstract:

The coast of SE-Vietnam, extending between Nha Trang and Phan Thiet, was explored in terms of beachrock formation, sea-level fluctuations and shallow water temperature during the mid-Holocene in comparison with present time.

Beachrock formations were found at three places. Petrographic observations, chemistry analyses of Mg and Sr as well as isotopic results of $\delta^{18}O$ and $\delta^{13}C$ indicated beachrock lithification in marine environment within the phreatic zone. The early cement types are constituted by micritic high-Mg calcite and aragonite crystals. In addition, blade cement type was found indicating meteoritic recrystallization of the most elevated beachrocks which are located today in supratidal position.

The age of the beachrocks covers a period from 6721 to 642 cal yr BP. It can be divided into three intervals: 6721 to 5869 cal yr BP as an older period of beachrock formation, followed by 3760 to 3272 cal yr BP showing a probable second stage of cementation, and the youngest cement formation from 1210 to 642 cal yr BP.

The age of the beachrocks were correlated with other sea-level indicators such as beachridge, backshore and washover deposits. They were explored in order to determine the sea-level fluctuations from mid-Holocene to the present time.

Records of sea-level highstand started between 6721 to 5869 cal yr BP with an average of 1.32 m above the modern mean sea level (amsl) indicated by oldest beachrocks. Subsequently, it rose until 2.67 m as maximum spring-tidal level between 5687 to 5377 cal yr BP, measured in at the base of Ca Na beachridge. This corresponds to a mean sea-level of 1.52 m after subtraction of the half-tidal range of 1.15 m. The drop of the sea-level started after the 5377 cal yr BP with a linear decrease from 4500 cal yr BP until present time.

Therefore, the probable coastal scenery during the mid-Holocene sea-level highstand shows that the beachrocks formed within the intertidal zone and beachridge was deposited in the

supratidal zone. Both indicators denote the same period of formation within the interval of 6721 to 5377 cal yr BP during mid-Holocene sea-level highstand.

From the Ca Na beachridge a sample of *Spondylus sp*, bivalve dated at 5537 ± 55 cal yr BP was analysed for $\delta^{18}O$ and $\delta^{13}C$ isotopes along its growth-path. From the stable isotope records shallow-water temperatures during the mid-Holocene sea-level highstand were calculated. Paleotemperature values were compared to present water temperature from NOAA at two different geographic positions, inside and outside of the investigation area taking into account a costal upwelling.

The results of the comparison paleotemperature and modern water temperature in two positions showed a seasonal difference. During summertime the water temperature in the mid-Holocene was approximately 1° C warmer than at the present water temperature.

Higher paleotemperatures found in shallow water along the SE-Vietnam coast during the mid-Holocene could be responsible for excessive coral mortality. The following hypothesis is suggested: firstly, warm water temperatures induced the bleaching of corals; secondly, beachridge deposit consisting mainly of skeleton from marine organisms might indicate the deposition after their death.

The present study demonstrates that the coastal evolution in SE-Vietnam was strongly influenced by mid-Holocene sea-level highstand and the warming of coastal waters.

Kurzfassung

Die Küste von SO-Vietnam wurde zwischen den Städten Nha Trang and Phan Thiet untersucht. Im Mittelpunkt stand die Bildung von Beachrocks im Zusammenhang mit Meeresspiegelschwankungen und die Rekonstruktion der Wassertemperatur während des mittleren Holozäns.

Die Beachrocks wurden an drei Standorten gefunden. Die petrographische und chemische Auswertung sowie die Isotopenwerte von $\delta^{18}O$ und $\delta^{13}C$ zeigt, dass die Beachrocks im marinen Milieu innerhalb des phreatischen Bereichs gebildet wurden. Der Originalzement der Beachrocks besteht aus Mikrit mit hoch-Mg Calzit und Aragonit. Außerdem wurde in den heute höchstgelegenen Beachrocks in supratidaler Position ein Bladezementtyp gefunden, der ein Anzeichen für den Einfluss von Süßwasser ist.

Das Alter der Beachrocks erstreckt sich über einen Zeitraum von 6721 bis 642 Kalenderjahren vor heute, der in drei Phasen unterteilt ist: von 6721 bis 5869 Kalenderjahren vor heute entstand die älteste Beachrockformation, darauf folgt von 3760 bis 3272 Kalenderjahren vor heute die zweite Phase, in der Beachrocks gebildet wurden, und die jüngste Beachrockformation entstand zwischen 1210 und 640 Kalenderjahren vor heute.

Das Alter der Beachrocks wurde gemeinsam mit Ablagrungen vom Strandwall, Oberen Strand und Durchbruchsfächer als weitere Anzeichen der Meeresspiegelschwankungen vom mittleren Holozän bis in die Gegenwart untersucht.

Die Meeresspiegelschwankungen begannen zwischen 6721 bis 5869 Kalenderjahren vor heute mit einem Mittelwert von 1.32 m über dem heutigen mittleren Meeresspiegel, was aus den Werten der Beachrocks berechnet wurde. Infolgedessen lag der Anstieg bis zum Meeresspiegelhochstand zwischen 5687 und 5377 Kalenderjahren vor heute bei + 2.67 m als maximale Springtide und bei + 1.52 m als mittlerer Meeresspigel. 1.52 m wurde aus dem Höchststand (2.67 m) minus 1.15 m berechnet, der Hälfte des Wertes des heutigen Tidenhubs.

Nach 5377 Kalenderjahren vor heute sank der Meeresspiegel ab 4500 Kalenderjahren linear zum heutigen Niveau ab.

Dadurch entstanden an der Küste im mittleren Holozän Beachrocks in der Gezeitenzone und Strandwälle in der supratiden Zone. Die beiden Meeresspiegelindikatoren deuten auf die gleiche Zeit hin, nämlich zwischen 6721 bis 5377 Kalenderjahren vor heute, den Höchstand des Meeresspiegels.

Am Beachridge von Ca Na wurde eine Schale der Muschel *Spondylus sp* analysiert. Die Muschel wurde auf 5537 ± 55 Kalenderjahre vor heute datiert. Aus der Schale wurden entsprechend dem Schalenwachstum eine Serie von Karbonat-Mikroproben entnommen und das stabile Isotop ^{18}O gemessen. Aus den stabilen Isotopenwerten wurde die Wasser-Paläotemperatur berechnet.

Die Ergebnisse der Paläotemperaturrekonstrution wurden mit den heutigen Wassertemperaturen an zwei unterschiedlichen geographischen Positionen verglichen, innerhalb und außerhalb des Untersuchungsgebiets, da an der sudöstlichen Küste von Vietnam ein Auftriebgebiet liegt.

Die Paläotemperaturergebnisse, verglichen mit der heutigen Wassertemperatur an diesen zwei Positionen, zeigen einen saisonalen Unterschied an. Während der Sommersaison war die Wassertemperatur im mittleren Holozän um ca. 1° C höher als die derzeitige Wassertemperatur.

Die erhöhte Temperatur der Küstengewässer von SO-Vietnam während des mittleren Holozäns war vermutlich verantwortlich für die erhöhte Mortalität der Korallen. Diese Hypothese basiert auf folgenden Annahmen: Erstens führte die warme Wassertemperatur das „Bleaching“ der Korallen herbei. Zweitens könnte der Strandwall eine Ablagerung dieser Korallen nach ihrem Tod sein, weil seine Ausgestaltung hauptsächlich aus Skeletten von Meeresorganismen besteht.

Aus den oben beschriebenen Untersuchungen lässt sich der Schluss ziehen, dass die Küstenentwicklung von SO-Vietnam durch den Meeresspiegelhochstand und die Erwärmung der flachen Küstengewässer im Mittelholozän stark beeinflusst wurde.

Acknowledgements

- I would like to express my sincere thanks to Prof. Dr. Karl Stattegger for giving me the opportunity to work in a very important project for his proposal, and also to carry out my Ph.D. thesis here in Kiel.

- I want to express my deepest gratitude to my dear partner Stefanie, her family and my family in Brazil for the support, affection, understanding and encouragement. Without their support I could have never been successful.

- I thank the Deutscher Akademischer Austauschdienst (DAAD) for support my Ph.D. scholarship in Germany, and particularly Mrs. Maria Salgado Martinez. As also for the Deutsche Forschungsgemeinschaft (DFG) for give me the finance support to realize this thesis through the project STA 401/10-1.2.

- I would like to express my thanks to Dr. Nils Anderson for his suggestions and productive discussion during my work accomplished in the Leibniz laboratory for stable isotope measure; also to Dr. Klaus Schwartzer for the help during the fieldworks in Vietnam.

- My thanks also for to all Vietnamese scientists which participated during two cruises in the South China Sea on board of R/V Nghien Cuu Bien; and also to the new scientific colleges of Nha Trang and Hanoi Institutes of Oceanography, particularly to Bui Quang Nghi, Dan Quang Minh and Nguyen Trung Thanh.

- I gratefully acknowledge the following persons for their help: Dr. Beate Bader and Mrs. U. Schuldt for the work in Scanning Electron Microscopic (SEM); Mr. Wolfgang Reimers for the thin sections; Mrs. Petra Fiedler for the analyses in X-Ray Diffraction laboratory; Mrs. Barbara Mader who that provided assistance with electron microprobe analyses; Dr. Thomas Muller-Lupp for the photos of bivalve shells in the IFM-GEOMAR institute and Mrs. Barbara Wolf for support of every bibliography during my work.

List of figures and tables

1. Introduction

2. General Methodology

3. Holocene beachrock formation the SE coastal of Vietnam

needles. (f) Big forms of aragonite needles; “M” indicates the presence of micritic cement. (g) Isopachous aragonite of needle “A” covering the algae fragment. (h) Fibrous isopachous aragonite with a black arrow pointing to a dark formation and the white arrow showing the bladed form of cement. (i) to (n) SEM-images: (i) The arrow indicates how rim cement covers the sediment. (j) Showing the form of aragonite needles. (k) Mesh of needle cement. (l) Needles growing onto the sediment. (m) Aragonite needle in Ca Na Beachrock. (n) Shows aragonite needle with bioclastic sediment in supratidal zone.
AF-Algae fragment, Q-Quartz, P-Pore.

Fig. 3.5. The biological constituents found on the cement in SEM-image. (a) Elliptical nannobacteria growing on an aragonite needle identified as nannobacterias. (b) Endolithic filament of an alga. (c) Bacterial film growing on a cement beachrock with its reproductive structure.

Fig. 3.6. Cross-plot of carbon versus oxygen isotopic from cement of beachrocks introduced by Milliman 1974, modified by James & Choquette, 1983, including the marine cement fields.

Fig. 3.7. Sediment size distribution from beach sand, where Ca Na Beachrocks were localized. The results identified standards in medium and coarse sand. Similar sedimentary distributions were found in beachrocks.

Fig. 3.8. The beachrocks and their respective ages are shown in two places. “A” represents the ages for the Ca Na Beachrock, whereas “B” represents the ages for the Son Hai Beachrock with its uppermost position without dating.

Table 3.1. Samples of beachrocks collected at three locations with their respective elevations above the maximum neap-tidal level (amntl) and above the maximum spring-tidal level (amstl).

Table 3.2. Oxygen and carbon isotope values and chemical concentration of $MgCO_3$ Mol ‰ and Sr ppm; from different cements precipitated in beachrocks.

Table 3.3. Dating of marine fossils sampled in beachrocks, with their position in relation the maximum neap-tidal level and above maximum spring-tidal level (cf. Table 2.1). The values of carbon isotope were acquired by Accelerator Mass-Spectrometer.

4. Holocene sea-level history of SE-Vietnam coast

Fig. 4.1. The working area. Positions of each sample as well as their respective sea-level indicators. The tide gauge used from Mui Dinh for correcting the vertical heights is also presented.

Fig. 4.2. Picture “a” shows a bivalve cemented in beachrock. Picture “b” within the circle is also a bivalve collected from beachridge. Both shells still show their valves connected, indicating a short time since they died until deposition.

Fig. 4.3. Geological indicators of sea level presented in the relief on the SE-Vietnamese coast. Beachridge is found in elevation position, whereas beachrocks are identified close to the water.

fossil shell Spondylus sp. “C” is a picture of SEM, showing the cross-lamellar structure of aragonite.

Fig. 5.3. Cross-plot $\delta^{13}C$ vs.$\delta^{18}O$ of mollusc shells from SE-Vietnam shows the distribution range from marine to freshwater fields of modern and fossil shells.

Fig. 5.4. Stable isotope profile measured on the shells. Grey areas are light $\delta^{18}O$ values, represented by S1, S2 and S3 in modern shells and Y1 to Y5 in fossil shell.

Fig. 5.5. Precipitation and temperature values from the Nha Trang coast from August 2001 to August 2005, used to calibrate $\delta^{18}O_{PDB‰}$ fractions from shells.

Fig. 5.6. Calibration between shell profiles of $\delta^{18}O_{PDB‰}$ with precipitation rate from the Nha Trang Bay. The upper graphic shows the precipitation variability from October 2001 to August 2005 with warm periods (WP), provided by NOAA/CIRRES; the points represent monthly average. The lower graphs contain $\delta^{18}O_{PDB‰}$ from modern shells. The exact months are directly linked with $\delta^{18}O_{PDB‰}$, while those that represent the probable months are indicated by dash lines.

Fig. 5.7. Monthly variation of SST from January 2002 to June 2005 with the respective temperature $\delta^{18}O_{PDB‰}$ of shells; the normalization of points measured in the shell to calendar months is required to equalize the seasonal temperature variation with the shells` growth.

Fig. 5.8. Linear regressions between salinity values and $\delta^{18}O$ PDB ‰ measured in modern shells.

Fig. 5.9. $\delta^{13}C$ vs. $\delta^{18}O$ values in linear regression from a series of shell samples used to recognize the kinetic effect.

Fig. 5.10. The plot shows two profiles: in “a” the probable paleotemperature$_{\delta 18OPDB‰}$ records concern the distance on the shell from 36 to 104 mm with $\delta^{18}O_w$ varying from 0 to 0.5 ‰ (continued line) and the values of temperatures just at 0 ‰ and - 0.5 ‰, showing the hydrologic balance between low and high precipitation rates respectively (dashed line). In “b” the temperature of modern shells is compared with paleo-water-temperature calculated on smow from 0 to 0.5 ‰.

Fig. 5.11. “A” shows the SST of Feb. 1999; in “B” shows the SST in the summer season of July 1999. Arrow indicates cold water upwelling from the coast towards the open ocean. The shell samples as well as the ESRL water temperature in 12° 24` N were collected in the area of upwelling, whereas the ESRL water temperature at 10° 30` N is outside of the upwelling area.

Fig. 5.12. The water-temperature records sought to ESRL are presented in two positions. The temperature at 10° 30` N is warmer than at 12° 24` N, being a result linked to different isotherm.

Fig. 5.13. Comparison between water paleotemperatures ($\delta^{18}O_w$ from 0 to -0.5 ‰) sampled in the dorsal position from 36 to 104 mm of Spondylus sp and water temperatures ERSL indices at the latitude of 10° 30` N from January 2000 to December 2006. The arrows show warmer temperature in summer than today. Colder water temperature during winter in 5537 ± 55 cal yr BP might be linked to the warmer isothermal at 10° 30` N.

Contents:

1. Introduction

1.1 General introduction

The present PhD thesis is a contribution to the Vietnamese-German cooperation in marine research sub-project "Holocene coastal evolution, sea-level fluctuations, terrigenous sedimentation and sediment dynamics on the continental shelf between the Mekong Delta and Nha Trang, Southeast-Vietnam".

This Ph.D. thesis is elaborated in nine chapters: 1) Introduction, in which the general topics of the study as well as the description of the research area are presented; 2) General methodology; 3) Holocene beachrock formation; 4) Holocene sea-level history; 5) Paleoceanography of coastal waters; 6) General discussion; 7) Conclusions; 8) References; 9) Appendix.

1.2. Regional setting

Vietnam is the easternmost country on the Indochina Peninsula (Fig. 1.1). Vietnam extends 2.000 km from the north to the south, with a total land area of approximately 331.688 km^2. Moreover, the country stretches along 3260 km of the coast between China and Cambodia.

In general, Vietnam's topography consists of hills and is densely forested. Mountains account for 40 % with smaller hills accounting 20 % of the area, whereas tropical forests covered 40 % of the country. Northern shoreline is the Red River Delta and Tonkin Shelf, whereas central shoreline small embayment and coastal plains with mountains nearby and narrow shelf are found. The southern shoreline is characterized by Mekong Delta and Sunda shelf.

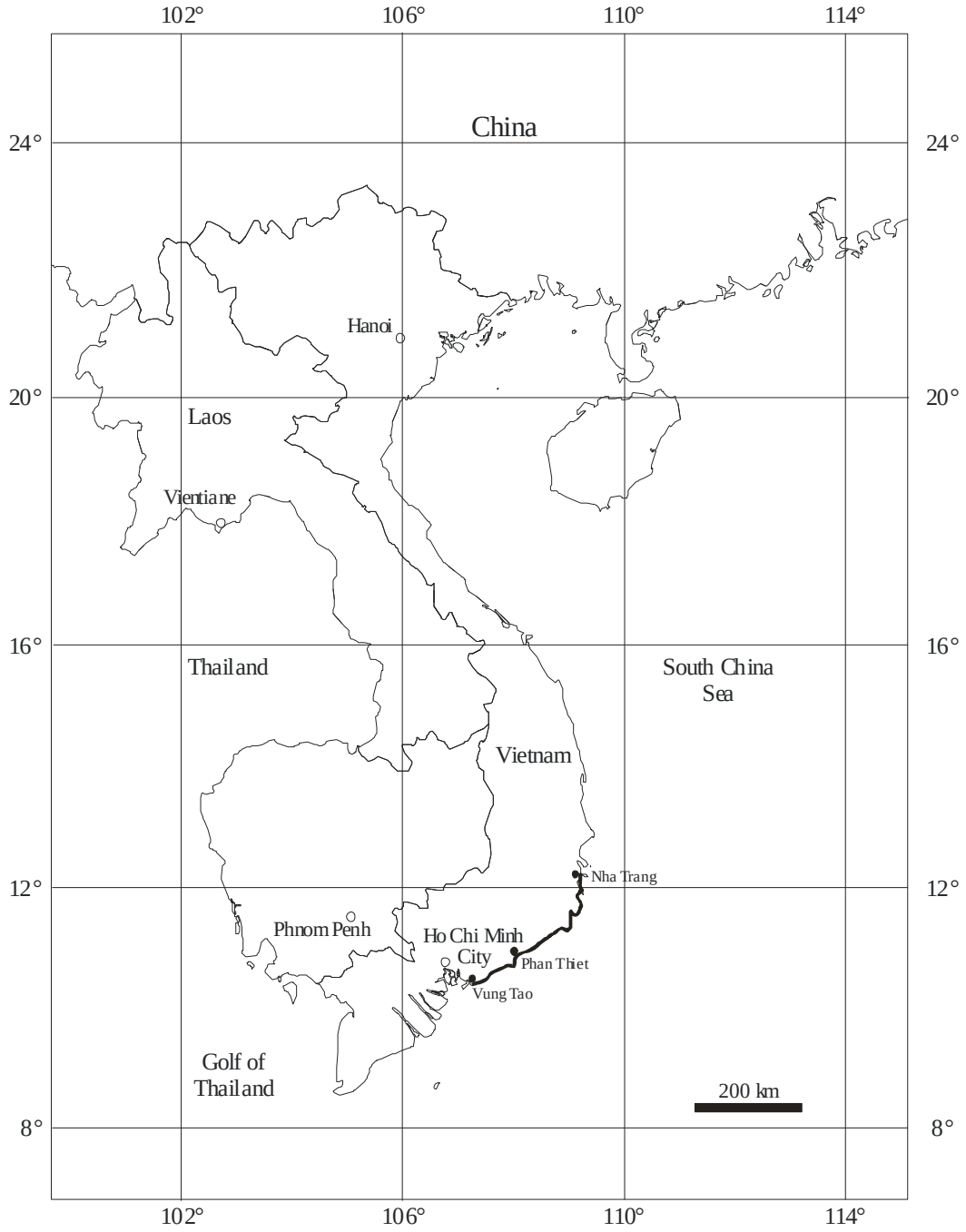

Fig. 1.1. Map localizing the work area between the towns of Nha Trang and Vung Tau on the SE-Vietnam coast.

1.2.1. Geology

Vietnam, together with Cambodia and Laos, belong to the Indochina block on the southeastern part of the Eurasian plate. It is one of the several fragments of Gondwana. The formation of the Indochina Block arose from the Precambrian metamorphic basement, Palaeozoic, Mesozoic and Cenozoic sedimentary rocks (Fontaine & Workman, 1997; Thuy et al., 2004).

According to Fontaine & Workman (1997), there is an important dislocation in the southern region of Vietnam termed the 110° fault, which runs parallel to the Vietnam coast reaching the study area in the east. Two fault zones in the region of Nha Trang, trending SW-NE, join the 110° fault. They were formed by SE movement of the Indochina block during the Himalayan orogeny.

As far as the tectonic-sedimentation evolution is concerned, the southeast coast of Vietnam can be divided into two zones with a different history. The first zone is northern Phu Khanh basin, region of Nha Thang town, which has mainly been uplifting since the Neogene. The second zone is the southern coastal zone with the Mekong Delta, which was continuously subsiding during the Neogene and the Quaternary. The geological features of southern part of Vietnam are presented in figure 1.2.

Actually, the coastal evolution resulted in a variety of morphological structures which are genetically related to different coastlines, comprising sea terraces, coastal dunes, salt water swamps, coastal plains, basaltic plateaus and inselbergs. A mountainous relief occurs on the landward side, reaching several hundred meters in altitude. It is only a few kilometres away from the coast, controlling the topography of the hinterland mainly in the northern coastal area. Mountain ranges dominate the scenery in the north-south and several branches in the east are striking WNW-ESE. They built peninsulas and islands. At some places attached to them small alluvial plains and bays occur. Moreover, most of the coastline in the northern part consists of rocks and sandy beaches or tidal flats which can only be found inside the bays, where small alluvial plains developed.

Neotectonic movements since the latest Pleistocene up to the Holocene characterise the SE coastal area up to the Vinh Hai region, which was a result of a westward tectonic compression caused by a transgression of plate movement in the Philippines (Choi et al., 2005). In the south region of the Mekong Delta sedimentary compositions show an absence of tectonic movements in the Holocene epoch (Nguyen et al. 2000).

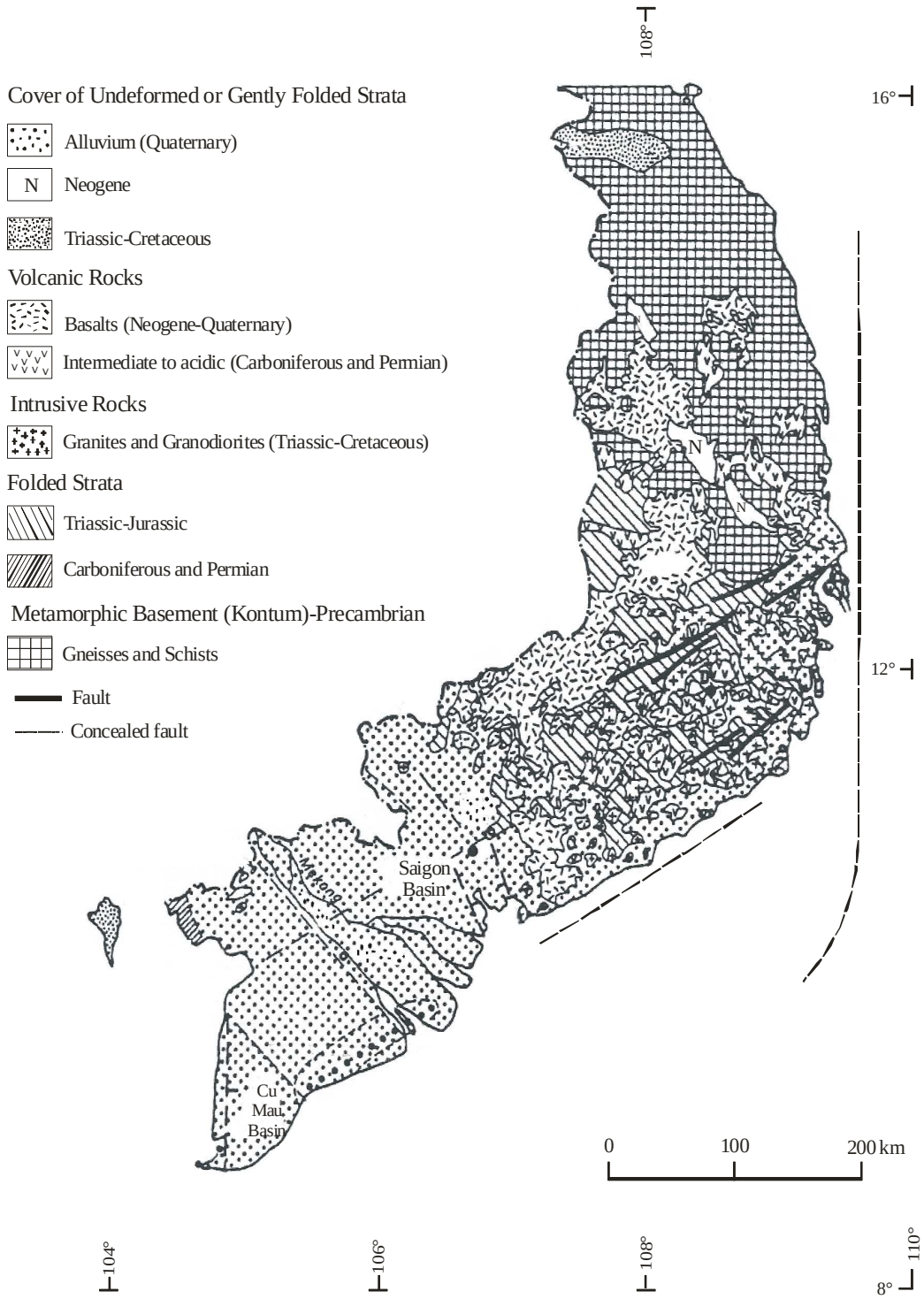

Fig. 1.2. Principal geological features of the southern part of Vietnam (cf. Fontaine & Workman, 1997).

1.2.2. Quaternary geology

Coastal plains are the geomorphologic characteristic of the Vietnamese coast. They are sediment deposits originating from the Neogene and the Quaternary periods, completely filling depressions formed during tectonic movements in the Cenozoic era. Neogene

sediments are distributed largely at the bottom of the plains and are mainly covered by Quaternary deposits with two types of accumulation.

Coastal plains are distributed along the shoreline reaching from the foot of the mountains' margin and going seaward. They have a maximum thickness of 200 m, are formed at the mouths of the rivers and occupy 1/3 of Vietnam (Tanabe et al. 2003).

Quaternary sediments of the Vietnamese coastal plains can be subdivided into four lithostratigraphic units (see Table 1.1). They are mainly composed of sand and gravel showing a predominance of terrestrial environment. Some layers are characterized by silt and clay and portions of marine fossils. Other marine layers are formed as elevated terraces (Tam, 1991; Mathers and Zalasiewicz, 1999).

Units	Name	Thickness	Lithology	Age	Reference
1° Horizon	Sam Son Horizon	Bottom of costal Plains	Continental sediment facies, Polymictic pebble, gravel and sandy	Late-Pliocene and Early-Pleistocene (N_2-Q_1)	
2° Horizon	Yen Mo Horizon	>100 to 60 m	Clay sediments with marine layers	Middle Pleistocene (Q^1_{II})	Nghi et al. (1998), An (1999)
3° Horizon		100 to 10 m	Fluvial Lithofacies, Polymictic pebble, gravel, sandy and Marine sediments	Late Pleistocene (Q^2_{II}, Q^3_{III})	
4° Horizon		80 to 10 m	Intercalated suits of fluvial and marine sediments		
Uppermost layer	Don Da	Maximal 5 m	Sand, Clay, Peat, Marine sediment and Microfauna	From 12,000 to present	Tam (1991)

Table. 1.1. The lithostratigraphic units of coastal plains in Vietnam.

1.3. Climatic Conditions

The climate in Vietnam is affected by the monsoon cycle that is by the northeast monsoon in winter and southwest monsoon in summer. Vietnam belongs to the humid and warm tropical zone; it is basically characterized by two distinct seasons. The summer season is associated with heavy rainfall for 6 months from May to November. The winter is associated with the dry season, although higher-range climatic periodicities were found (Fairbridge, 1986).

The mean annual rainfall in the working area is not homogeneous. Near Nha Trang it amounts to 1300 mm yr^{-1} and in the southern area, the Mekong Delta region, reaches 1700 mm yr^{-1} (Nguyen, et. al., 2000), with an evaporation of approximately 1000 mm yr^{-1} (Jia et. al. 2006).

The mean air temperature in the central and south region, deduced from the last 30 years, is 27 - 30° C. The maximum temperature measured is 39.9° C, whereas the minimum temperature is 17.7° C (Thong et al., 2000).

1.4. Oceanography

1.4.1. Circulation

The major circulation in the South China Sea (SCS) is driven by the monsoon winds (Wyrtki, 1961). During wintertime the circulation is dominated by the northeast monsoon, and during the summer the circulation is caused by the southwest monsoon. It is associated with the geographic characteristics of the SCS, where semi-enclosed basin exchanges water with the subtropical Pacific Ocean through the Luzon Strait. Furthermore, the water of the tropical Java Sea and Indian Ocean flows across the shallow Sunda Shelf to the southwest. The described circulation system in the western SCS drives strong currents, causing large anticyclonic circulation during the southwestern monsoon and a cyclonic circulation during the northeastern monsoon (Ho, et al., 2000; Hu et al., 2000; Fang, et al., 2002) (Fig. 1.3).

Due to this displacement, the wind develops a strong southward current along the coast of Vietnam with approximately 0.5 m s^{-1} during the northeast monsoon from October to February. The contrary happens from May to August, when the northeastward current during

the southwest monsoon reaches approximately 0.7 m s^{-1} (Wyrtki, 1961). Between 11° and 14° N, the strong northeast current leaves the coast of southeast Vietnam and diffuses toward the northeast (Shaw & Chao, 1994).

By inducing a northeastward current, the southwest monsoon provokes a vertical movement of water masses resulting in a seasonal upwelling. This upwelling event during the summer months was already described for the southeast coast of Vietnam by Tang, et al. (2004), Rojana-anawat, et al. (2000), and Shaw & Chao, et al. (1994).

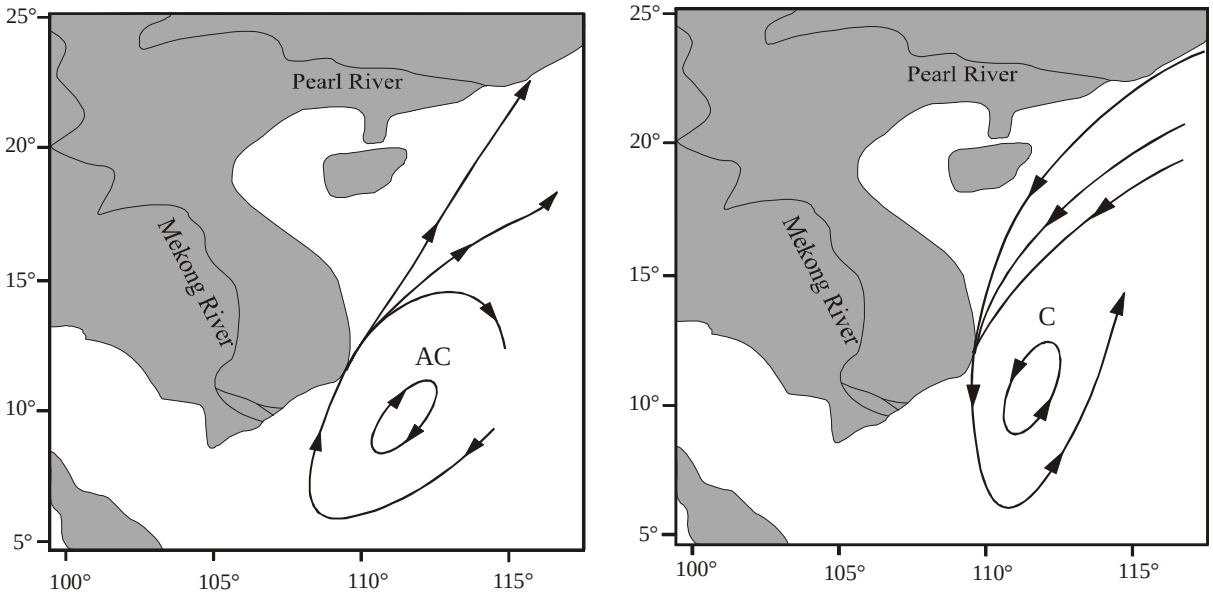

Fig. 1.3. Upper layer circulation patterns on the western SCS; "AC" represents the anticyclonic eddy in the summer season during the southwest monsoon, and "C" represents the cyclonic eddy formation in the winter season during the northeast monsoon.

1.4.2. Temperature

The sea-surface temperatures of the western SCS were monthly surveyed; the data are from the NODC (Levitus) World Ocean Atlas provided by the NOAA-CIRES Climate Diagnostics Center – CO, USA http://www.cdc.noaa.gov., presented by Jia et al. (2006). According to this database the mean annual surface temperature increases from 26.5°C to 28°C from the north to the south of the western SCS (Fig.1.4).

Temperatures to a depth of 5 m were researched along the Vietnamese coast in May 1999 (Thong et al., 2000). The research revealed a maximum temperature of 27° C in the north,

increasing southward. Along the Nha Trang coast the maximum temperature was 28°C, and southeastward along the Vung Tau coast the temperature reached 30°C.

During the southwest monsoon in summer, an upwelling event along the southeast coast of Vietnam carries cold water to the sea surface (Rojana-anawat et al., 2000). Tang et al. (2004) provide SST measurements from the AVHRR (Advanced Very High Resolution Radiometer) through satellite images from NOAA satellites, showing the summer upwelling (Fig. 5.11).

1.4.3. Salinity

The salinity values are affected by the geographical position of the SCS in a tropical region, adding to monsoonal climates that result in a large annual variation of the salinity grade. The monsoon circulation from the northeast carries high saline water from the Pacific Ocean with a salinity of about 34 psu southward to the Vietnamese coast. During the southwest monsoon, the situation is reversed: water with a salinity of about 32.8 psu is transported along the coast of Vietnam to the north, bringing a salinity of approximately 33.4 psu in the central region (Jia et al., 2006, and Wyrtki, 1961) (Fig. 1.4).

The salinity is lower in the western SCS along the coast of Vietnam with an annual salinity value less than 34 psu caused by the average of rainfall, which exceeds the evaporation in the summer. During the dry season, the salinity increases as a result of the immense evaporation. With the beginning of the rain season, a great interchange of saline waters takes place. It is induced by the monsoon changing the circulation, which produces a mixing of low and high saline water masses (Wyrtki, 1961).

The very high precipitation and freshwater input from the rivers affect the sea-surface salinity, resulting in very low salinity rates of about 31.5 psu along the Mekong Delta. Towards Nha Trang the salinity increases to about 33.5 psu due to the dissipation of low saline currents from the Mekong Delta. In summer, during the southwest monsoon an upwelling event brings even more salty water to the southeast Vietnamese coast (Rojana-anawat, 2000).

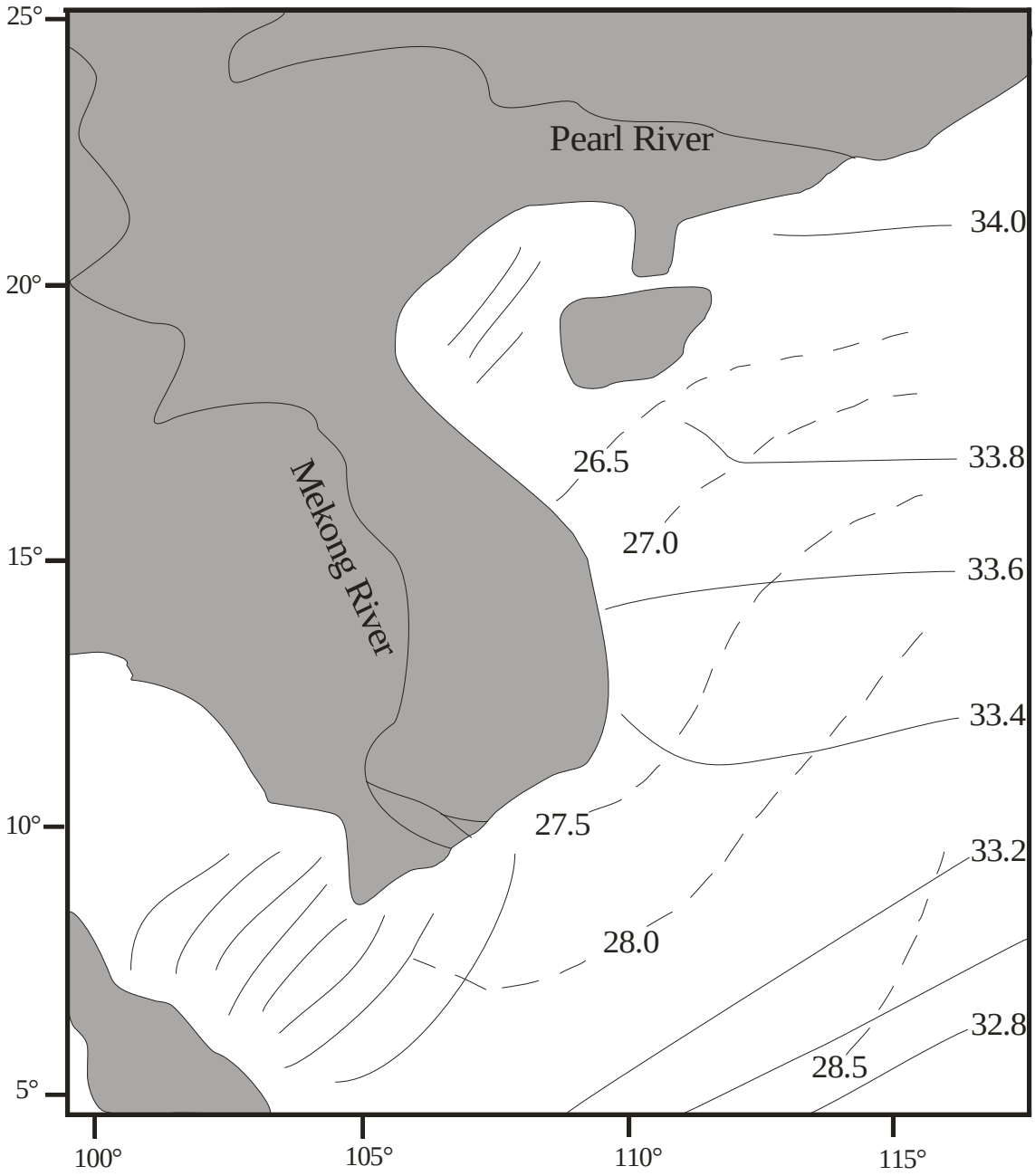

Fig. 1.4. The average sea-surface temperature in °C (dashed line) and salinity in psu (solid line) distributions in the western part of the South China Sea near the Vietnamese coast (cf. Jia et al. 2006).

1.4.4. Tide

The Vietnamese coast is characterized by diurnal, semidiurnal and mixed tidal regimes, with the mixed tidal regime being predominant (Huang et al. 1994) (Fig. 1.5). The spring-tidal range reaches about 4.0 m in the north and south, whereas in the central region the range decreases to 0.5 – 0.7 m.

The study area in the southeast region is characterised by a mesotidal range, presenting maximum spring tide of approx. 3.7 m in Vung Tau. The tide in Vung Tau is a mixed tide of

predominantly semi-diurnal character being twice as large as further north. Different tidal regimes can be found from Nha Trang to Phan Thiet with mixed tide diurnal character prevailing. It varies in amplitude from 0.48 m during neap-tide and 1 m during spring-tide in Nha Trang. The tide occurs at nearly the same time in all locations evaluated. Tidal data were used from the Atlas of Natural Conditions, edited by Lanh (1997) and the software WXTidal-32 version 4.0.

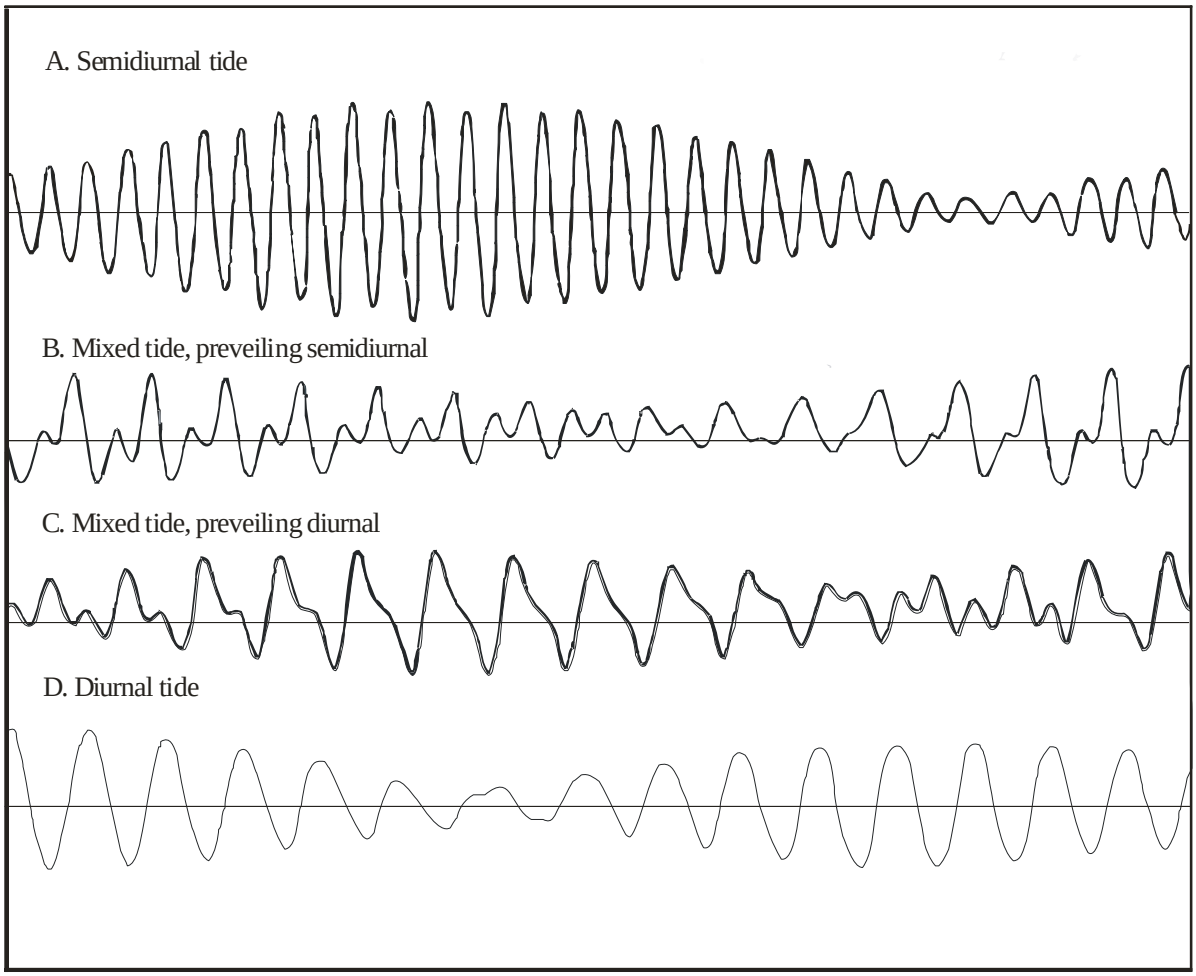

Fig. 1.5. Different tidal patterns.

2. Methods

Fieldwork was performed during two periods, the first from 3rd to19th November 2003 and the second from 4th to 7th of May 2005, between Nha Trang and Vung Tau, covering more than 400 km of the coast. Several potential sedimentary indicators of the coastal evolution linked with sea-level fluctuation were identified. As the principal evaluated indicators were found between Nha Trang and Phan Thiet, the work was restricted to this region (Fig. 2.1).

During these field studies, 26 samples were collected at five locations along the SE-Vietnamese coast (Fig. 2.1). In the north of the working area, in Nha Trang, living shells were collected for the reconstruction of the sea-water temperature. Near Phan Rang in the south a beachridge was found. Field research in Son Hai followed, where beachrock samples were collected, being the principal sea-level indicator examined in this work.

In the area around Ca Na, the largest numbers of samples was taken at two stations. In addition to beachrocks and beachridges, two more sea-level indicators were evaluated: washover and backshore. In order to estimate the sea-water temperature in the mid-Holocene a fossil bivalve shell was collected from as beachridge sea-level highstand indicator.

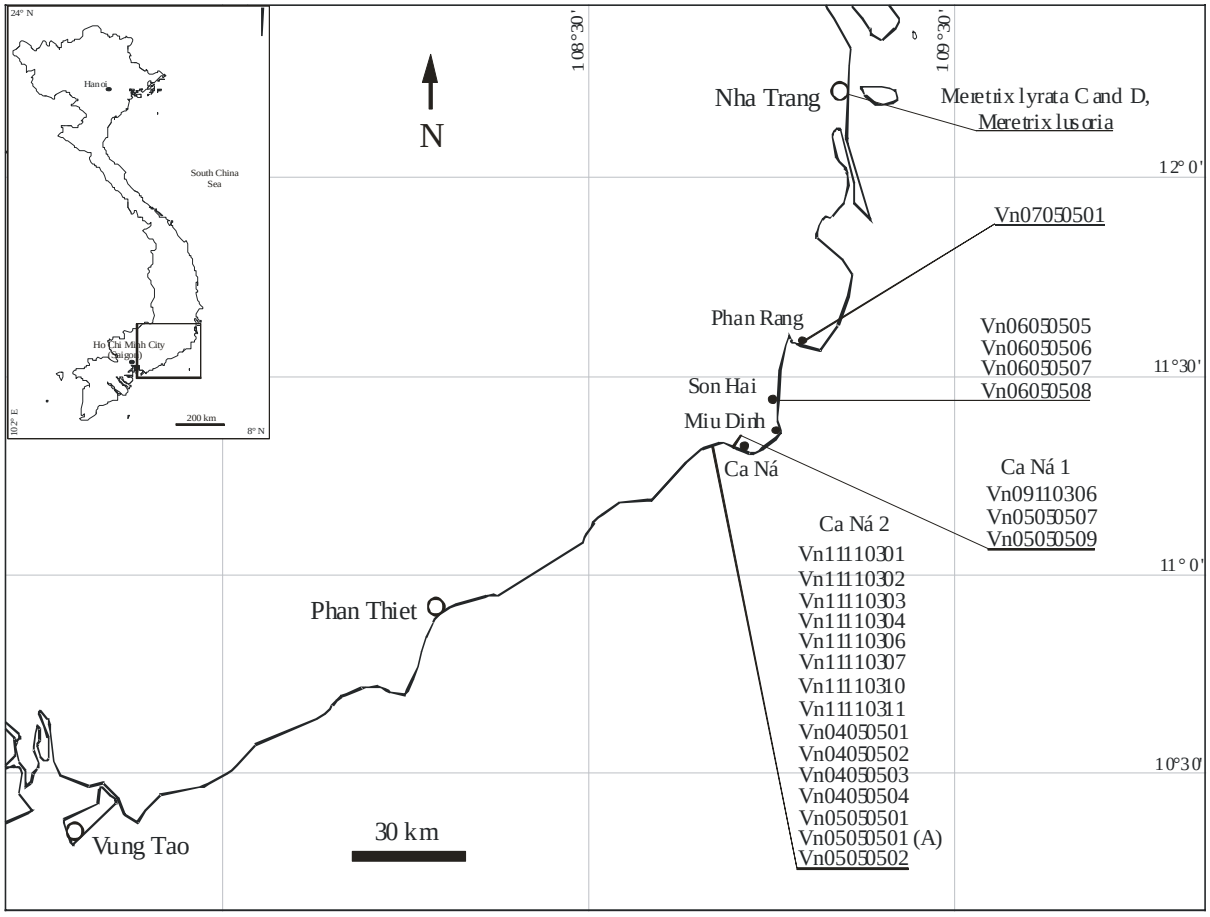

Fig. 2.1. The working area between Nha Trang and Phan Thiet. The figure shows the field research stations and the respective identification of samples.

2.1. Measurement of vertical height and tidal correction

The samples were gathered in the field using the Global Positioning System (GPS). The elevation in relation to the sea level at the time of sampling (Fig. 2.2) was measured by standard geodetic methods using a theodolite.

The vertical positions, determined in the field, were referenced to different tidal levels, using the tidal table supplied by the Mui Dinh chart Datum (Fig. 2.1) in Admiralty Chart 3883, Point Lagan to Cap Varella, 1:200000 (1971). The Mui Dinh tide is characterized by a mesotidal range with a mean sea level (msl) at 0.95 m as reference elevation, a maximum neap tide (mnt) at 1.40 m and a maximum spring tide (mst) at 2.1 m, presenting a mixed tide regime of a prevailing diurnal character.

When the tidal datum in Mui Dinh was established, all samples to construct the sea-level curve were corrected to this datum. The description of the beachrocks was corrected to above the present mean sea level, mean neap tide and maximum spring tide from the tide stand at the moment of sampling. The heights of the tides at the moment of sampling were determined by the tidal software WXTidal-32 v. 4.0, which is a tide program with a reference gauge in Manila – Philippines and a substation at Mui Dinh, showing the same levels found in the Admiralty Chart 3883 (1971) (Tab. 2.1).

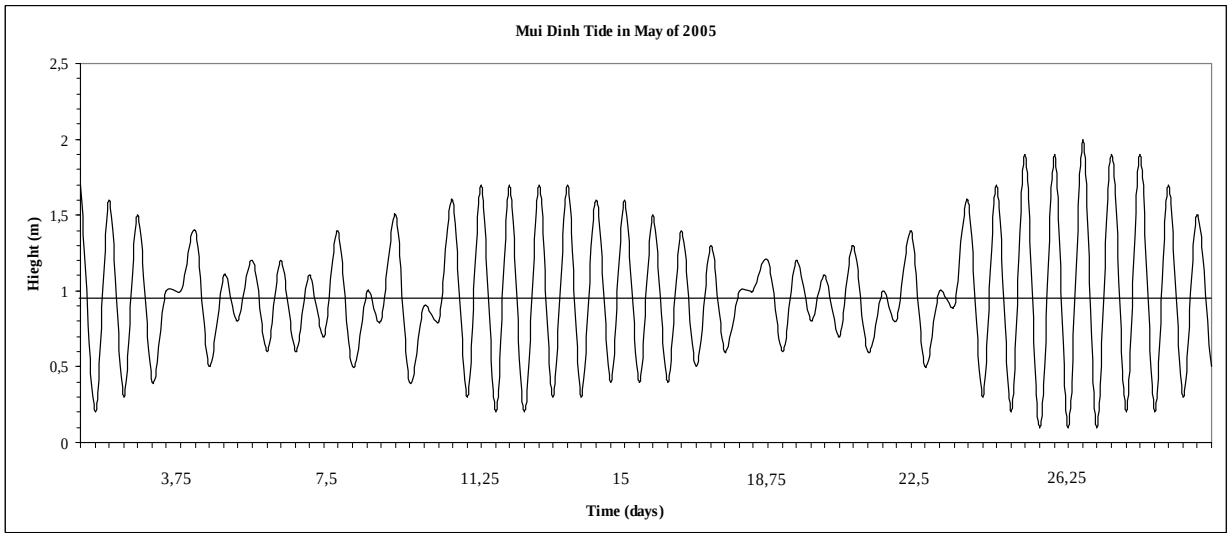

Fig. 2.2. Tidal elevations at the Mui Dinh sub-station that occurred during the fieldtrip in May of 2005.

Number of samples	Position	Sea-level indicator	Time of sampling	Sample position above sea level at the time of sampling (m)	Tide at the time of sampling (m)	Mean sea level (m) at the Mui Ding	Maximum neap tide (m) at Mui Ding 45 cm above msl	Maximum spring tide (m) at Mui Dinh 115 cm above msl	Elevation above mean sea level (m) for Mui Dinh gauge	Elevation of sampling above maximum neap tide (m)	Elevation above maximum spring tide (m)
Vn 09110306	11° 19,975`// 108° 52,320`	Beachrock	16:36	1.01	1.11	0.95	1.4	2.1	1.17	0.72	0.02
Vn 11110302	11°19,434`// 108°50,260`	Backshore	7:24	1.70	0.92	0.95	1.4	2.1	1.67	1.22	0.52
Vn 11110306	11°19,796`// 108°50,496`	Beachridge	9:18	3.59	0.93	0.95	1.4	2.1	3.57	3.12	2.42
Vn 11110307	“	Beachridge	9:18	2.69	0.93	0.95	1.4	2.1	2.67	2.22	1.52
Vn 11110310	11°19,803`// 108°50,550`	Beachrock	12:06	0.70	1.47	0.95	1.4	2.1	1.22	0.77	0.07
Vn 11110311	11° 20,305`// 108° 51,041`	Washover	16:45	1.80	1.33	0.95	1.4	2.1	2.18	1.73	1.03
Vn 04050501	11°19.958`// 108°50.774`	Beachrock	16:07	0.30	1.36	0.95	1.4	2.1	0.71	0.26	-0.44
Vn 04050502	“	Beachrock	16:07	0.20	1.36	0.95	1.4	2.1	0.61	0.16	-0.54
Vn 04050503	“	Beachrock	16:07	1.04	1.36	0.95	1.4	2.1	1.45	1.00	0.30
Vn 04050504	“	Beachrock	16:07	1.04	1.36	0.95	1.4	2.1	1.45	1.00	0.30
Vn 05050501	11°19,801`// 108°50.495`	Beachridge	7:20	2.99	0.93	0.95	1.4	2.1	2.97	2.52	1.82
Vn 05050501 A	“	“	“	2.37	0.93	0.95	1.4	2.1	2.35	1.90	1.20
Vn 05050502	“	“	“	2.27	0.93	0.95	1.4	2.1	2.25	1.80	1.10
Vn 05050507	11°19.993`// 108°52.429`	Beachridge	9:30	1.27	1.15	0.95	1.4	2.1	1.47	1.02	0.32
Vn 05050509	“	Beachrock	9:57	0.98	1.19	0.95	1.4	2.1	1.22	0.77	0.07
Vn 06050505	11°24.946`// 109°00.622`	Beachrock	15:30	0.92	0.90	0.95	1.4	2.1	0.87	0.42	-0.28
Vn 06050506	“	Beachrock	15:30	1.65	0.90	0.95	1.4	2.1	1.60	1.15	0.45
Vn 06050507	“	Beachrock	15:30	0.94	0.90	0.95	1.4	2.1	0.89	0.44	-0.26
Vn 06050508	“	Beachrock	15:30	0.94	0.90	0.95	1.4	2.1	0.89	0.44	-0.26

Table 2.1. Sample elevation corrections according to Mui Dinh tide gauge control.

2.2. Determination of mineral phases by X-ray diffraction

The material for radiocarbon ^{14}C dating had been examined before by X-ray diffraction, an analysis used for the determination of the mineral phase of the carbonate samples. Since in most mollusc shells the mineral aragonite is the original component of carbonate, its alteration can be identified through replacement by the mineral calcite. In this thesis carbonate-shell material that presented $\geq$ 10 % of alteration of the original mineral was not taken into consideration.

The X-ray diffraction analyses were carried out at the Institute of Geosciences at the University of Kiel. The equipment used was a Philips PW1710, whose signal impulse was converted to % of aragonite and calcite, using a methodology elaborated by Milliman (1977).

2.3. Scanning Electronic Microscope (SEM) analysis

The SEM observations were carried out on beachrocks in order to identify the precipitated cement type as well as in order to observe the framework relationship prevailing between cement and sediment. Afterwards, photos were taken of microorganisms growing on the cements.

The bivalve fossils were observed under the SEM with the objective to detect the aragonite mineral through the identification of the cross-lamellar structure. The observations were accomplished in the Scanning Electronic Microscope Laboratory at the Institute of Geosciences at the University of Kiel. The equipment used was a CanScan CS-44.

2.4. Radiometric AMS ^{14}C age dating

The AMS radiocarbon ages were determined using a 3 MV High Voltage Engineering Europe, Tandentron, 4130 AMS-system at the Leibniz Laboratory for Radiometric Dating and Isotope Research, Kiel. The analytical precision for counting and machine statistics is 0.25-0.3% for modern samples (Nadeau et. al., 1997 and Schleicher et. al. 1998).

In order to calibrate AMS ^{14}C years to calendar years B.P., the program CALIB rev. 5.0.1 was used (Stuiver and Reimer, 1993) (HTML version). For each calibrated age 1σ – range was

calculated. The marine reservoir age correction approximates 190 ± 35 years with a ΔR value of -70 ± 30 years measured in the *Porite lutea*, which is a scleractinian coral from the Con Dao Island (Dang et. al., 2004). (source http://calib.qub.ac.uk/marine/ by Paula Reimer). In the research region a reservoir age of 253 ± 23 years was identified in the *Arca fusca* bivalve which was not used in this study, though.

2.5. Stable isotopes $\delta^{18}O$ and $\delta^{13}C$

The carbonate powder on the filter was treated with 100% orthophosphoric acid under vacuum at 73° with a Finnigan MAT 251 gas isotope mass spectrometer at the Leibniz Laboratory for Radiometric Dating and Isotope Research, Kiel. The isotope values are reported as parts per mil (‰) in the usual δ-notation relative to the PDB ‰ (Pee Dee Belemnites) based NBS-19. The error external amounts to less than ± 0.07 ‰ and ± 0.05 ‰ for $\delta^{18}O$ and $\delta^{13}C$ respectively.

3. Holocene beachrock formation on the SE-Vietnamese coast

Abstract:

Three beachrock formations were identified along the SE coast of Vietnam between Nha Trang and Phan Thiet: two in the region of Ca Na town and one in Son Hai town. The uppermost position of the beachrocks was vertically measured, relative to the waterline during the sampling. In order to identify the sediment types, petrographic thin sections of beachrock samples were examined. The formation of cement fabrics and their influence on the coastal environment and vice versa were identified using $MgCO_3$ and Sr and isotopic records of $\delta^{18}O$ and $\delta^{13}C$. The age of the beachrocks was determined using radiocarbon measurements from fossil shells and fragments of corals lithificated in the beachrocks.

The identification of terrigenous sediment and the skeletal constituents of the beachrocks enabled us to make some assumptions about the probable sediment source, the agents of transport, and the diagenetic alteration. From the origin of the sediment, it was possible to identify a strong link to the upper layer of the coastal plain formation, serving as sediment source. The early cements were identified as micritic high-Mg calcite and aragonite crystals, indicating precipitation in the marine phreatic zone. Additionally, blade cement, resulting from meteoritic alteration in the supratidal zone was detected.

Chemical cement analyses confirm the predominance of marine diagenesis. The values of $MgCO_3$ in cement ranged from 5.69 to 6.82 mol ‰. Sr linked to aragonite reached a value of 4329 to 11123 ppm. The isotopic composition also revealed marine conditions with some influence of freshwater for $\delta^{18}O$, ranging from - 2.30 to - 0.97 ‰PDB. Freshwater influence is restricted to most elevated beachrocks with supratidal position today. The $\delta^{13}C$ value reached from 2.46 to 3.86 ‰PDB.

AMS-radiocarbon dating covers the time from 6721 to 642 cal yr BP. It can be divided into three intervals: 6721 to 5869 cal yr BP as an older stage of beachrock formation; followed by 3760 to 3272 cal yr BP, showing a probable second stage of cementation; and the youngest cement formation from 1210 to 642 cal yr BP.

Considering the geochemical and geomorphological characteristics with tropical conditions, a scenario of beachrock lithification in Son Hai town could be developed. The formation of beachrocks

is induced by their exposure during low tide and by their high porosity. The high porosity enhances water percolation during high tide. During the low tide, the water filling the voids evaporates because of high air temperatures, which is a normal condition in tropical coastal regions such as SE-Vietnam. Consequently, the supersaturated carbonate dissolved in the water precipitates, followed by the growing of crystalline cement.

3. 1. Introduction

Beachrocks are sediment bodies frequently observed on tropical and subtropical sandy beaches. They are formed by sand and gravel including fossils of shells, fragments of corals and skeletons of carbonated algae, cemented within the intertidal zone by the precipitation of calcium carbonate (e.g. Ginsburg, 1953; Russell, 1959; Mabesoone, 1964; Stoddart & Cann, 1965; Taylor & Illing, 1969; McLean, 1974; Siesser, 1974; Hanor, 1978; Strasser et al., 1989; Omoto, 2001, 2004). Beachrocks can also occur in regions of temperate climate (e.g. Alexandersson, 1972; Holail & Rashed, 1992; Sellwood, 1994; Calvet et al., 2003; Rey et al., 2004) and more exceptionally in cold climates or even in lake systems (e.g. Jones et al., 1997; Kneale & Viles, 2000).

Early cement is formed by the process of marine carbonate lithification within the intertidal zone, although it can also occur in the upper part of the subtidal zone (Alexandersson, 1972) and the lower part of the supratidal zone (Holail & Rashed, 1992) as well as in the swash zone (Badyukov, 1986; Bernier & Dolongeville, 1996; Kelletat, 1989; Kelletat, 2006). However, some authors suggest that the intertidal zone is probably the interval, in which the early cementation processes develop most intensively due to the constant occurrence of waves and the generation of tidal action.

The early cementation processes have been discussed at great length. Warm water becomes supersaturated with calcium carbonate and is in a high-energy condition due to the water flux in the intertidal zone. Thus, interface water-sediments with high percolation and porosity are created, allowing the necessary volume of water to move through the sediment and bring

about its cementation. Additionally, this interface water-sediment has to be a stable substrate with a slow sedimentation rate (Bathurst, 1971; Scoffin, 1987; Moore, 1989). Therefore, the process is believed to occur beneath the beach surface within the agradational relief (Badyukov, 1986).

Three possible processes are suggested to explain the scenario of cement precipitation. The majority of authors suggests that to the chief processes involved belongs the physicochemical process such as occurs by supersaturation with carbonate through direct evaporation of seawater (e.g. Scoffin, 1970; Moore & Billings, 1971; Milliman, 1974; Beier, 1985). Another possible process is the way groundwater influences the CO_2 degassing at the phreatic/vadose limit (Hanor, 1978; Gischler & Lomando, 1997). The third suggested process describes the precipitation occurring from brackish water in the mixed zone of marine and meteoric water fluxes (Schmalz, 1971; Moore, 1973). The focus of other authors (Krumbein, 1979; Bernier et al., 1990; Pedone & Folk, 1996; Neumeier, 1999; Khadkikar & Rajshekhar, 2003) has also been the process of cement precipitation somehow controlled and/or induced by microbial activity.

Minerals of high-Mg calcite and aragonite are the earliest cement crystals precipitated in the intertidal zone. After the precipitation process, these metastable crystals undergo replacement effects, adopting highly varied and complex morphologies and textures, usually stipulating for the change of environment (e.g. Folk, 1974; Schroeder, 1973; Longman, 1980; Beier, 1985; Meyers, 1987; Gischler & Lomando, 1997; Font & Calvet, 1997; Spurgeon et al., 2003; Guerra et al., 2005).

In addition to the interest in their formation, beachrocks are widely studied as modifier agents of coastal geomorphology. They have been identified as reducers of the littoral sediment volume, changing the coastal morphology as well as the preservation potential of the shoreline face (Cooper, 1991; Guerra et al., 2005; Winterholler, 2006). They are also involved in the reconstruction of coastal morphology processes (Semeniuk & Searle, 1987).

As a consequence, these characteristics also influence their formation in the intertidal zone. Beachrocks are very good indicators of former sea-level stability, mainly during the Holocene (e.g. Omoto 2004 and Caldas et al., 2006), and also until the late Pleistocene, depending on their state of conservation (Ramsay & Cooper, 2002). Beachrocks have been investigated for at least 167 years. One of the first scientists dealing with them was Darwin (1841) in his studies about NE-Brazil. Beachrock research was intensified at the beginning of the 1950s, dealing with many regions where their formation could occur.

The task of this study is to identify and describe the formation of beachrocks on the southeast Vietnamese coast, being a coastal region widely fragmented and constituted of several different types of landforms. Furthermore, this study aims to develop a model based on cement precipitation events in these beachrocks.

Investigations of beachrocks from the Vietnamese coast are very scarce. They were previously used as indicators of sea-level curve reconstruction by Korotky et al. (1995) on the Re Island. Tam (1991) used the term “outcrops” for describing some structures in the north of Vietnam, but it is not clear whether the outcrops are beachrocks or not.

3.2. Methodology

3.2.1. Beachrock bodies

Beachrocks were found during two field campaigns in SE-Vietnam between the cities Nha Trang and Phan Thiet (Fig. 3.1). They were geometrically investigated: their length, width and height were measured. The vertical distance from the waterline to the top of the beachrocks was measured. And the position of each sample in the beachrocks was determined from the waterline of the time of sampling to above the mean sea level.

The identification of the tidal level enabled to observe a considerable influence of the marine water on the beachrocks` bodies. The cement in the beachrocks changes its shape in relation to different tidal levels. Therefore, especially the mean neap-tidal level at + 0.45 m and the

maximum spring-tidal level at + 1.15 m above the mean sea-level were used as reference levels (cf. table 3.1).

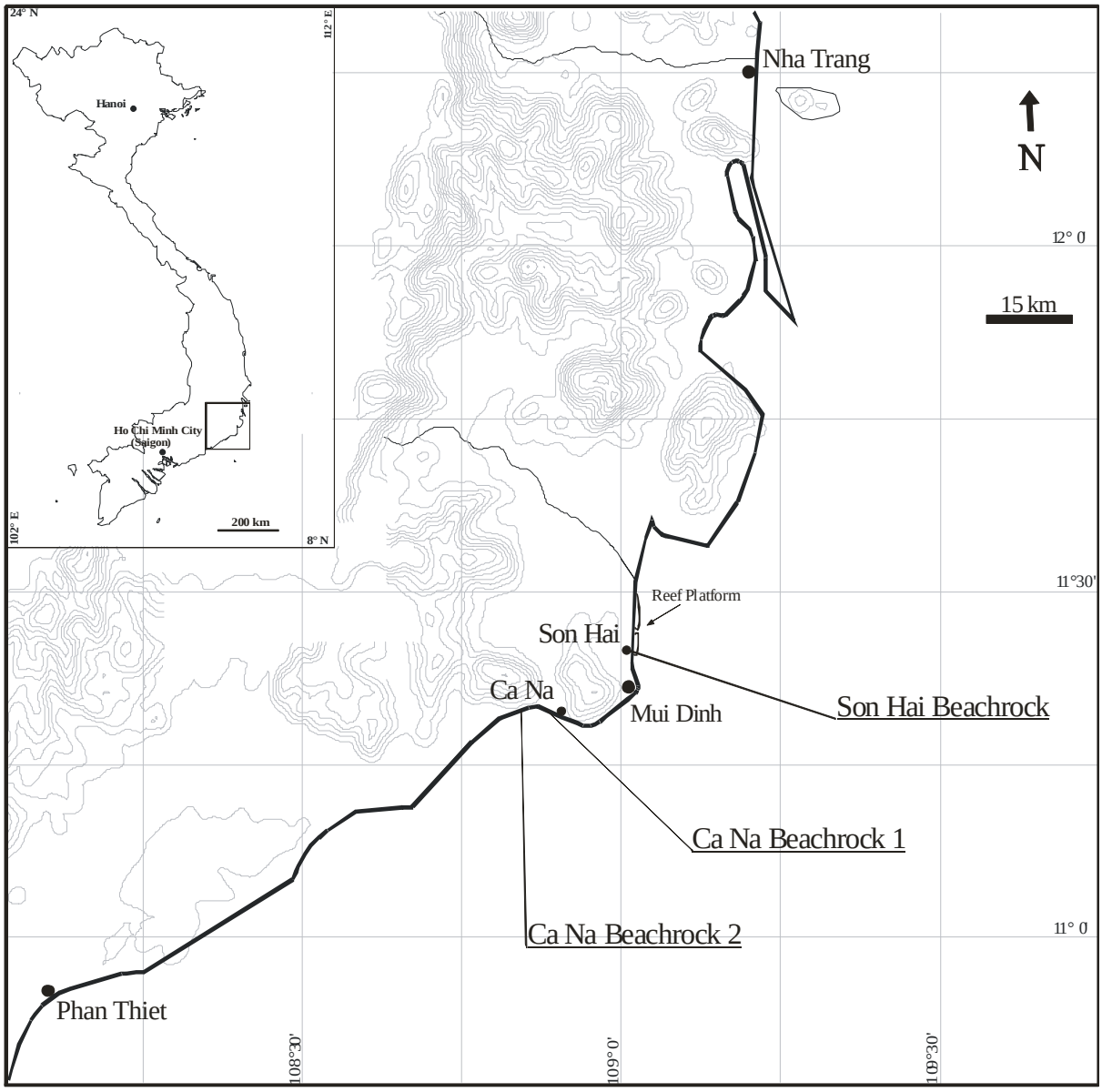

Fig. 3.1. The research area is located between Nha Trang and Phan Thiet in SE-Vietnam. The positions of the three beachrocks are shown. The Mui Dinh tide gauge was used to correct the height of the beachrock samples in relation to the tidal range.

Beachrock	Coordinates	Dating sample	Position above maximum neap tide (m)	Position above maximum spring tide (m)
Ca Na 1	11°19.975/ 108°52.320	Vn 09110306	0.72	0.02
	11°19.993/ 108°52.429	Vn 05050509	0.77	0.07
Ca Na 2	11°19.958/ 108°50.774	Vn 04050501	0.26	- 0.44
	"	Vn 04050502	0.16	- 0.54
	11°19.958/ 108°50.774	Vn 11110310	0.77	0.07
	11°19.803/ 108°50.550	Vn 04050503	1.00	0.30
		Vn 04050504	1.00	0.30
Son Hai	11°24.946/ 109°00.622	Vn 06050505	0.42	- 0.28
	"	Vn 06050507	0.44	- 0.26
	"	Vn 06050508	0.44	- 0.26

Table 3.1. Samples of beachrocks collected at three locations with their respective elevations above the maximum neap-tidal level (amntl) and above the maximum spring-tidal level (amstl).

3.2.2 Beachrock samples

In the laboratory, beachrock samples were cut to prepare petrography thin sections. The set-up was done in respect of the direction of the beachrock's growth. Six petrographic thin sections of beachrocks were investigated, so that the textural constituent of lithoclasts and biological fragments could be identified. The following methodology, used for describing the contents of petrographic thin sections as well as the framework between the cement precipitation and the sediment, is summarized by Tucker (1981).

An amount of aragonite and micritic high-Mg calcite from precipitated cements was taken with the intention of measuring the fractionation of $\delta^{18}O$ and $\delta^{13}C$. It was observed that the micritic high-Mg calcite cement is not a single mineral. Normally, it fills the pores along with many fragments of carbonate organisms, which cannot be observed under the optical microscope. In order, to avoid a misinterpretation as regards the examination of isotopes in cement, the samples were searched under an X-ray scanner in microprobe analysis. These

images provide information, which is not recognizable under an optical microscope. In this way, cement precipitated in pores without contaminating primary fragments was chosen.

Fractions of $\delta^{18}O$ and $\delta^{13}C$ of cement were analysed in order to get information about the environments in which precipitation took place (Emrich et al., 1970). The environments, which were identified, were the marine phreatic zone and the meteoritic zone. The marine phreatic zone is found below the mixing zone (Fig. 3.2). The meteoric zone is constituted by the meteoritic phreatic zone found under the water table and by the vadose zone identified above the water table and described as the region of unconsolidated sediment and passage of freshwater to the phreatic zone (e.g. Moore, 2004).

Fractions of $\delta^{18}O$ and $\delta^{13}C$ in cements are connected with the marine environment with a value close to zero (Fig. 3.2). Precipitation in freshwater represented by a concentration systematically negative like: $\delta^{13}C$ - 5 to - 15 and $\delta^{18}O$ - 5 to - 10, with negative values also indicating post-depositional exchanges with meteoric waters (Land & Goreau, 1969; Magaritz et al. 1979; Margaritz, 1983; Veizer, 1983; Coudray & Montaggioni, 1996). The fractionations of both proxies are also indicators of biological influence on cement formation. The liberation of methane during the fermentation process by microbes shows carbon isotope values of $> 10_{PDB\,‰}$ (James & Choquette, 1983; Hudson, 1977; Milliman, 1974).

The cement material was taken from the rubbed surface of beachrock pieces, previously used in the preparation of petrographic thin sections. The largest pores were chosen under the magnifying glass in order to avoid the mixing of cement with the carbonate of bioclastic constituents. While sampling, the cement from the beachrock pieces was taken using millimetre fraise equipment under the magnifying glass.

Isotope fractionation alone indicates only the tidal zone which influences the different parts of beachrock. It does not tell anything about the chemical composition of the early precipitated cement. Through investigation of the chemical concentrations of Sr and $MgCO_3$ in carbonate cements, it is possible to identify crystals of aragonite and high-Mg calcite

(micritic). The early diagenetic aragonite cement forms in shallow marine tropical water, presenting a range from 7 to 10 parts per thousand (ppm) of Sr (Kinsman, 1969; James & Ginsburg, 1979; Veizer, 1983; Morse & Mackenzie, 1990) and more than 5 mol ‰ of $MgCO_3$ for high-Mg calcite (Friedman & Sanders, 1978; Coudray & Montaggioni 1986). However, in some places the concentration of $MgCO_3$ in cement of calcite range from 12 to 18 mol ‰ (Alexandersson, 1972; Caldas, 2002).

Six thin sections of Sr and $MgCO_3$ were analysed in the Electronic Microprobe (EMP) laboratory, performed at the Mineralogy Division, University of Kiel. The equipment used was a Cameca, a Camebax-Microbeam with four wavelengths-dispersed spectrometers. The operating conditions consisted of 15 kV accelerating voltage and a 15nA beam current, which allowed a beam diameter smaller than 10 µm.

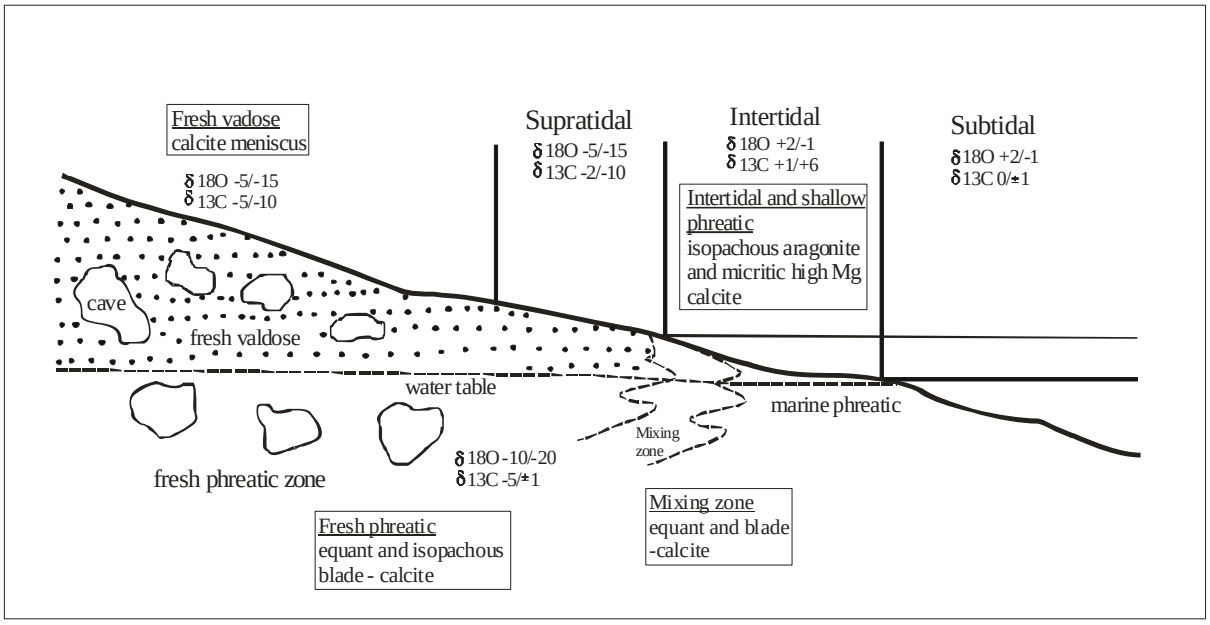

Fig. 3.2. The environments of inorganic calcium carbonate precipitation, indicating the typical crystal fabric as well as their range value of $\delta^{13}C$ and $\delta^{18}O$ (Margaritz, 1983; Coudray & Montaggioni, 1986).

3.3. Beachrock location

Three beachrock were detected along 270 km of the southeast Vietnamese coast between Phan Thiet and Nha Trang. The first two beachrocks were found on the coast near Ca Na town, situated 112 km south of Nha Trang. The first beachrock, identified as Ca Na 1, was about 2.03 km away from Ca Na town and the second one, identified as Ca Na 2, was about 4.95 km away from Ca Na town (Fig. 3.1).

The geomorphology of the coast in Ca Na can be described as narrow shore, followed by a backshore zone formed of a field of small dunes. The mountainous system starts behind the dune fields, characterised by the crystalline basement rocks.

The second beachrock position was located in Son Hai town, a small fisherman village approx. 97.7 km south of Nha Trang town. This region was also characterized by a narrow strip of beach, followed by an extensive dune field. A platform reef was found adjacent to the beachrock. It was characterized by fringe morphology, with a length of approximately 1 km (Fig. 3.1). Petrographical observations revealed that the platform reef was constituted of siliciclastic sediment, but no signs of constructor organisms, such as corals or algae were detected. More details about platform reefs can be found in Moore (2004, p. 106).

3.4. Beachrock characterisation

Ca Na Beachrock 1 was found facing the Ca Na Beach Resort. Its complete description was not possible, because houses were built on the beachrocks (Fig. 3.3). Ca Na Beachrock 1 lies between the intertidal zone and the supratidal zone with a length of approx. 60 m and a width of approx. 5 m. Its uppermost position reaches an elevation of 0.07 m above the actual maximum spring-tidal level (amstl) (Tab. 3.1). At this station samples were only collected for dating analyses, but not for petrographical observation.

Ca Na Beachrock 2 was also found between the intertidal and the supratidal zone. Its uppermost position reached 0.30 m amstl. Additionally, it had a length of about 80 m and a width of 6 m. This beachrock originally had a bed-like form, lying on the sand. Today its form is characterized by polygonal slices from 1 m^2 up to 3 m^2 in size and a thickness of approximately 30 cm (Fig. 3.8a). This fragmentation probably occurred due to a combination of wave action and tidal regime.

Samples from three different altitudes of Ca Na Beachrock 2 were collected. For the petrographical observation of the lowest position, a sample was collected at - 0.54 m amstl. The second sample was collected at - 0.44 m amstl, and the third was collected at the highest position, which was at 0.07 m amstl (Tab. 3.1).

The third beachrock was found in Son Hai town, having a cylindrical form and lying on the beach (Fig. 3.3). Its length was approximately 60 m, with a width of circa 3.50 m. Its uppermost position reached 0.45 m amstl (Tab. 3.1). Moreover, its structure showed a series of bodies of approx. 15-20 m in height, located landward on the beach. This sequence was buried into the beach, where only the top of the beachrock appeared (Fig. 3.8b). The beachrocks is strong recrystalized and was not take into considerations for detailed studies (see p. 45).

From the Son Hai Beachrock, samples were collected for petrographical observations and dating analyses. The samples were taken at a height of - 0.28 m amstl, and two other samples

were collected on different seaward dipping layers of the beachrock at the same altitude of -0.26 m amstl. They were identified as Vn 06050507 on the landward side and as Vn 06050508 on the seaward side.

Ca Na Beachrock 1: approx. 60 m in length and 5 m in width.

Ca Na Beachrock 2: approx. 80 m in length and 6 m in width.

Son Hai Beachrock: approx. 60 m in length and 3.5 m in width.

Fig. 3.3. The three bodies of beachrocks found on SE-Vietnamese coast.

All the explored beachrocks could be identified as seaward-dipping beachrocks. This type of beachrock is formed like a bed inclining towards the sea and extends close to the coast line (Fig. 3.8), (Purse, 1980).

3.5. Results

3.5.1 Petrographical description

Petrographic observation revealed several sedimentary features. With regard to the roundness of the components, with angular, sub-angular and sub-rounded forms and low sphericity was identified. The mean grain-size was variable, with medium sand 0.436(2x) and 0.390 mm being the size of samples from the Ca Na Beachrock 2. The samples from the Son Hai Beachrock revealed fine sand, with a size of 0.234, 0.218 and 0.156 mm. They were poorly-sorted, moderately-sorted and well-sorted respectively, with the last feature being more frequently found. Moreover, the maturity stage was identified. The maturity stage indicates that the matrix-cement consists of grain-supported fabric. Fabric-supported grains were predominantly observed in the samples, where micritic cement occurred. Porosity was more frequently observed in beachrocks with fibrous cement rather than in beachrocks with micritic cement.

All thin sections showed that on average 54.7 % of components are of terrigenous origin. The frequency percentile value for each sedimentary constituent yielded 35.7 % of quartz, (including monocrystalline and polycrystalline grains), feldspar 9.5 %, fragment rocks 4.8 %, glauconite 4.7 % and minor amounts of mica and ironstone. Carbonate bioclasts occurred in smaller quantities of about 38 %. 7 % of the total grains could not be identified.

3.5.2. Cement composition and morphology

Micritic subtranslucent crystals of high-Mg calcite were identified as the early cement in the Ca Na Beachrock 2 (Fig. 3.4a). Micritic high-Mg calcite was found at - 0.54 m amstl, filling completely the voids in intragranular and intergranular spaces. Micritic high-Mg calcite in most cases is formed by rhombic crystals, with the diameter measuring between 4 and 30 µm

(Schroeder, 1973; Moore, 1973; Hattin & Dodd, 1978; Land & Moore, 1980 and Milliman; 1977).

Micritic cement as the early cement of beachrocks, sometimes displays a bimodal-phase texture, reminiscent of peloidal forms (Fig. 3.4b). The peloidal texture was identified at - 0.44 m amstl. The pellets measured from 40 to 100 µm in diameter. Following Macintyre's classification of pellets (1977, 1985), they are 20 - 60 µm in diameter, which suggests the formation of this kind of cement in the beachrocks in SE-Vietnam. This texture of cement was already described for Grand Cayman (Moore, 1973), Hawaii (Meyers, 1987), Belize (Gischler & Lomando 1997) and for Reunion Island (Font & Calvet, 1997).

Isopachous aragonite was also found at - 0.54 m amstl in the Ca Na Beachrock 2, growing onto the particles, with micrite occupying the pores (Fig. 3.4c). More aragonite cement was found at - 0.26 m amstl in the Son Hai Beachrock. Its fabrics were identified as isopachous fringes in distal position (Fig. 3.4d), which are followed by rims covering the grains, characterized by a brown-clear colour (plane-polarized-light). Isopachous aragonite is an indicator of cementation within the marine phreatic environment in the intertidal zone. Many authors identified aragonite isopachous cement in the intertidal zone as e.g. Ginsburg (1953), Moore (1973), Beier (1985), Strasser et al. (1989), Kindler & Bain (1993).

Fig. 3.4e demonstrates aragonite fibres found at the same elevation as the isopachous fringes aragonite, which was at - 0.26 m amstl in the Son Hai Beachrock. The average size of its crystals was 100 µm in length and 4 µm in width. Furthermore, examples of meshes of aragonite needles were also identified, showing the specific characteristic of cement needles grows in every direction (Fig. 3.4e and 3.4k SEM).

Aragonite needle cement was also found in the Ca Na Beachrock 2 at an altitude of - 0.54 m amstl. Its crystals were 90 µm in length and 2.2 µm in width (Fig. 3.4f, and 3.4j SEM). On this cement it was possible to visualise the growth orientation of crystal fibres, being

approximately perpendicular to the surface grains (Fig. 3.4l and m SEM). Figure 3.4f illustrates how micritic high-Mg calcite fills the pores, where aragonite needles do not occur.

Cement aragonite needle were also found at an elevation of 0.07 m amstl in the Ca Na Beachrock 2 (Fig. 3.4g, n SEM). This height represents the maximum influx of the present sea-level stand. Aragonite cement appears, covering terrigenous and biological grains. Moreover, a dark film covers the cement needles (Fig. 3.4h). In recent works it has been identified as an organic deposition (Vieira & De Ros, 2006). According to the same authors, organic deposition occurs, where a stagnant condition allows its development.

Under the microscope a crystal fabric, identified as calcite blade, was observed in Ca Na Beachrock 2 (Fig. 3.4h). The crystal is not elongated and it has a width of about 28 µm. The apex of the crystal has an extremity in the form of a "V". Bladed cement is usually mentioned together with cement characterized by marine environment (Meyers, 1987; Gischler & Lomando, 1997). However, the bladed shape also occurs in the supratidal or mixing zones, where it shows a greater influence by freshwater (Schroeder, 1979; Longman, 1980; Coudray & Montaggioni, 1986; Given & Wilkinson, 1985a; James & Choquette, 1990). Rim cements, covering the sediment, were observed at - 0.28 m amstl (Fig. 3.4i) as well as at - 0.26 m amstl (Fig. 3.4d) in the Son Hai beachrocks.

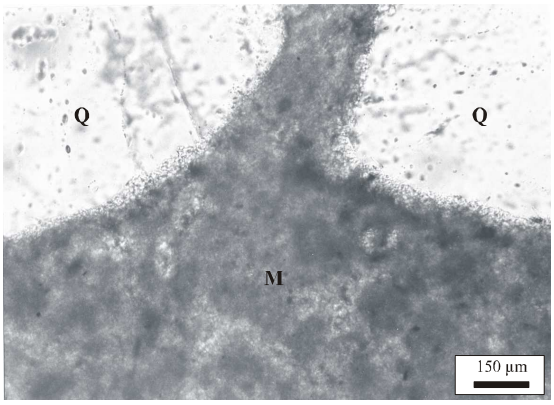
Q
Q
M
150 µm

(a)

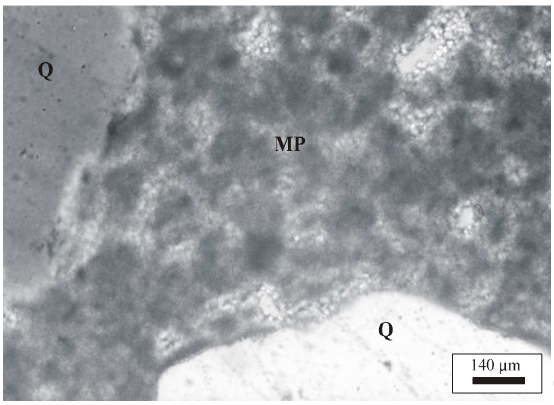
Q
MP
Q
140 µm

(b)

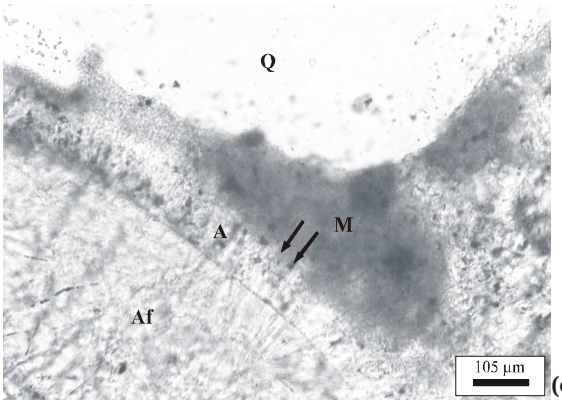
Q
A
M
Af
105 µm

(c)

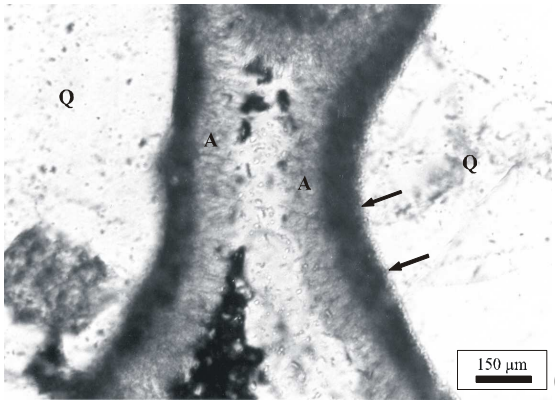
Q
A
A
Q
150 µm

(d)

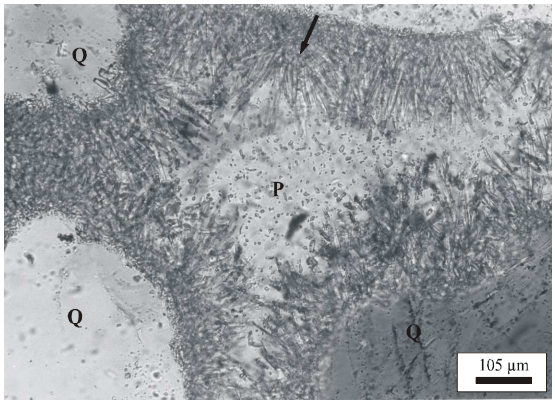
Q
P
Q
Q
105 µm

(e)

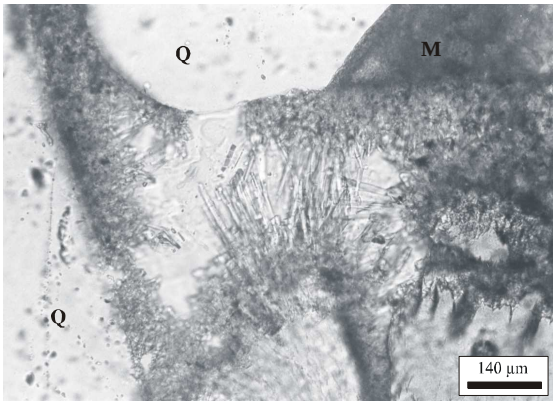
Q
M
Q
140 µm

(f)

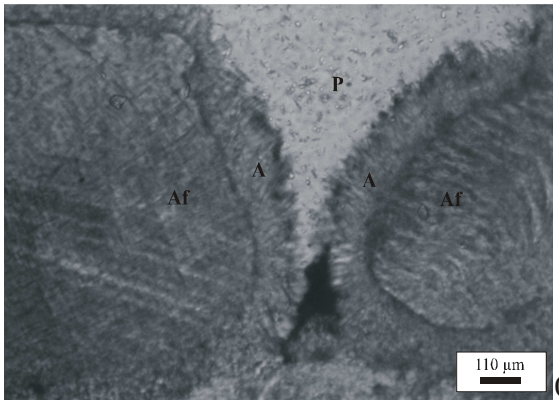
P
A
A
Af
Af
110 µm

(g)

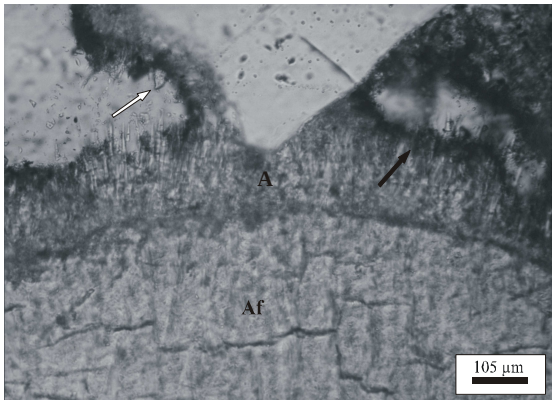
A
Af
105 µm

(h)

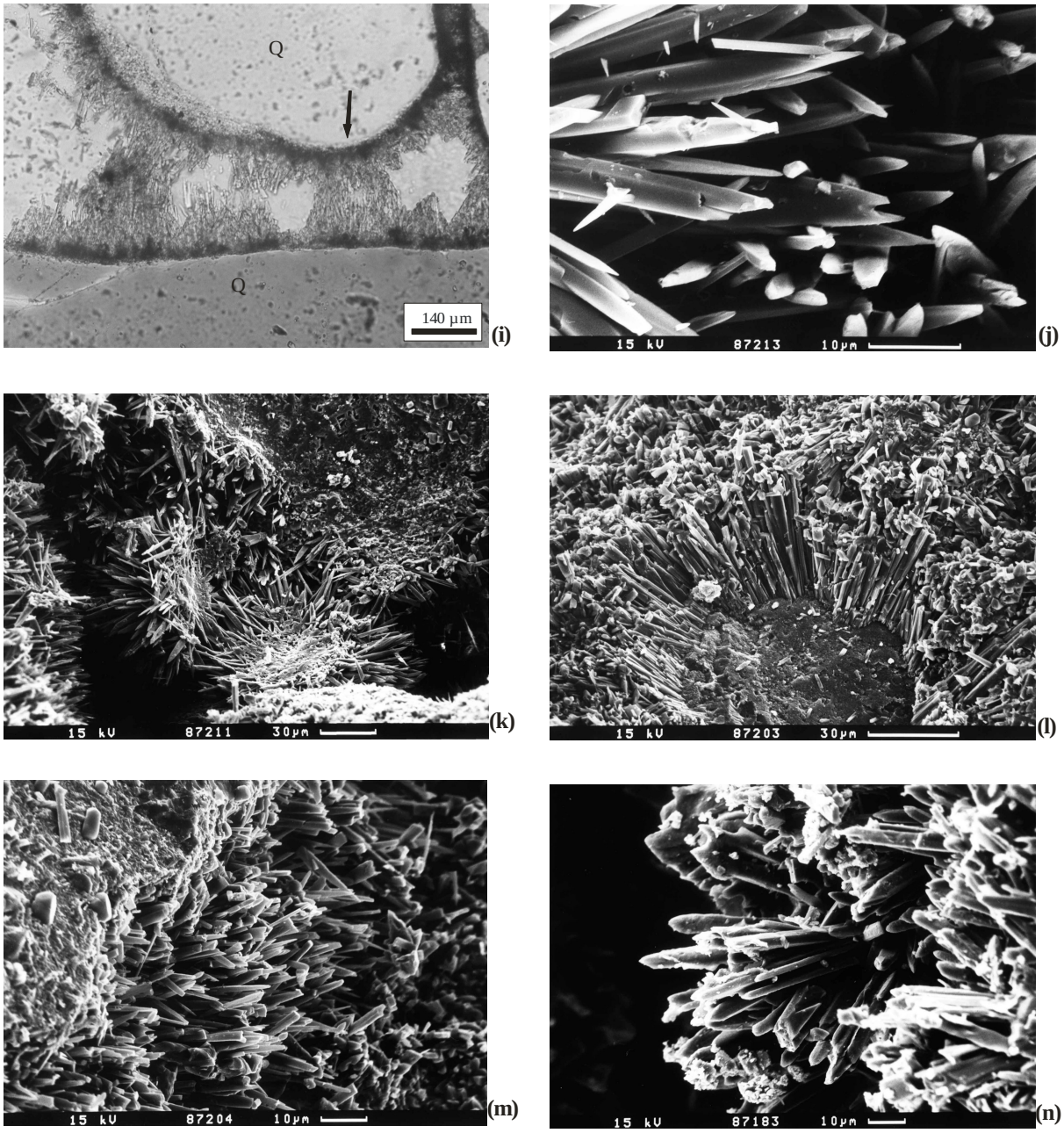

Fig. 3.4. Sequence of cementation events and morphological forms of cement, displayed in plane polarized light. (a) Formation of micritic high-Mg calcite cement represented by “M”. (b) Peloidal feature “MP”. (c) Isopachous aragonite “A” on the bioclastic sediment. The black arrows indicate the boundary between aragonite and micritic cement. (d) The formation of isopachous aragonite fringe “A” in distal positions. The arrows indicate the rim covering the sediment. (e) Fibrous aragonite. Black arrow shows the presence of a mesh of aragonite needles. (f) Big forms of aragonite needles; “M” indicates the presence of micritic cement. (g) Isopachous aragonite of needle “A” covering the algae fragment. (h) Fibrous isopachous aragonite with a black arrow pointing to a dark formation and the white arrow showing the bladed form of cement. (i) to (n) SEM-images: (i) The arrow indicates how rim cement covers the sediment. (j) Showing the form of aragonite needles. (k) Mesh of needle cement. (l) Needles growing onto the sediment. (m) Aragonite needle in Ca Na Beachrock. (n) Shows aragonite needle with bioclastic sediment in supratidal zone.
AF-Algae fragment, Q-Quartz, P-Pore.

3.5.3. Bacterial flora in the beachrock cement

In the Son Hai Beachrock, nannobacteria were identified by Scan Electronic Microscopy (SEM) at the position of - 0.26 m amstl. These organisms were observed on the surface of aragonite needle cement (Fig. 3.5a). In accordance with Folk (1993), Pedone & Folk (1996) and Neumeier (1999), nannobacteria have been described in cements of aragonite and high-Mg calcite. They are characterized by an elliptical biomorphology and are very small in size, normally less than 1 µm.

The endolithic filament algae (Fig. 3.5b) were found growing among the grains. They were also observed at - 0.26 m amstl in the Son Hai Beachrocks. According to Moore (2004, p.102), the filament forms bind the grains together. Chacón et al. (2006) showed the development of algal filaments in limestone within the intertidal zone.

A bacterial film community was identified at - 0.54 m amstl in the Ca Na Beachrock 2 (Fig. 3.5c). The figure demonstrates a phase of the bacterial reproductive cycle, occurring on the micritic cement surface. The structure was identified according to Perry & Staley (1997).

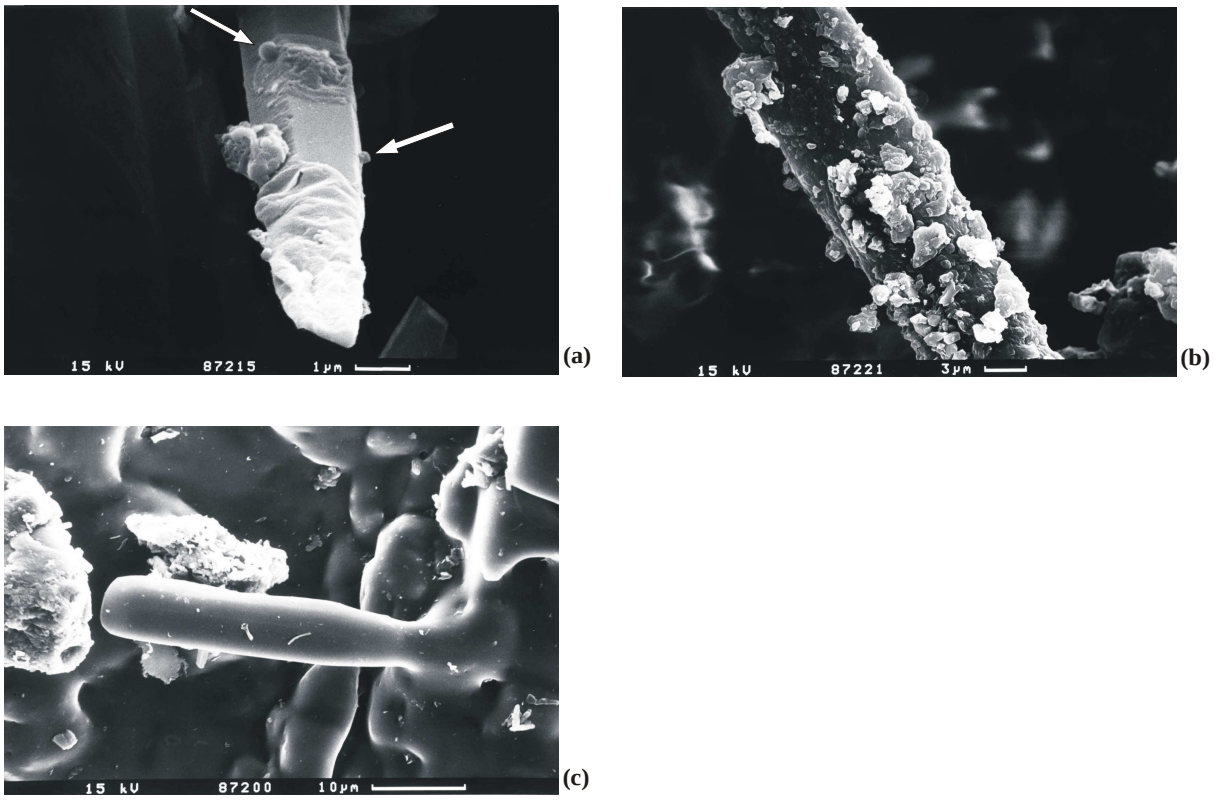

Fig. 3.5. The biological constituents found on the cement in SEM-image. (a) Elliptical nannobacteria growing on an aragonite needle identified as nannobacterias. (b) Endolithic filament of an alga. (c) Bacterial film growing on a cement beachrock with its reproductive structure.

3.5.4. Isotopic concentration of $\delta^{18}O$ and $\delta^{13}C$ in cement

High-Mg calcite and aragonite cements were collected in order to analyze the stable isotopes $\delta^{18}O$ and $\delta^{13}C$. The results are shown in Tab. 3.2; the values are plotted on the cross-plot describing environmental conditions (Fig. 3.6).

The value of $\delta^{18}O_{PDB‰}$ in cement beachrocks averages out at - 1.72 ‰, ranging from - 0.97 to - 2.30 ‰. In the Ca Na Beachrock 2 (- 0.44 m amstl) a value of - 0.97 ‰ $\delta^{18}O_{PDB}$ for micritic cement was found. According to Coudray & Montaggiani (1986), a value of - 0.97 ‰ $\delta^{18}O_{PDB}$ is characteristic of the intertidal zone. Micritic cement in Ca Na Beachrock 2 (- 0.54 m amstl) contains - 1.30 ‰ $\delta^{18}O_{PDB}$ a value also identifying the intertidal zone. Fibrous aragonite, sampled at 0.07 m amstl, has a value of - 2.21 ‰ $\delta^{18}O_{PDB}$.

Identification samples	Cements	Above maximum spring-tide (m)	$\delta^{18}O_{PDB‰}$	$\delta^{13}C_{PDB‰}$	Mean of $MgCO_3$ (mol ‰)	Mean of Sr (ppm)	n (Sr and Mg)
Vn 04050501	Micritic / Peloidal	- 0.44	- 0.97	3.08	6.82	349	36
Vn 04050502	Micritic / Aragonite Isopachous	- 0.54	- 1.30	2.90	5.69	821	52
Vn 11110310	Fibrous aragonite of needle and bladed	0.07	- 2.21	2.96	1.29	4329	120
Vn 06050505	Fibrous isopachous aragonite	- 0.28	- 1.87	3.73	0.09	8032	65
Vn 06050507	Aragonite isopachous fringe and mesh of needle	- 0.26	- 1.69	3.86	0.11	8012	35
Vn 06050508	Aragonite isopachous Fringes	- 0.26	- 2.30	2.46	0.06	11123	82

Table 3.2. Oxygen and carbon isotope values and chemical concentration of $MgCO_3$ mol ‰ and Sr ppm; from different cements precipitated in beachrocks.

Cements in the Son Hai Beachrock from - 0.26 m amstl are formed by fringes of isopachous aragonite. Their cement isotopic concentration ranges between - 1.69 ‰ $\delta^{18}O_{PDB}$ on the landward side of the beachrock and - 2.30 ‰ $\delta^{18}O_{PDB}$ on the seaward side. At the position of - 0.28 m amstl, the crystals formed by fibrous isopachous aragonite have a value of - 1.87 ‰ $\delta^{18}O_{PDB}$.

The values of oxygen isotopes in beachrock cements from SE-Vietnam are lower than those of aragonite cements in Mediterranean beachrocks (- 1.0 ‰), but they are higher in calcite (- 3.5 ‰) (Magaritz 1979). Beier (1985) showed an average of - 0.88 ‰ $\delta^{18}O_{PDB}$ in beachrock cement from San Salvador, which is higher than that in beachrocks from SE-Vietnam. In the Red Sea and the Mediterranean, beachrocks have a mean of 0.5 ‰ $\delta^{18}O_{PDB}$, which is higher than the values applying for the Vietnamese beachrocks (Holai & Rashed, 1991). On the Canary Islands the mean is lower than in SE-Vietnam (- 3.6 ‰) (Calvet et al., 2003). In SW-Madagascar beachrock cement formed by fibrous aragonite was found in the intertidal and

the supratidal zone. This cement displays values of oxygen isotope between - 0.35 and - 0.90 ‰, which are lower values than those derived from the same type of cement in SE-Vietnam.

The results of the investigation of carbon isotope are less homogeneous than those of oxygen isotope. The mean of $\delta^{13}C$ in cement beachrock remained at 3.16 ‰, ranging from 2.46 to 3.86 ‰ $\delta^{13}C_{PDB}$.

In the Ca Na Beachrock 2 the concentration of micritic high-Mg calcite cement, had a value of 3.08 ‰ $\delta^{13}C_{PDB}$ in - 0.44 m amstl. At the lower position of - 0.54 m amstl, 2.90 ‰ $\delta^{13}C_{PDB}$ was measured. At the position of 0.07 m amstl, aragonite cement contains 2.96 ‰ $\delta^{13}C_{PDB}$. The values of carbon isotopes from this beachrock are linked to the intertidal zone.

The cement in the Son Hai Beachrock is formed by isopachous aragonite crystals. The concentration of $\delta^{13}C$ was 3.86 ‰ $\delta^{13}C_{PDB}$ landward and 2.46 ‰ $\delta^{13}C_{PDB}$ seaward, measured at - 0.26 m amstl. Fibrous isopachous aragonite cement demonstrated a value of 3.73 ‰ $\delta^{13}C_{PDB}$ at - 0.28 m amstl, which is the highest result of $\delta^{13}C$ for crystal cement in the SE-Vietnamese beachrocks.

In comparison, Magaritz (1979) presented values of 1.2 and - 1.7 ‰ $\delta^{13}C_{PDB}$ for aragonite and calcite respectively in Mediterranean beachrocks, which are lower values than those found in the Vietnamese beachrocks. Holai & Rashed (1991) also investigated Mediterranean beachrocks and determined a mean of 1.6 ‰ $\delta^{13}C_{PDB}$, which is again a lower value in comparison with the values from Vietnam. In contrast to the Mediterranean beachrocks, cement beachrocks in the Red Sea displayed a mean of 3.3 ‰ $\delta^{13}C_{PDB}$, being similar to the Vietnamese beachrocks. In San Salvador, Beier (1985) identified a mean of 4.91 ‰ $\delta^{13}C_{PDB}$, being much higher than the values presented above (Tab. 3.2). Calvet et al. (2003) identified a mean of 4.5 ‰ $\delta^{13}C_{PDB}$ for the Canary Islands, which is again higher than the values applying for SE-Vietnam. The carbon isotope of aragonite cement beachrocks in SW-Madagascar ranges from 2.84 to 3.88 ‰ $\delta^{13}C_{PDB}$, presenting values similar to those in SE-Vietnam.

The cross-plot of $\delta^{18}O$ vs. $\delta^{13}C$ (Fig. 3.6) was elaborated in order to identify the origin of the isotopic concentration. All the isotopic results plot into the field of green algae. The samples from the Ca Na station as well as the sample Vn 06050508 from the Son Hai station demonstrated isotopic values of Shallow-water Molluscs and Foraminifera field (Milliman, 1977). No value was found for the shallow-water limestone field.

Hudson (1977) and James & Choquette (1983) propose representative values for beachrocks through a field of marine cement. The samples 1, 2, 4 and 6 were found within this field, while samples 3 and 5 are positioned in the overlap of green algae and in the Shallow-water Molluscs and Foraminifera field (Fig. 3.6).

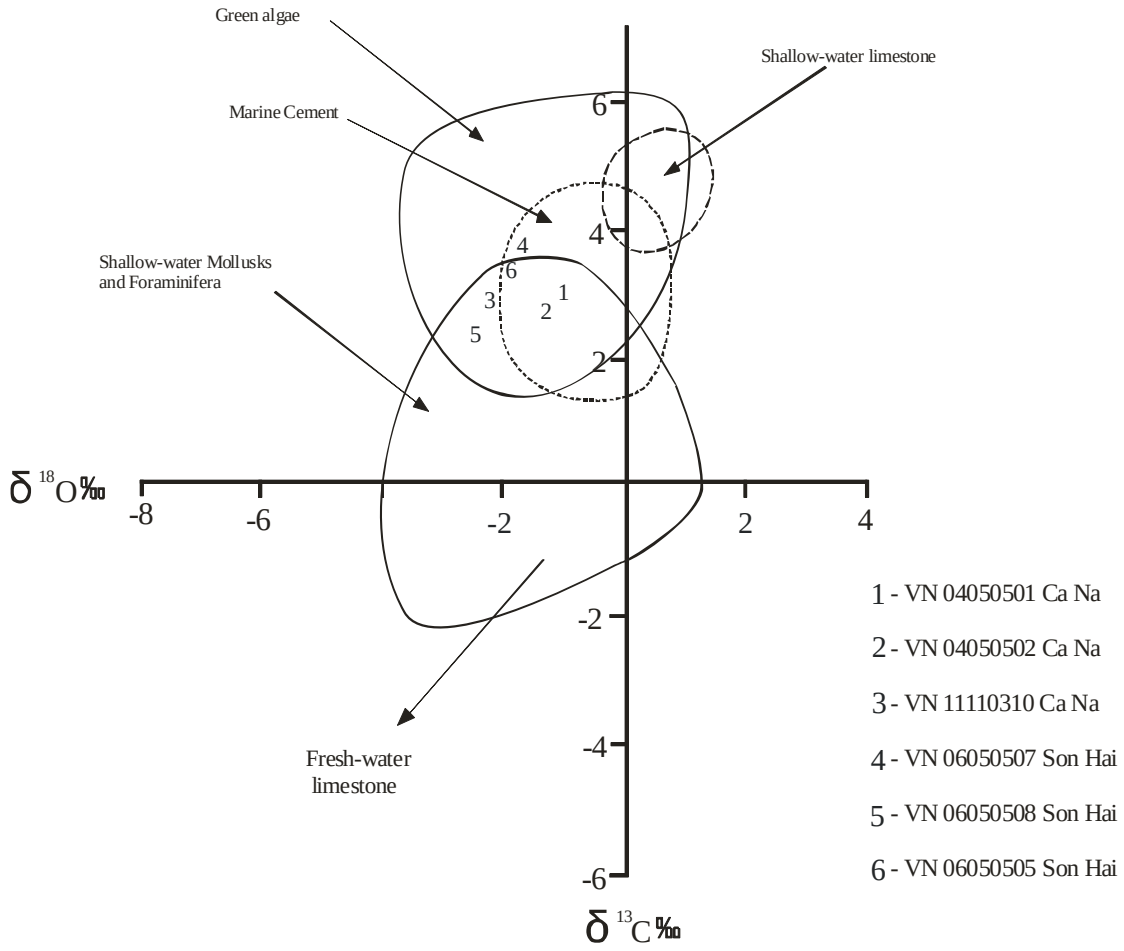

Fig. 3.6. Cross-plot of carbon versus oxygen isotopes from cement of beachrocks introduced by Milliman 1974, modified by James & Choquette, 1983, including the marine cement fields.

3.5.5. Chemistry of cements

The concentration of Sr and $MgCO_3$ was measured to confirm the early cementation process. It can be determined through the identification of micritic high-Mg calcite and aragonite, as well as through their alteration during the change of marine to freshwater environment. All results of Sr and $MgCO_3$ are an average measured at several points of the microprobe thin sections. Tab. 3.2 presents the concentration of $MgCO_3$ and Sr, showing a very good correlation between micritic high-Mg calcite and aragonite cement.

The chemical concentration of micritic cement in the Ca Na Beachrock 2 (- 0.44 m amstl) represented an average of 6.82 mol ‰ of $MgCO_3$, ranging from 5.24 to 7.45 mol ‰. Micritic cements constituted an average of 349 ppm, ranging from 260 to 1600 ppm for Sr. In addition, the Ca Na Beachrock 2 (- 0.54 m amstl) had an average of micritic cement of 5.69 mol ‰ $MgCO_3$, ranging from 3.85 to 6.75 mol ‰. The Sr in aragonite cement measured 821 ppm, ranging from 90 to 3580 ppm.

In contrast to the previous results, different measurement results were obtained in the Ca Na Beachrock 2 (0.07 m amstl) as regards fibrous aragonite cement. The concentration of $MgCO_3$ reached 1.29 mol ‰, ranging from 0.005 to 2.821 mol ‰. The concentration of Sr displayed an average of 4329 ppm, ranging from 1680 to 5920 ppm.

In the Son Hai Beachrock, isopachous aragonite finger cement was detected at - 0.26 m amstl. The measured average of $MgCO_3$ was 0.11 mol ‰, ranging from 0.02 to 0.74 mol ‰. The Sr concentration averaged out at of 8012 ppm, varying from 4720 to12060 ppm. On the other side of the Son Hai Beachrock, a sample was collected at the same height as the first sample. The cement was also formed of isopachous fringes aragonite. The molar concentration of $MgCO_3$ had an average of 0.06 mol ‰, ranging from 0.01 to 0.37 mol ‰. The Sr concentration had an average of 11123 ppm (± 942), ranging from 7680 to 13010 ppm. The third sample from the Son Hai Beachrock (- 0.28 m amstl) consisted of fibrous isopachous aragonite cement. The concentration of $MgCO_3$ reached an average of 0.09 mol

‰, ranging from 0.033 to 0.304 mol ‰. Sr averaged was reached in 8032 ppm, ranging from 6020 to 11690 ppm.

3.5.6. Age of beachrocks

The age of radiocarbon can be identified by carbonate material mineralized by marine organisms (e.g. corals and shells), which died in their original habitat. They are carried away from these places to the intertidal zone by waves and coastal currents. Afterwards this material is cemented into the beachrocks by the lithification process. The ages of the Vietnamese beachrocks were measured by AMS (see chapter 2). The beachrock ranged in age from 6721 to 640 cal yr BP. (Tab. 3.3). Three age periods were detected.

The youngest age interval was found in the Son Hai Beachrock with 1210 to 640 cal yr BP. The youngest radiocarbon age of 640 cal yr BP was deduced from the sample collected at - 0.28 m amstl. The last two samples were dated at a position of - 0.26 m amstl (Tab. 3.3).

The oldest dating was found in the Ca Na Beachrock 1, representing an interval from 6721 to 5869 cal yr BP. The youngest material, found at 0.02 m amstl, dates from 5869 cal yr BP. Older material was found at 0.07 m amstl, dating from 6130 cal yr BP.

The age dated in the Ca Na Beachrock 2 could be connected to the intermediate age of the beachrocks in Vietnam. But it showed a range from 6720 to 3270 cal yr BP, which represents intermediate as well as old dates, similar to those in the Ca Na Beachrock 1.

The position of the samples collected at - 0.54 m amstl was dated to 3270 cal yr BP. At the next position of - 0.44 m amstl, an age of 3600 cal yr BP was determined. The last age identified at the Ca Na Beachrock 2 and considered as intermediate was found at 0.07 m amstl and dated to 3760 cal yr BP. The two older ages in the Ca Na Beachrock 2, dating to 6720 and 6680 cal yr BP respectively, were found at the highest position of 0.30 m amstl.

The results of $\delta^{13}C$ measured by AMS showed very different values, which varied from - 2.88 ‰ to 4.11 ‰. The results from all the dated material, confirmed marine origin.

Beachrock	Identification	Above maximum neap tide (m)	Above maximum spring tide (m)	AMS ^{14}C age (ky B.P.)	Calibrated age 1σ (ky B.P.)	$\delta^{13}C$ (‰)
Ca Na 1	Vn 09110306	0.72	0.02	5420 ± 30	5869	1.78 ± 0.05
	Vn 05050509	0.77	0.07	5650 ± 40	6131	3.13 ± 0.19
Ca Na 2	Vn 04050501	0.26	- 0.44	3615 ± 25	3605	- 1.57 ± 0.08
	Vn 04050502	0.16	- 0.54	3325 ± 30	3272	0.95 ± 0.20
	Vn 04050503	1.00	0.30	6160 ± 35	6680	0.04 ± 0.17
	Vn 04050504	1.00	0.30	6210 ± 35	6721	0.84 ± 0.28
	Vn 11110310	0.77	0.07	3745 ± 30	3760	0.21 ± 0.11
Son Hai	Vn 06050505	0.42	- 0.28	1005 ± 25	642	0.69 ± 0.05
	Vn 06050507	0.44	- 0.26	1095 ± 35	706	4.11 ± 0.30
	Vn 06050508	0.44	- 0.26	1570 ± 35	1210	- 0.18 ± 0.07

Table 3.3. Dating of marine fossils sampled in beachrocks, with their position in relation to the maximum neap-tidal level and maximum spring-tidal level (cf. Table 2.1). The values of carbon isotope were acquired by Accelerator Mass-Spectrometer.

3.6. Interpretation

3.6.1. Sedimentological setting

The observation of the petrographic constituents of the Vietnamese beachrocks confirmed their origin from the transitional zone of sediment (e.g. Badyukov, 1986). The sediment of the beachrocks is composed of a mixture of constituents, originating from many sources.

The beachrocks mainly consist of grains of quartz, rock fragments and feldspar, which represent normal terrigenous sediment that can be found on tropical beaches. Other types of sediment such as glauconite and heavy mineral-like tourmaline were found in small fractions. The presence of glauconite confirms a strong influence of beachrocks on the marine environment. Glauconite is associated with diagenetically formed minerals, being usually formed by the reduction process in pre-existing particles such as carbonate grains, clay minerals and faecal pellets (Odin & Matter, 1981; Odin, 1988). The bioclastic contents were formed by many carbonate-shell-building organisms. These sediments were found in every level of the investigated beachrocks.

In order to confirm the origin of the beachrocks, sedimentary parameters from the Ca Na Beach were investigated and well-sorted sediment of medium and coarse sand (Fig. 3.7) was

identified. The sediments of the medium sand of the Ca Na Beachrock 2 were compared with those of Ca Na Beach, showing similar parameters.

The morphological characteristics of the terrigenous grains revealed a low sphericity and displayed different categories of roundness from angular to sub-rounded forms. These characteristics show that the transport of the sediments from its source to the depositional environment is not far, indicating that the source of sediment is near the deposits. The presence of mountains near the coastal region and the existence of cleaved quartz grains confirm this interpretation. Therefore, the scarcely developed beachrock formation on the southeastern Vietnamese coast can be explained by the restricted sediment supply from the hinterland.

Moreover, little sediment is carried to the shoreline and maybe transported away by the coastal currents. This can be confirmed mainly by the fragmentary landforms on the coast, where mountains frequently occur near the water. Thus, missing accommodation space for sediment deposition of the shoreline could be another reason for the lack of beachrock development.

In addition, the sedimentary contents of beachrocks are very similar to those observed in coastal plain deposits. Coastal plains are marine deposits originating from transgressive events, but they do not occur throughout the Vietnamese coast. These deposits do not exceed 5 m in altitude, with an average between 3 and 2 m above the actual sea level. In general, they are formed by sand, clay, marine fossils and microfauna (Tam, 1991). More information is given in chapter 1. In this connection it is important to mention that coastal plain deposits might have some influence on the formation of beachrocks, mainly on the upper layer of coastal plain deposits, where the sediments are reworked and afterwards carried to the lithification zone.

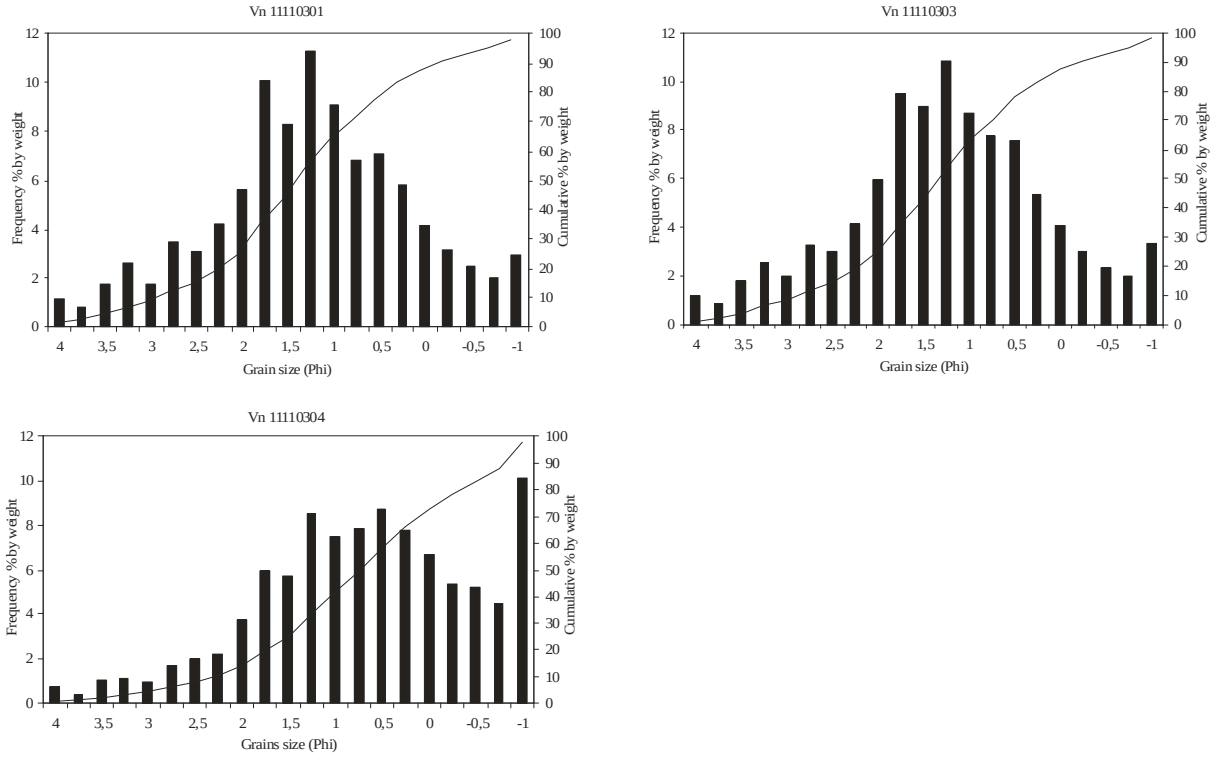

Fig. 3.7. Sediment size distribution from beach sand, where Ca Na Beachrocks were localized. The results identified standards in medium and coarse sand. Similar sedimentary distributions were found in beachrocks.

3.6.2. Cement diagenesis

In the Ca Na Beachrocks 2 diagenetic forms of micritic and peloidal cement (Fig. 3.4 a, b) were identified. The presence of these cements goes along with the early cementation, being also confirmed by the high concentration of $MgCO_3$ between 5.69 and 6.82 mol ‰ (Tab. 3.2). The results of oxygen isotopes revealed normal marine condition for cements of the Ca Na Beachrock 2. The sequence of beachrocks formed by micritic cement (Vn 04050502) displayed a depletion of $\delta^{18}O$, which could indicate a loss of marine condition (Tab. 3.2). However, performance in microprobe analyses demonstrated values of 5.69 mol ‰ of $MgCO_3$, confirming the influence of intertidal zone (Tab. 3.2).

Micritic cement is enriched in carbon isotope with values of 3.08 ‰ and 2.90 ‰. This is considered normal for shallow water in tropic marine regions, where the dissolution of calcium carbonate in water is high (Holail & Rashed, 1991; Beier, 1985).

The precipitation of micritic cement is associated with microbiological influence, as is suggested by some authors (Webb, 1999 and Font & Calvet, 1997). The influence of microorganisms on cement formations of Vietnamese beachrocks will be further elucidated at the end of this chapter.

At 0.07 m amstl in the Ca Na Beachrock 2, the cement is formed by fibrous aragonite and blade fabrics. These types of cement are associated with marine and meteoritic environments respectively (James & Choquette 1984 and 1990). Isotope measurements confirm the natural marine conditions of reduced $\delta^{18}O$ and enrichment by $\delta^{13}C$ isotopes. The chemical concentration also shows a low value of 4329 ppm of Sr in crystal of aragonite. The same applies to $MgCO_3$, with values reaching 1.29 mol ‰ (Tab. 3.2). The chemical concentration indicates that at 0.07 m amstl, the beachrock in Ca Na is still influenced by marine conditions. However, the marine influence changes to meteoritic influence in the supratidal zone. The presence of bladed cement supports this observation (Fig. 3.4h); bladed aragonite is an index of freshwater influence by vadose or meteoritic zones (Longman, 1980; Given & Wilkison, 1985; James & Choquette, 1990; Font & Calvet, 1997).

The predominate cement in the Son Hai Beachrock is aragonite, which consist of diagenetic fabrics such as fringe, needles, mesh of needles and rim (Fig. 3.4 d, e, i). These cements type are representative of marine intertidal zone and the meteoritic influence in supratidal zone (e.g. James & Choquette, 1983, 1990; Gischler & Lomando, 1997; Font & Calvet, 1997). The chemical concentration of Sr and $MgCO_3$ gives important information about the cement formation in the Son Hai Beachrock, which consists only of aragonite crystals in marine conditions. The Microprobe analyses do not indicate the presence of $MgCO_3$, in contrast to Sr, which is significantly higher, suggesting a high concentration of aragonite.

Oxygenic isotopic values, measured by sampling in the intertidal zone (cf. Table 3.2), present depleted values, which normally are > - 1 ‰PDB indicating an influence of the marine environment. As regards the Ca Na Beachrock 2, this is not too apparent, as the results

indicate a shift of the environmental influence in sample Vn 11110310 (Table. 3.3), observed in Sr and $MgCO_3$ results. In the Son Hai Beachrock, depleted values of $\delta^{18}O$ were observed. Possible factors linked with the relatively small oxygen isotope might be: the low temperature of the seawater, the influence of meteoric water and the concentration of salinity. However, the low temperatures of the sea water cannot be appreciated as an explanation because the mean water temperature in southeast Vietnam is 28° C, with the temperature reaching 29.1° C in summer. Additionally, the analysed temperature of coastal water ranges between 29° to 30° C in the region where the beachrocks were found (Rojana-anawat, 2000). Freshwater might be the reason for a small reduction of the isotopic value. But the elevated contents of Sr in aragonite indicate a strong influence of the marine environment. Thus, the influence of the salinity concentration in the water may be added as a more appropriate factor, forcing the concentration of lighter $\delta^{18}O$. Calvet et al, (2003) whose work in La Palma (Canary Islands) showed a low concentration of salinity in the sea water. This suggests that the lower values of $\delta^{18}O$ of precipitated cement in the Vietnam beachrocks is a consequence of the low concentration of salinity in the shallow coastal water of the SCS, showing values between 33.0 and 33.6 ‰ psu.

Taking the isotopic fractions into consideration (Fig. 3.6), the cross-plot does not show any tendency towards freshwater conditions. Furthermore, it is difficult to discern a correlation between the values and the marine cement field. In only two cases of high-Mg calcite, they are exactly within this field. Other values show diverse concentrations of marine dissolved carbonate fields, which are identified to consist of green algae and Shallow-water Molluscs and Foraminifera fields.

To find out more about the influence of microorganisms on the precipitation of carbonate cement, the samples were observed under SEM. These observations revealed the presence of spherical nannobacteria on the surface of aragonite needle (Fig. 3.5 a). But these organisms are not involved in the process of cement precipitation.

The precipitation of micritic cement is also described as a result of the influence of microorganisms, but this cannot be taken into account in this work due to the lack of appropriate dates. The emergence of nannobacteria on aragonite cement can be associated with cement precipitation through the fermentation process. This is suggested by $\delta^{13}C$ isotopic concentrations, which are increased up to 10 ‰ PDB due to residual methane liberated at the end of the fermentation process (Moore, 2004; p: 79). However, this was not found in the aragonite crystals in the Vietnamese beachrocks.

3.6.3. Age of beachrocks

The ages of the beachrocks reveal that there are three generations of beachrocks in SE-Vietnam (Fig. 3.8). The first generation was localized in the Ca Na Beachrocks at the uppermost position of 0.30 m amstl. The age ranges from 6720 to 5869 cal yr BP. The second generation dates from 3600 to 3270 cal yr BP and was found at the position of - 0.44 m and - 0.54 m amstl. The third generation was located in Son Hai town. Evidence for its development was found in the intertidal zone at circa - 0.28 m amstl, with ages from 1210 to 640 cal yr BP (Tab. 3.3).

The ages indicate that the beachrock were found during different sea-level positions. This can be observed at the end of the early-Holocene with ages ranging from 6721 to 5869 cal yr BP, found above the present mean sea level. The same applies to the period after the mid-Holocene, which ages ranging from 3760 to 640 cal yr BP.

As regards the Son Hai Beachrock, its uppermost position was measured at 0.45 m amstl. In order to determine its age, a coral fragment was collected (Vn 06050506). Since it consisted of 32 % of altered aragonite, it was not suitable for age-dating. These two characteristics of the Son Hai Beachrock suggested that it might have originated from the same formation cycle as the Ca Na Beachrock. But this assumption could not be confirmed because of the lack of data from uppermost position of the Son Hai Beachrock.

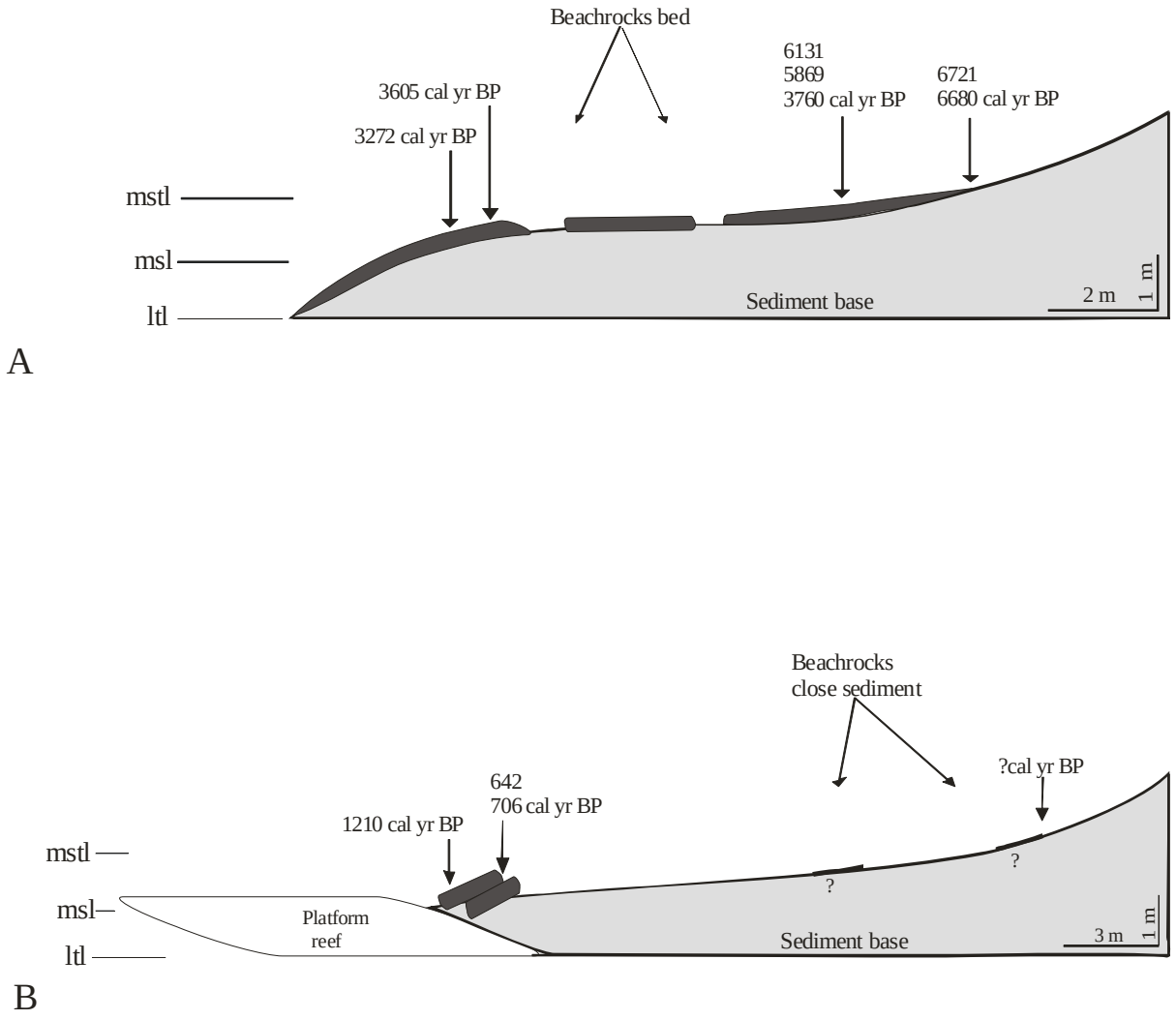

Fig. 3.8. The beachrocks and their respective ages are shown in two places. “A” represents the ages for the Ca Na Beachrock, whereas “B” represents the ages for the Son Hai Beachrock with its uppermost position without dating.

3.6.4. Cement precipitation event

As was presented in the introductory chapter, the beachrock cementation process has been supported by three main theories. We tried to observe events of cementation in the beachrock based on these theories in both places along the Vietnamese coast.

The physicochemical process of CO_2 degassing was not investigated in this work. This type of cement precipitation, as suggested by Hanor (1978), occurs in the vadose zone. Through the observation under SEM, microorganisms were found on the fibrous cement. Nonetheless, geochemical results did not indicate any signal of the microorganisms developing cement. Our own observations of cement precipitation showed that cement is associated with a

physicochemical process, induced by evaporation of water supersaturated in carbonates (Scoffin, 1970).

Cement formation was assumed in the Son Hai Beachrock because of the beachrock's position in the upper half of the intertidal zone and its young age. The principal cement that was found was fibrous aragonite cement, whereas micritic high-Mg calcite, typical cement of the marine phreatic zone, could not be observed.

The intertidal position of the beachrock in Son Hai prevents the tide flux from washing and drying its structure. During the high tide, the body of the beachrock is submerged and its void filled with water supersaturated. During the low tide, the water leaves the beachrock surface wet. Thus, the supersaturated water inside the voids can precipitate the carbonate through the evaporation of the sea water, forming fibrous cement inside the voids. Additionally, the sediment is supplied by a flux of the tidal current.

The tidal regime was observed from Mui Ding gauge with the intention of counting the days of the seawater being above the beachrock. We observed the influence of the tide during one year at three different standards: mean sea level at 0.95 m, neap-tide at 1.4 m and the maximum spring-tide at 2.1 m.

The behaviour of the tidal regime showed that its influence on the beachrock started in 50 % of the days at the base of the beachrocks, indicated by the mean sea level. For the position of 1.4 m, the influence in days was 31 %, not covering the whole body of the beachrock. The beachrock remained fully covered only during 6 % of the time, which was during all days of maximum spring tide.

The intention of the observations of these stages is to present the maximal percentage of days at different levels of the tide. It is evident that the beachrock body is influenced by the water, more than 50 % of the time due to the effect of the waves as well as due to the splash from the washing area.

The interaction between the processes of wetting and drying is necessary in order to trigger the evaporation, which stimulates the precipitation of $CaCO_3$. This can be described as an uninterrupted process of flood tide and ebb tide, connected with a warm air temperature and a direct incidence of sunlight.

The Son Hai Beachrock has some geomorphological characteristics that allow a process of cementation, as are: it lies within the intertidal zone; the exposition of the beachrock facilitates the movement of water as well as the influence of the sunlight; it has a high rate of intergranular porosity and fibrous crystals of aragonite. Some authors, as Scoffin (1970) Pyökäri (1982) Beier (1985) have already observed cement precipitation in beachrocks induced by direct evaporation of sea water.

3.7. Conclusions

1. The early cements identified in the Vietnamese beachrocks are micritic high-Mg calcite and aragonite, which are types of cement normally found in the intertidal zone. The values of Sr and $MgCO_3$ as well as the fractions of isotopes ^{18}O and ^{13}C confirmed their strong marine influence and the precipitation in the intertidal zone.
2. A more complete sequence of cement formation was detected in the Ca Na Beachrock 2. Furthermore, it was ascertained that in the intertidal zone the precipitation of micritic cement and peloidal cement correlates with each other. However, a bladed form was found above the maximum spring tide position, indicating a loss of marine influence, being followed by the increase of meteoritic influence on the supratidal zone. This change was confirmed by a low $MgCO_3$ value and decreasing Sr values.
3. In the Son Hai Beachrock, the cement displayed aragonite isopachous forms originating from the intertidal zone, whereas micritic high-Mg calcite could not be identified. The cementation process seemed to be very young. However, in a sample that was collected in the uppermost part of the Son Hai Beachrock recrystallized coral

fragment was found. Hence, the conclusion can be drawn that the beachrock is older than the ages presented in this study.

4. In both beachrock places, biological-agent originating cement could not be identified. The isotopic carbon values were very low and did not indicate any influence of fermentative processes by microorganisms.
5. The correlation between the ages and the heights of the explored beachrocks suggested the existence of three generations of beachrocks in SE-Vietnam. The first generation was found between 0.02 to 0.45 m above the maximum modern spring-tidal level. In this position, the older ages of Vietnamese beachrocks were found, dating from 6721 to 5869 cal yr BP. The ages found in the modern intertidal zone are related to the last two generations of beachrock formation, with ages from 3631 to 642 cal yr BP.
6. The mechanism of cement precipitation in the Son Hai Beachrock was associated with its geomorphological characteristics, which facilitate the lithification of beachrocks. The seaward position of the beachrock enables a flux of water that fills the voids during the high tide. During the low tide, with the beachrock drying out and being exposed to high air-temperatures, which results in the development of fibrous aragonite inside the voids.
7. From the investigation of geomorphological features, sediment contents, cement chemistry, geochemistry and dating records, it was possible to conclude that the beachrocks on the coast of SE-Vietnam are closely linked to the Holocene coastal evolution. Their evolution is a result of sea-level fluctuations, which occurred during the Holocene.
8. The comparison between Vietnamese beachrock with the Madagascar Beachrock confirmed that distinct places show similar principles of sedimentation, widely influenced by the sandy beaches, where they are found. The lithification process is

driven by physicochemical agents of water coupled with geomorphological characteristics of the beachrock places themselves.

4. Holocene sea-level history of the SE-Vietnamese coast

Abstract:

Beachrocks, beachridge, washover and backshore deposits were investigated at the southeast Vietnamese coast in order to reconstruct Holocene sea level changes. From the above mentioned sea-level indicators, eighteen samples were collected and analysed by AMS radiocarbon dating. In addition, three sea-level index points from salt marsh deposits, sampled in the upper Mekong Delta were included with the reconstruction (Tamura et al., 2007).

The Holocene sea-level history reconstructed by these indicators ranges in age from 8000 cal yr BP to present. Ages between 7960 to 7340 cal yr BP marks the last phase of the early Holocene linear deglaciation. Furthermore, the period between 6721 to 5869 cal yr BP with an average height of 1.32 m above modern mean sea-level (amsl) was identified by beachrocks.

In addition, a slight sea level rise was identified as the likely maximum highstand position in the mid-Holocene (5687 to 5377 cal yr BP). This highstand position is represented by beachridge which serves as an indicator of the uppermost spring-tidal sea level below beachrigde deposition (2.67 m amsl). This corresponds to a maximum mean sea-level of 1.52 m amsl found for the subtraction of the half modern tidal range of 1.15 m.

The mean sea level differs by 0.20 m between beachrocks and beachridge deposits. Thus, the probable scenery for the mid-Holocene sea-level highstand shows beachrocks deposited in the intertidal zone and beachridge deposits in the supratidal zone. Both indicators denote the same period of formation within the interval of 6760 to 5377 cal yr BP representing the highstand period. Sea-level dropped after 5377 to 3600 cal yr BP reaching 0.71 m amsl measured on beachrocks. Since this time to 642 cal yr BP, the age of the youngest beachrock, sea level converged towards modern sea level.

A rate of 3.8 mm yr^{-1} of sea-level rise was calculated from salt marsh indicators and concerns beachrocks with 2.9 m of height within the period of 7730 to 6700 cal yr BP. Then sea-level rise decelerated strongly from 6700 until 5500 cal yr BP reaching finally the highstand. After 5500 cal yr BP sea level started the drop slightly, for the last 4500 years a linear drop of 0.29 mm yr^{-1} was calculated.

The Holocene sea-level fluctuation observed in Southeast Vietnam resulted from glacio-isostatic processes: The sea-level rise up to the mid-Holocene highstand was provoked by the last melting phase of polar ice-sheets at the end of the last glaciation. The process of Equatorial Ocean Siphoning due to isostatic relaxation movements of the lithosphere in high latitudes induced subsequent sea-level lowering in low latitudes since the mid-Holocene.

4.1. Introduction

Sea-level changes during the Holocene have been an important topic of research; mainly because the sea level reached a highstand position in mid-Holocene time on most equatorial coasts (e.g. Long, 2001; Pirazzoli, 1991). Research also focuses on the processes that induced this elevation during the mid-Holocene. The relative sea-level rise in the mid-Holocene between approx. 7000 to 5000 years ago is initially a result of the end of the last glaciation about 21 ky ago (e.g. Peltier, 1994; Hanebuth et al., 2000). When the melting of the ice sheet started, two processes were activated: the glacio-isostatic and the hydro-isostatic movement of the lithosphere.

Glacio-isostatic processes characterize incremental changes in the sea level as a result of the deformation of the earth surface due to the melting of ice sheets. Subsequently a second process starts, which is the so-called hydro-isostatic process being a contribution to the adjustment of the earth to the redistributed-melt-water load into the oceans (Lambeck & Johnston, 1998). These processes are described as the rheology movement of the lithosphere and are provoked by the dwindling of the polar ice-sheet in the northern hemisphere coupled with a reduction of the Antarctic ice sheet. When the last postglacial eustatic sea-level rise had begun, it had a far-reading effect on the mid-Holocene relative sea level (e.g. Nakada & Lambeck, 1989; Peltier, 2002; Fleming et al. 1998) Due to these complex geophysical events associated with constancy and rapid sea-level responses, which were manifested themselves in different places of the equatorial region, there exists a wide interest in Holocene sea-level fluctuations.

Previous studies in the region of Southeast Asia have shown a mid-Holocene sea-level highstand induced by the processes described above. However, the sea-level fluctuation in this region is not well known. Therefore, there is only a small number of research works; and not every works are taken into consideration possible variable influences the sea-level fluctuation, as was explained recently to Woodroffe & Horton (2005).

Most of the research works about sea level on the Vietnamese coast were done on the delta regions and some islands. For the delta of Song Hong - Red River in North Vietnam, Mien & Phon (2000) and Tanabe et al. (2003 and 2006) have presented a Holocene sea-level curve based on marine notch, mangrove clay and shell midden. As far as the South Vietnam region is concerned, Nguyen et al. (2000) and Ta et al. (2002) have attributed to elevated relict deposits, flood plains and beachridge the evolution of the Mekong Delta. Tamura et al. (2007) have investigated the Holocene deposits in intertidal and supratidal zones and have described them as results of deglaciation sea-level rise.

Furthermore, Korotky et al. (1995) collected a great number of samples from islands localized in the vicinity of Vietnam's coast. Based on these dates, An (1996) has proposed a sea-level curve interpolated the different of elevations sea level. Boyd & Lan (2004) have proposed a sea-level curve for North Vietnam (Ha Long Bay) only one index dating sampled from a wave cut notch. Finally, Lam & Boyle (2000) have presented a sea-level history for the Bac Bo Golf derived from Holocene coastal deposits which formed during sea-level rise.

The objective of the present research paper is to elaborate a sea-level curve from the mid-Holocene for the SE-Vietnamese coast. The most important sea-level indicators are beachrocks and beachridge in highstand position. The vertical heights of sea-level indicators were referenced to a known tidal gauge datum measured at Mui Dinh substation, in the vicinity of the sample positions.

4.2. Indicators of sea-level reconstruction

The sea-level reconstruction on the SE-Vietnamese coast was performed with the help of two main indicators: beachrock and beachridge. Beachrock is widely recognised as a former indicator of sea-level stability. It was investigated in many regions like on the Maly-Thai peninsula (Tjia, 1996), in South Africa (Ramsay & Cooper, 2002, Ramsay, 1995) - with beachrocks submerged onto the continental shelf – on the Nansei Islands in southwestern Japan (Omoto, 2001, 2004) and in Northeast of Brazil (Caldas et al., 2006; Vieira & De Ros, 2006).

The structure of beachrock is formed by sand and gravel including fossils and skeleton fragments of coral. Beachrocks developed in the intertidal zone by cement precipitation from carbonate, a process which occurs mainly takes place in tropical and sub-tropical regions under favourable conditions as far as the lithification process is concerned, which implies solubility of carbonates and a high rate of evaporation (Moore, 2004).

However, the difficulty of associating beachrocks with sea-level stability is related to the tidal regime, because the formation of beachrocks is directly linked to the tidal range. Therefore, some authors believe that beachrocks are more reliable sea-level indicators on microtidal coasts (e.g. Hopley, 1986; Guilcher, 1988; Cooper, 1991; Kindley & Bair, 1993; Ramsay, 1995; and Ramsay & Cooper, 2002). Nevertheless, when research works are accomplished on mesotidal coasts, they are realized with regard to the beachrocks` characteristics and involve petrographic description, precise levelling of the vertical position in relation to present sea level, as well as sample from the uppermost level of beachrock. These characteristics are appropriate to take accurate indexes of the sea-level history (Oliveira et al., 1990, Bezerra et al., 1998, and Caldas et al., 2006). Furthermore, the coastal environment influences the diagenetic features identified by chemical and geochemical analyses (Longman, 1980; Vollbrecht & Meischner, 1993; and Font & Calvet, 1997) and evaluated by radiocarbon dating. All these items provide sufficient material to reconstruct former sea levels.

The next important sea-level indicator, which was found, was beachridge deposit. It is a sedimentary deposit developed by storm-surge events. However, beachridge is not considered as a geomorphological indicator of ancient sea-level stability.

A definition of beachridge is presented by Hesp et al. (2005), who analysed the terms of prograded barriers. They describe beachridge as swash aligned deposits. According to them a beachridge develops when swash and storm waves build deposits or ridges. They are primarily formed from sand, pebbles, cobbles or boulders, or from a combination of these sediments, but also from various kinds of other marine or organic sediments (e.g. from shell, coral and wood). They are typically formed at or above the normal spring tide level, being generally persistent. They are marine deposits formed by wave action.

From the present definition it may be assumed that abandoned shoreline beachridge plays an important role as a sea-level indicator if the predicted maximal sea-level amplitude is represented by the beachridge base. The building sequence corresponds to the deposition accomplished not within the sea-level range, but above the maximum sea level.

Beachridge as a former sea-level indicator has been investigated in coastal areas of Thailand (Tjia, 1996; Sinsakul, 1992) and West Java (Rimbaman, 1992). Following these authors, beachridge is described as a linear geomorphic element found on land generally 1 m above the high tide and running parallel to the present shoreline.

Apart from these indicators washover and backshore deposits were also evaluated. Washover deposits have a bar or barrier shape and are accumulated by storm-surge events (e.g. Donnelly et al., 2004). They can be understood as a former sea-level indicator only when they are found above the maximum spring-tidal level, because deposition induced by storm-surge does not correspond to intertidal zone. Backshore is defined as a deposit found in the upper shore zone beyond the advance of the present waves and tides. It is also known as backbeach and beach-backshore.

4.3. Material and methods

The area studied is localized on the SE coast of Vietnam, with an extension of 270 km between the cities of Nha Trang and Phan Thiet (Fig. 4.1). During two field campaigns potential sea-level indicators were sought. After that could be characterize former sea-level fluctuation throughout this coastal area. Through field observation and personal communication with Vietnamese scientists we were able to identify two major deposit types. These structures were found at four stations, with the largest distance between them being 34.8 km along the coastline (Fig. 4.1).

The principal sea-level indicators, which were evaluated, are beachrocks and beachridges in highstand position. Shell and coral fragments were sampled from beachrocks and beachrigdes for ^{14}C radiometric datings. The positions of the samples as well as the beachrocks and beachrigde uppermost positions were accurately surveyed in relation to the water-line using a theodolite. After that, the heights measured were regarding the mean sea level and the maximal spring tide by tidal data from the Mui Dinh tidal-gauge substation.

All carbonate materials were carefully collected in order to obtain the depositional age of the beachrocks. Only fossils that were transported rapidly from their death place to the depositional environment were sampled in the field. This condition is represented by molluscs with well-preserved shell, and particular by bivalves with both valves still connected (Fig. 4.2). In laboratory, the fossils were removed from the consolidated beachrock pieces using a dentist driller; because of the high-duration of beachrock and the importance to take fossils with good preservation for their identification. Afterwards every carbonate sample chosen for dating was analysed by XR-Diffraction in order to observe a possible alteration of the original mineral-phase aragonite to diagenetic calcite. The recrystallized samples were discarded. Thus, a group of 18 fossils mainly consisting of bivalves and corals were dated. The methodology of ^{14}C dating has been set forth in chapter 2.

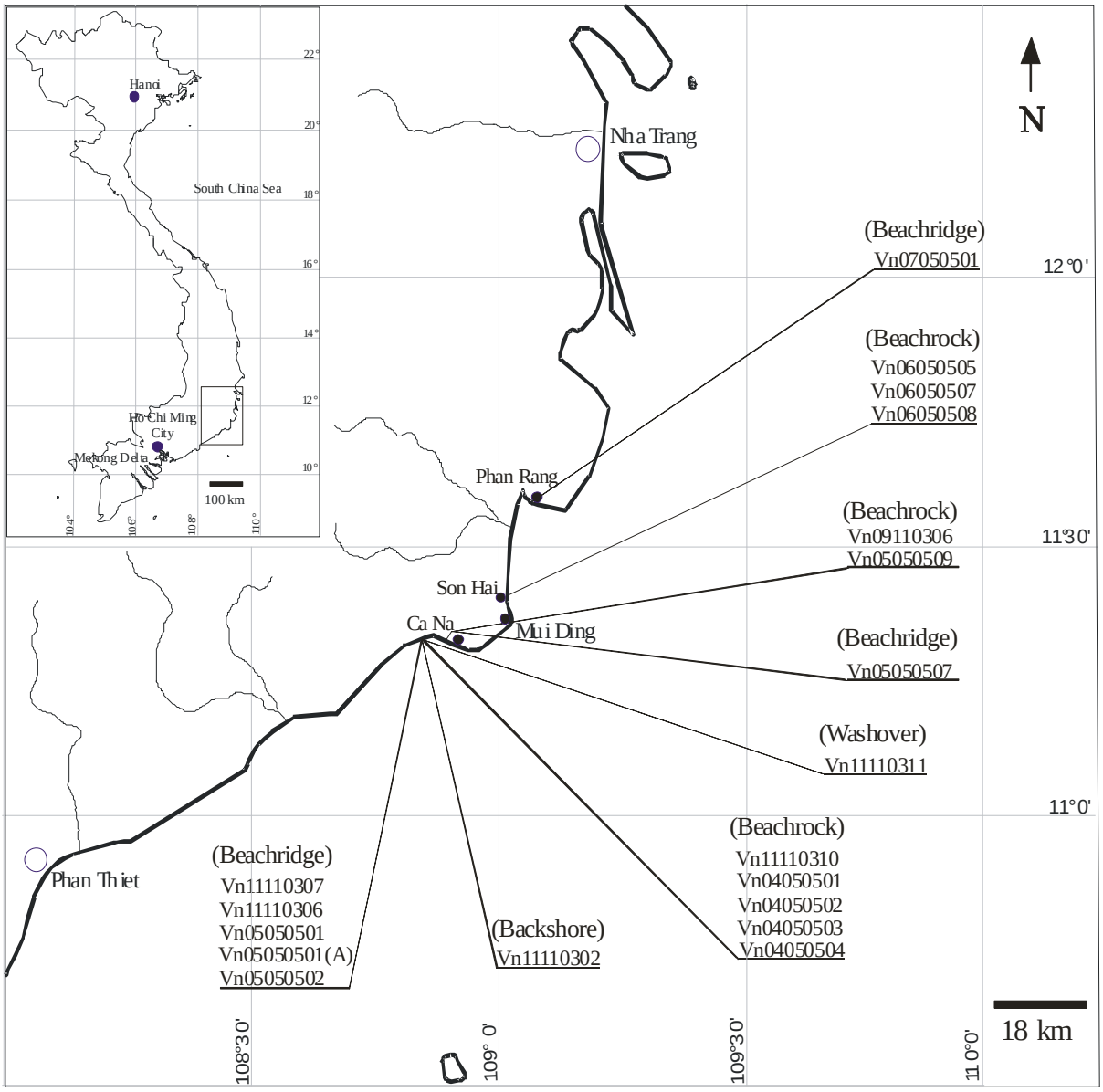

Fig. 4.1. The working area. Positions of each sample as well as their respective sea-level indicators. The tide gauge used from Mui Dinh for correcting the vertical heights is also presented.

Fig. 4.2. Picture "a" shows a bivalve cemented in beachrock. Picture "b" within the circle is also a bivalve collected from beachridge. Both shells still show their valves connected, indicating a short time since they died until deposition.

4.4. Results

4.4.1. Sea-level indicators

The main indicators of ancient sea-level stability found in the investigated coastal area were beachrocks that lie landward in the intertidal zone and beachridge deposit in the supratidal zone (Fig. 4.3). The beachrocks were found at three locations on the SE-Vietnamese coast, deposited in the intertidal zone. Two bodies were detected in the vicinity of Ca Na town and the third was found in the fishing village of Son Hai (Fig. 4.1).

The Ca Na Beachrocks measured between 60 and 80 m in length and their vertical position attained 0.30 m above today's maximum spring tide (amst), corresponding to the uppermost position. The Son Hai Beachrock with 60 m of length has an uppermost position of 0.45 m amst; see table 1 chapter 2.

The investigation of beachrocks showed marine influence with early cement formation consisting of micritic high Mg-calcite and aragonite crystals. Cementation occurred under marine phreatic conditions in an intertidal environment, indicated by high chemical concentration of Mg and Sr. Furthermore, bladed cement formed by freshwater in a mixed marine-freshwater environment. In the more elevated positions of beachrocks it has replaced

the original marine cement. The characterisation of beachrocks in the study area is given in the third chapter.

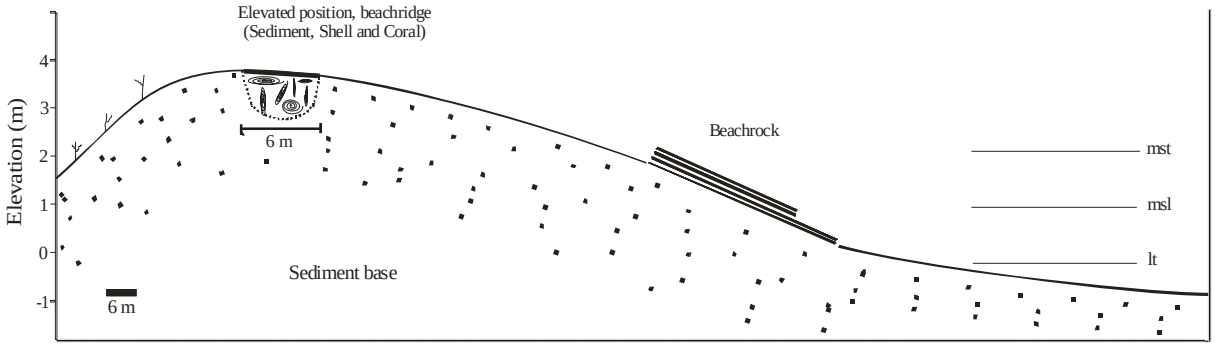

Fig. 4.3. Geological indicators of sea level presented in the relief on the SE-Vietnamese coast. Beachridge is found in elevated position, whereas beachrocks are identified close to the water.

Beachridge was not easy to find in the study area because deposit was buried in the dunefields, which made its detection difficult. It was detected in places where temporary rivers had cut the relief transversally as well as in places where anthropogenic activities such as the building of houses occur. For these reasons, it was not possible to make clear inferences about beachridge geomorphology.

The observation of beachridge deposits revealed two very distinct features. The upper part of beachridge deposit is formed by a massive layer of bioclastic debris. The lower part consists of bioclastic horizons of coral fragments, gastropods and bivalves, which are separated by sandy layers.

The beachridge section is situated on the backshore with a transversal distance of 94 m from the waterline and with 6 m in width. The maximum vertical height or uppermost position from the waterline was measured at 3.57 m amsl, and the maximal height of deposit amounts to 1.80 m. The thickness of the lower stratified and the upper no stratified units reached 0.90 m each (Fig. 4.4).

The beachridge seems to run parallel to the present shoreline above the present sea level, if the geomorphologic base allows it. However, this statement seems to be very difficult to

prove, mainly because fossil beachridge could only be found at three stations. Two samples were found in Ca Na town, and the third in Phan Rang, with very similar characteristics.

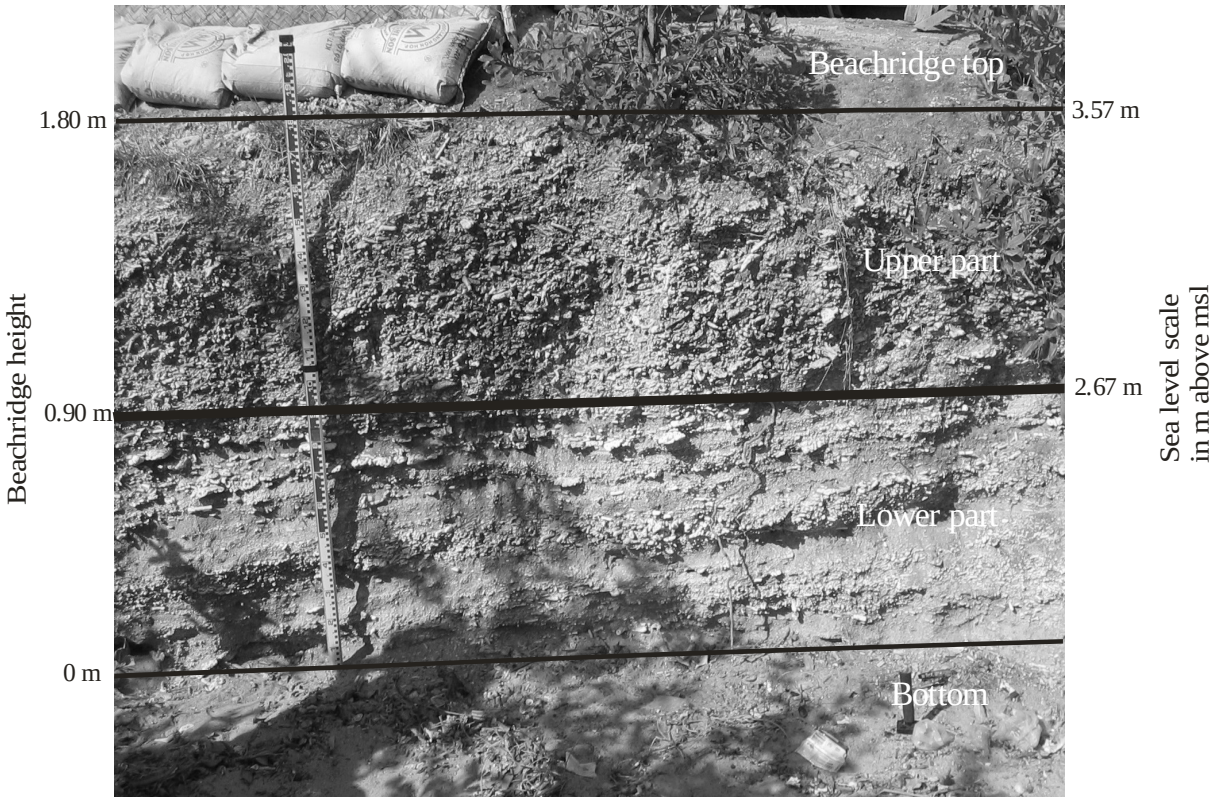

Fig. 4.4. The beachridge deposit found near Ca Na in SE-Vietnam shows two distinct units. The upper part is formed exclusively by bioclastic debris framework between 1.80 to 0.90 m. The lower part is from 0.90 to 0 m formed by alternating layers of bioclastic debris and siliciclastic sand. The sea-level scale is connected to the heights of the beachridge.

4.4.2. Radiocarbon age control

In four investigated sites within the study area 18 sea-level indexes were available. Each position of the locations as well as the identified samples are presented in Figure 4.1. The results of the determination of the ages from AMS radiocarbon dating with their elevations are presented in Table 4.1 as well.

a) Son Hai locality, station 1 (11° 24.946`N /109° 00.622`E)

The Son Hai station is located 97.7 km southward of Nha Trang town. At this locality a series of beachrocks parallel to the beach in front of Son Hai village which serve as sea-level

indicators. The index points of the sea level were measured in three levels of these beachrocks bodies.

The youngest sample was a coral fragment (Vn 6050505) collected at 0.87 m amsl and - 0.28 m above the maximum spring-tidal sea level (amstsl); it ranges in age from 681 to 603 cal yr BP. The following samples are identified as a coral fragment (Vn 06050507) collected at 0.89 m amsl and - 0.26 m amstsl with an age of 752 – 661 cal yr BP. The oldest sea-level index sampled in Son Hai station was also identified as a coral fragment (Vn 06050508). It was found at 0.89 m amsl and - 0.26 m amstsl representing an age of 1256 -1164 cal yr BP.

The ages dated from beachrocks in Son Hai indicated formation in the late-Holocene. However, the uppermost beachrock position was measured at 0.45 m amstsl, showing older beachrock formation than in the intertidal zone. Moreover, a coral sampled in this uppermost position could not be dated due to its high level of recrystallization, which is a signal of an older beachrock formation.

b) Ca Na locality (Ca Na 1), station 2 (11° 19,975`N / 108° 52,320`E)

In the coastal area near Ca Na town, located 112 km southward of Nha Trang, two former sea-level indicators were identified. The first station is Ca Na 1, located 2.03 km southwest of Ca Na town, representing beachrocks and beachridge.

The youngest sea-level index is a coral fragment (Vn 09110306) collected at 1.17 m amsl and 0.02 m amstsl, yielding an age ranging from 5928 to 5810 cal yr BP. The second index is identified as a bivalve shell (Vn 05050509) collected on the coordinate of 11° 19.993`N / 108° 52.429`E at 1.22 m amsl and 0.07 m amstsl. This fragment yields an age ranging from 6208 to 6055 cal yr BP.

The oldest sea-level index is a coral fragment (Vn 05050507) out of a bioclastic layer from top of a small beachridge which is 0.71 m high. This sample was collected at 1.47 m amsl and 0.32 m amstsl ranging in age from 7323 to 7203 cal yr BP. This sample is the oldest sample used for sea-level curve reconstruction on the SE-Vietnamese coast.

c) Ca Na locality (Ca Na 2) Station 3 (11° 19.803`N / 108° 50.550`E)

The third station is located 4.95 km southwest of Ca Na town. At this location, 12 indexes were sampled from beachrock and one from beachridge.

The youngest beachrock sample was a coral fragment (Vn 04050502) representing an age ranging from 3332 to 3213 cal yr BP at an elevation of 0.61 m amsl and - 0.54 m amstsl. The next sample, found in the same site as the first was identified as a coral fragment (Vn 04050501), dating from 3668 to 3542 cal yr BP and being located at 0.71 m amsl and - 0.44 m amstsl. The third index was also as coral fragment (Vn 11110310) collected at 1.22 m amsl and 0.07 m amstsl, yielding a ranging from 3826 to 3694 cal yr BP. The fourth sample, a bivalve (Vn 04050503), was collected at 1.45 m amsl and 0.30 m amstsl and represents an age ranging from 6742 to 6618 cal yr BP. The last sample was identified as coral fragment (Vn 04050504) collected at the same position as the anterior sample, representing a very similar range of age from 6791 to 6652 cal yr BP.

The position of beachrock samples at the Ca Na 2 station represented two different times of deposition. The first in the early mid-Holocene is dated to 6721 and 6680 cal yr BP, reaching 0.30 m amsl; the second within the late-Holocene dated 3760 cal yr BP.

Three sea-level indexes were found in beachridge the elevated position above the maximum spring-tidal level. The following datings were obtained: the youngest sample was a bivalve shell (Vn 05050501) found at 2.97 m amsl and 1.82 m amstsl (see Table 2.1 in chapter 2), yielding an age range from 5436 to 5319 cal yr BP. The second index of the beachridge was sampled in 3.57 m amsl and 2.42 m amstsl (see Table 2.1 in chapter 2) and was identified as a bivalve shell (Vn 11110306) dating from 5605 – 5470 cal yr BP. The third sample was a coral fragment (Vn 11110307) sampled at 2.76 m amsl and 1.52 m amstsl. This sample ranged in age from 5758 to 5616 cal yr BP.

The sequence of radiocarbon dates of beachridge is important for sea-level reconstruction, because they cover a period, which is not found in beachrocks. Therefore, it is a hiatus period

with regard to beachrock, but it formation supplies evidence for beachridge formation for the age interval between 5377 and 5758 cal yr BP (mid-Holocene).

Apart from of these samples from the Ca Na station 3, two different position of the former sea-level indicators were evaluated. The samples Vn 11110311 and Vn 11110302 were collected from two different abandoned shore deposits. They are described as washover and backshore respectively (Tab. 4.1).

The sample Vn 11110311 was identified as a gastropod mollusc and was collected in a washover deposit in the position of 2.18 m amsl and 1.03 m amstsl, yielding an age range from 1806 to 1682 cal yr BP. The second sample from the abandoned Backshore was identified as a bivalve mollusc (Vn 11110302) and was collected from a backshore deposit. The sample from the highest position was collected at 1.62 m amsl and 0.52 m amstsl, ranging in age from 1828 to 1713 cal yr BP.

Laboratory N°	Sea-level Indicators	Material dated	Elevation AMSL (m)	Elevation AMSTSL (m)	AMS ^{14}C age (ky. B.P.)	Arg[a] %	Calibrated age (ky. B.P.)	Calibrated age 1σ range (ky. B.P.)	δ^{13}C ‰
KIA 27723	Son Hai Beachrock Vn 06050505	Coral	0.87	-0.28	1005 ±25	99	642	681-603	0.69 ±0.05
KIA 29581	Son Hai Beachrock Vn 06050507	Coral	0.89	-0.26	1095 +35/-30	*	706	752-661	4.11 ±0.30
KIA 29367	Son Hai Beachrock Vn 06050508	Coral	0.89	-0.26	1570 ±25	98	1210	1256-1164	-0.18 ±0.07
KIA 26152	Ca Na 1 Beachrock Vn 09110306	Coral	1.17	0.02	5420 ±30	94	5869	5928-5810 5800-5794	1.78 ±0.05
KIA 29373	Ca Na 1 Beachrock Vn 05050509	Bivalve	1.22	0.07	5650 ±40	95	6131	6208-6055	3.13 ±0.19
KIA 27725	Ca Na 1 Beachridge Vn 05050507	Coral	1.47	0.32	6655 ±40	99	7263	7323-7203	-2.88 ±0.24
KIA 29372	Ca Na 2 Beachrock Vn 04050502	Coral	0.61	-0.54	3325 ±30	100	3272	3332-3213	0.95 ±0.20
KIA 29369	Ca Na 2 Beachrock Vn 04050501	Coral	0.71	-0.44	3615 ±25	92	3605	3668-3542	0.66 ±0.10
KIA 26151	Ca Na 2 Beachrock Vn 11110310	Coral	1.22	0.07	3745 ±30	100	3760	3826-3694	0.21 ±0.11
KIA 27721	Ca Na 2 Beachrock Vn 04050503	Bivalve	1.45	0.30	6160 ±35	98	6680	6742-6618	0.04 ±0.17
KIA 29368	Ca Na 2 Beachrock Vn 04050504	Coral	1.45	0.30	6210 ±35	99	6721	6791-6652	0.84 ±0.28
KIA 29370	Ca Na 2 Beachridge Vn 05050501	Bivalve	2.97	1.82	4965 ±30	91	5377	5436-5319	0.66 ±0.10
KIA 24556	Ca Na 2 Beachridge Vn 11110306	Bivalve	3.57	2.42	5120 ±55	100	5537	5605-5470	-0.34 ±0.22
KIA 26438	Ca Na 2 Beachridge Vn 11110307	Coral	2.67	1.52	5270 ±40	99	5687	5758-5616	0.88 ±0.16
KIA 34377	Ca Na 2 Beachridge Vn 05050501[a]	Coral	2.35	1.20	5010 ±30	*	5450	5384-5508	-2.34±0.23
KIA 34378	Ca Na 2 Beachridge Vn 05050502	Coral	2.25	1.10	5185 ±35	99	5610	5573-5653	-5.53±0.27
KIA 24557	Ca Na 2 Washover Vn 11110311	Gastropod	2.18	1.03	2075 ±30	99	1744	1806-1682	0.52 ±0.09
KIA 24560	Ca Na 2 Backshore Vn 11110302	Bivalve	1.67	0.52	2110 ±25	99	1770	1828-1713	2.36 ±0.07

Laboratory N°	Sea-level Indicators	Material dated	Elevation AMSL (m)	AMS ^{14}C age (ky. B.P.)	Calibrated age (ky. B.P.)	Calibrated age 1σ range (ky. B.P.)	δ^{13}C ‰	Reference
Beta 192748	Salt marsh deposits	Plant fragment	-0.08	6250 ± 40	7207	7253-7161	-27.9	Tamura et al. 2007
Beta 192749	Salt marsh deposits	Plant fragment	-0.90	6620 ± 40	7498	7521-7475 7566-7534	-27.9	Tamura et al. 2007
Beta 192751	Salt marsh deposits	Plant fragment	-2.08	7130 ± 40	7966	7998-7935	-28.1	Tamura et al. 2007

*Not enough material.
Arg. - Aragonite

Table 4.1. Radiocarbon ages of sea-level indicators. The elevations are referenced to above mean sea level (AMSL) and maximum spring-tidal sea level (AMSTSL) today. The results of ^{14}C dating with respective aragonite concentration were calibrated to 1σ, enclosing 68.3% of probable distribution area. Moreover, three additional samples from the upper Mekong Delta River are presented, representing the positions below the present mean sea level.

4.4.3. Holocene sea-level history

Figure 4.5 presents the reconstruction of the mid-Holocene sea-level curve for the southeast Vietnamese coast. It is a result of a precise AMS-radiocarbon dating and careful sampling of fossils together with elevation measurements on beachrock, beachridge, washover and backshore deposits.

The sea-level curve is based on 18 index points, calculated from the values above the present mean sea level. The three index points below the present mean sea level are AMS ^{14}C dated plant fragments from the upper Mekong Delta. They were sampled from salt marsh deposits from the intertidal to supratidal (Tamura et al. 2007). The vertical error bars in every sea-level index point originate from different tidal ranges, which depend on the local samples and sediment deposits.

The beachrock error bars are calculated from the maximum tidal range for the present time in the Mui Dinh datum. The tidal range in the Mui Dinh sub-station represented a maximal spring-tide corresponding to 2.1 m and a mean sea level at 0.95 m, analysed on the nodal cycle, which corresponds to 18.6 years. Therefore, the beachrock error bars correspond to 1.15 m half-tidal range on each side of the dots. However, concerning the last three younger ages, the errors bars extend 0.6 m upward and 1.7 m downward because the samples were collected very close to the top of beachrock bodies. With regard to salt marsh deposits, the error bars span 2.6 m, which is the tidal range in the Mekong River Delta, according to Tamura et al. (2007). The upward error bar reaches 0.7 m and downward reaches 1.9 m due to the deposits were found from intertidal to supratidal setting.

Beachridge error bars only extend on the downward side of the dots because they represent the uppermost position measured on the sea-level indicator. The interval of the error bar reaches 0.90 m in maximum, which corresponds to the thickness of beachridge deposit. It decreases successively relative to the sampling of the heights (Fig. 4.5 and Fig. 4.6). The sample Vn 05050507 was also sampled in beachrigde; its position has been corrected

downward 0.71 m, it yielded a vertical position of 0.76 m amsl. More information about the development of beachridge during sea-level history will be given below.

The error bar concerning the sea-level index from washover presents only a bar downward of the dot because according to the definition, washover is a deposit caused by storm-surge event.

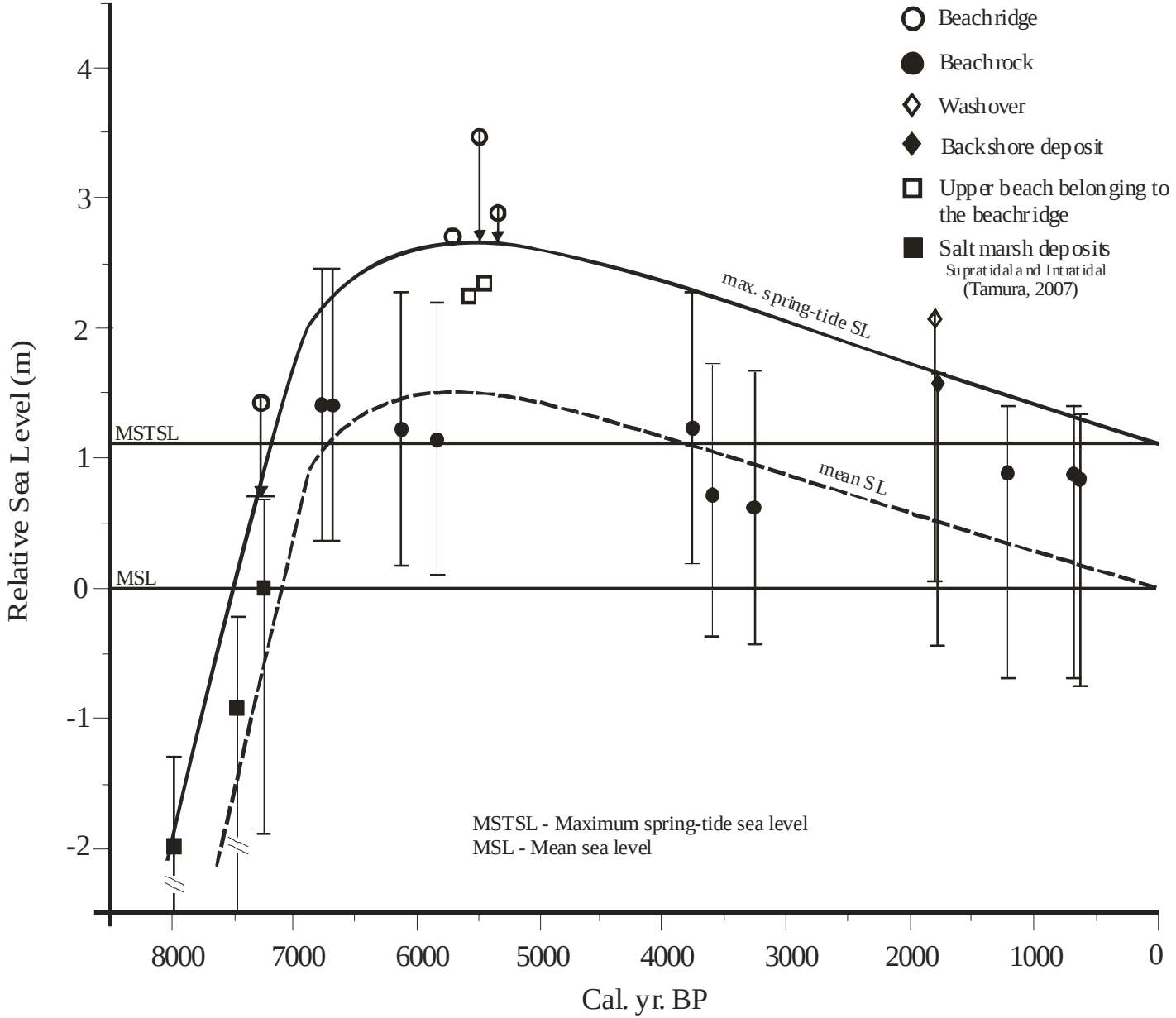

Fig. 4.5. Holocene sea-level curve for the SE-Vietnamese coast, for mean sea level and maximum spring-tide sea level based on different sea-level indicators. Vertical error bars mark intertide in beachrocks and minimum extension of supratidal deposits. Symbols cover 1σ range of calibrated AMS radiocarbon ages.

With regard to backshore deposit, the sea-level index also has a downward error bar because this deposit normally stays within the supratidal zone. Thus, from the position of the dot, the error bar extends 2.1 m downward (Fig. 4.5).

Sea-level index points below the present sea level and older than the mid-Holocene are available from the Mekong region. These index points vary from - 2.08 m to - 0.08 m within the age interval from 7966 to 7207 cal yr BP. These ages were connected with the highstand beachrocks` age and so doing we could reconstruct the last phase of the early Holocene linear sea-level rise, which amounts to 3 m in approx. 1000 years (Fig. 4.5).

The following segment of sea-level indicates the rise of the mean sea level to the highstand beachrocks, which show a range of ages from 6721 cal yr BP sampled at 1.45 m amsl until 5869 cal yr BP of 1.17 m amsl. Within this interval, two more sea-level index points with very similar height positions were measured (Table 4.1). This information about beachrocks confirms a low variation of sea level during a period of 852 yr with an elevation average of 1.32 m amsl from the heights measured, and therefore supports an occurrence of sea-level stability. Furthermore, recent work on the Singapore coast presents sea-level elevation similar to the beachrocks explored in Vietnam (Bird et al., 2007).

In comparison with the sequence of the sea-level trajectory regarding beachrocks, a slightly higher sea level is indicated by beachridge formation. The criterion for highstand positions is that the sea-level rise must be limited by the identification of an uppermost level, defined as the maximal amplitude for spring tide. Based on this criterion, the uppermost spring-tidal sea level for the southeast Vietnamese coast was found at 2.67 m amsl (Fig. 4.6).

The maximal amplitude of the sea level was identified by different features of the investigated beachridge. The base is at 1.77 m amsl, whereas the maximum height amounts to 1.80 m or 3.57 m amsl. The upper unit reaches from 3.57 to 2.67 amsl, consisting exclusively of bioclastic fragments of coral, bivalve, gastropod, deposited as a massive debris-layer (Fig. 4.6a). The lower unit extends from 2.67 m to 1.77 m amsl and is the most basal part with

exposed layers of intermissive bioclastic debris, which are separated by sandy layers. This transverse section of the beachridge was exposed by erosion of a small temporary river (Fig. 4.6a).

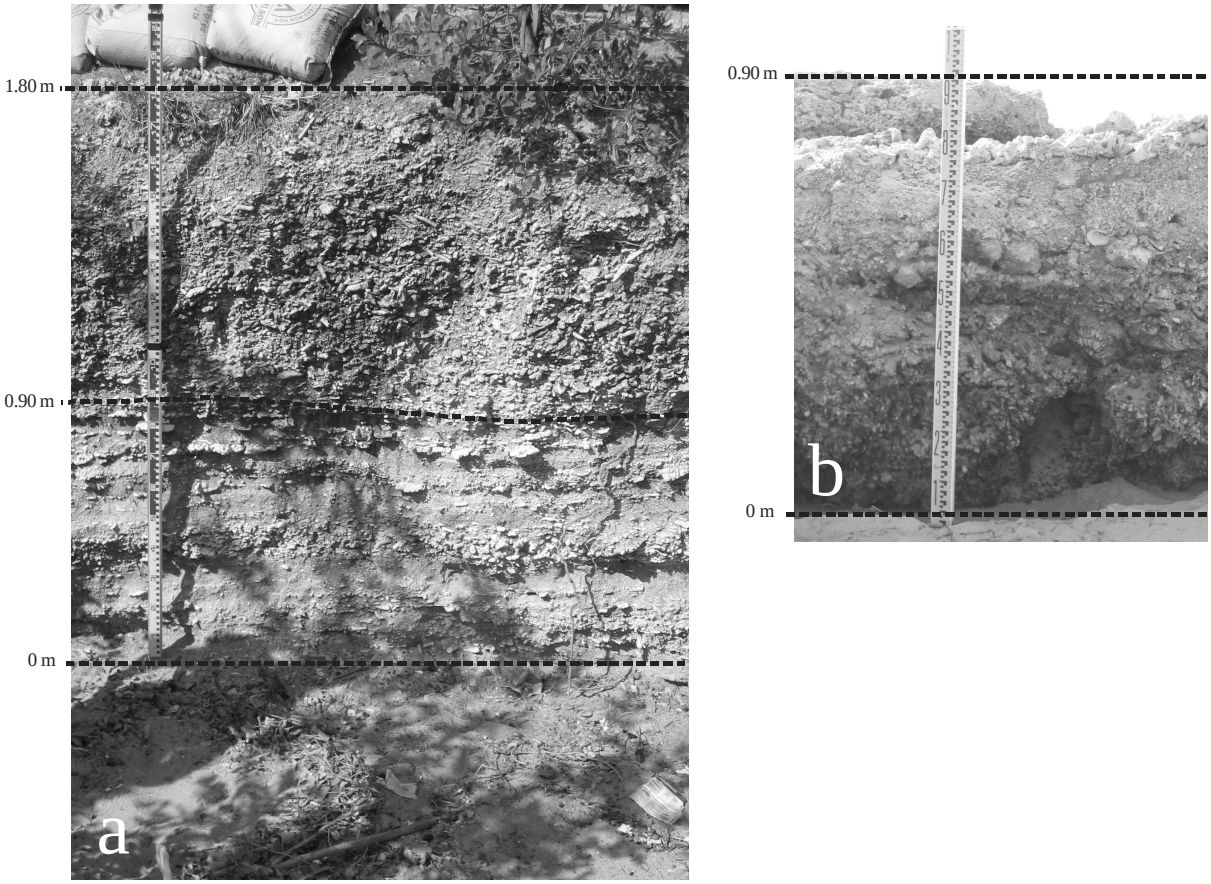

Fig. 4.6. Picture “a” shows the whole stratigraphic features with 1.80 m in height. Only the upper part corresponds to beachridge reached at 0.90 m; the lower part corresponds to sediment bases. Picture “b” shows the height of beachridge in Phan Rang town, which is the same as in Ca Na.

The grain-size of sandy layer in the lower unit ranges between medium sand and coarse sand, (Fig.4.7) representing typical beach sand (see chapter 3). Besides, two coral fragments were dated in 5450 and 5610 cal yr BP (Vn 05050501 A, Vn 05050502) (Table 4.1). They indicated the same period of deposition as the upper unit. From these results can be inferred that this part of the beachridge belongs to the upper beach sediment within the intertidal zone.

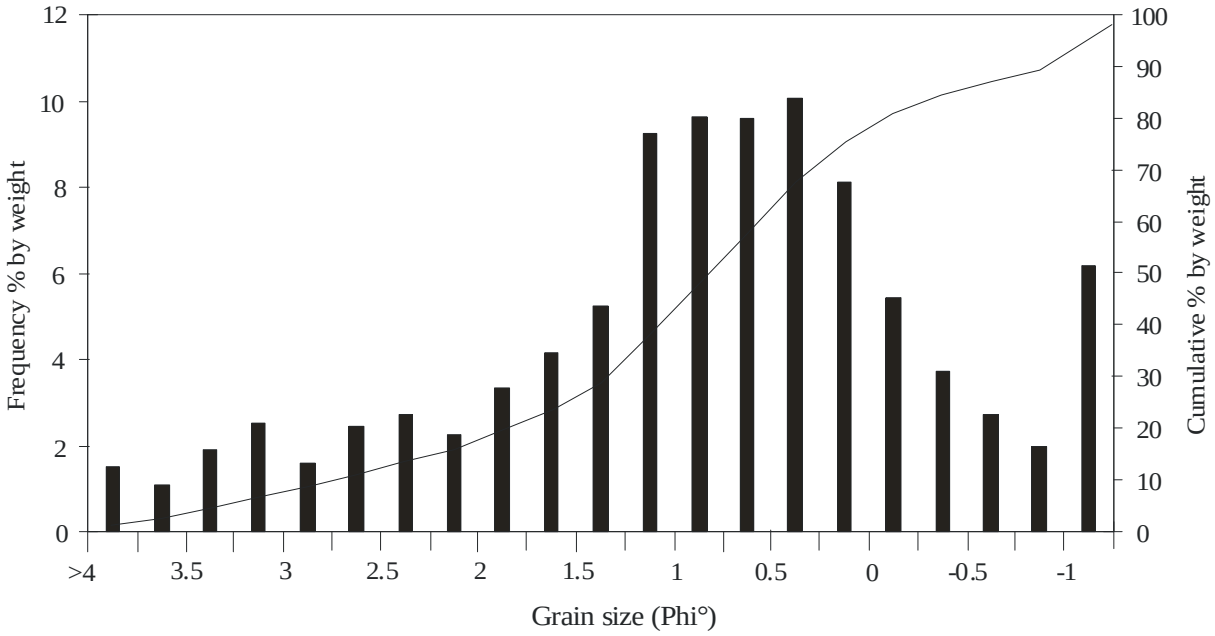

Fig. 4.7. Grain size composition of sediment sample Vn 05050502 from the lower part of beachridge deposit. The result shows a mixture of predominantly coarse and medium sand.

Real beachridge corresponds only to the upper layer. Thus, the highest sea level calculated for the mid-Holocene on the coast of southeast Vietnam is at 2.67 m amsl (Fig. 4.5) and makes the maximum spring-tidal level during the sea-level highstand in the mid-Holocene. It can be assumed that the sea-level reached its uppermost position at the base of the 0.90 m thick beachrigde of Ca Na that is 2.67 m amsl (Fig. 4.6a).

Therefore, all beachridge ages between 5760-5320 cal yr BP were corrected downward to 2.67 m. Hence, the oldest beachridge sample (Vn 11110307) was sampled at 2.67 m amsl making maximal spring-tide sea level. The second sample was taken from the top of the beachridge and was measured at 3.57 amsl (Vn 11110306). Regarding this sample the whole thickness of the beachridge had to be corrected. The third sample was collected at 2.97 m amsl (Vn 05050501), requiring correction up to the uppermost sea level of 0.30 m.

Once the value for the maximal spring tide in the mid-Holocene had been identified, the mean sea level for this time period could be calculated through subtraction of the half tidal range in the region, assuming no tidal variation between the studied time periods. As far as the tidal value of the working area in Mui Dinh is concerned the gauge indicates a mean sea level

corresponding to 0.95 m as the tidal-gauge reference value, with a mean spring tide at 1.92 m, a maximal spring tide at 2.1 m. That means a half-tidal range of 1.15 m.

From this information a maximum sea level of 1.52 m was inferred, based on the subtraction of 1.15 m, from 2.67 m, which indicated the position of the half present spring tide. In this way, the probable mean sea level during highstand position in the mid-Holocene was identified, but not completely established because the identified msl of beachrock highstand was 1.32 m, giving a difference of 0.20 m (Fig. 4.5).

The approach of identifying the mean sea level as well as its uppermost level under the formation of beachridge confirmed the mean sea-level fluctuation in the mid-Holocene passing by 1.52 m between the years 5687 - 5377 cal yr BP, with an interval time of 310 yr. Furthermore, with these values the rate of sea-level rise could be calculated. In fact, the more or less linear rise from salt marsh indicators below the Mekong Delta to beachrocks of Ca Na amounted to 2.9 m within the period between 7730 to 6700 cal yr BP. This presents a rate of sea-level rise of 3.8 mm yr^{-1}. In sequence, the sea-level rise decelerated strongly after 6700 until 5500 cal yr BP. The sea-level highstand was reached in the time 5687 to 5377 cal yr BP.

Figure 4.8 presents a model of the mid-Holocene highstand. The developed sea-level curve is put onto the beachridge features. The top has an elevation of 3.57 m amsl at 1.80 m of deposit. After that the maximum spring-tidal level in mid-Holocene appears at 2.67 m amsl at a height of 0.90 m. Subtracting half-tidal range of 1.15 m the mid-Holocene highstand can be calculated by 1.52 m above modern mean sea level.

Thus, the evidence that the lower part of the beachridge outcrop belongs to an ancient beach is based on the following discoveries: 1) As far as the difference between the upper and the lower units, is concerned the upper unit is built up almost exclusively by bioclastics, whereas the lower unit contains layers of bioclastics and layers of sand; 2) Grain size distribution classifies the lower unit as consisting of medium and coarse sand, corresponding to the

distribution of sand on the tropical beach; 3) The upper and lower Ca Na beachridge units have been deposited during the same period.

However, in Phan Rang town (Fig. 4.1) another beachridge with a 1σ range between 4889 - 4782 cal yr BP (Vn 07050501) was explored. At this outcrop the thickness of the beachridge was also 0.90 m, which corresponds to the thickness of the beachridge found in Ca Na. Moreover, it is composed of very similar sediment types (Fig. 4.6b). In contrast to the beachridge in Ca Na, the present msl measured on the beachridge in Phan Rang was approx. 1 m lower. While observing the region where this outcrop is exposed many anthropogenic effects were detected that had changed the original environment. It is also not sure, that this beachrigde rests in its original position. Therefore, the uppermost position measured against the present mean sea level at Phan Rang station was not taken into consideration.

The start of the sea-level drop was deduced from the sea-level curve indicating a sea-level drop starting around 5377 cal yr BP. The next beachrock index marks a position at 1.22 m amsl, which suggests an age of 3760 cal yr BP (Fig. 4.5). Two indexes, one at 0.61 m and the other at 0.71 m amsl, correspond to ages between 3605 and 3272 cal yr BP respectively.

The following group contains two samples with 1770 and 1744 cal yr BP from washover and backshore deposits respectively, which normally are deposited above the maximum spring tide. Therefore, their positions on the sea-level curve occur just above the ancient maximum spring tide.

The last group of ages is found 534 yrs after the penultimate group of ages. The position at 0.89 m suggests an age of 1210 cal yr BP. The next two samples were also taken at 0.89 and 0.87 m amsl with respective ages of 706 and 642 cal yr BP, showing already a stabilization of the sea level in the late-Holocene period (Fig. 4.5). The reconstructed sea-level curve shows a linear sea-level drop of 0.29 mm yr^{-1} for the last 4500 years, from the 1.30 m to the modern mean sea level.

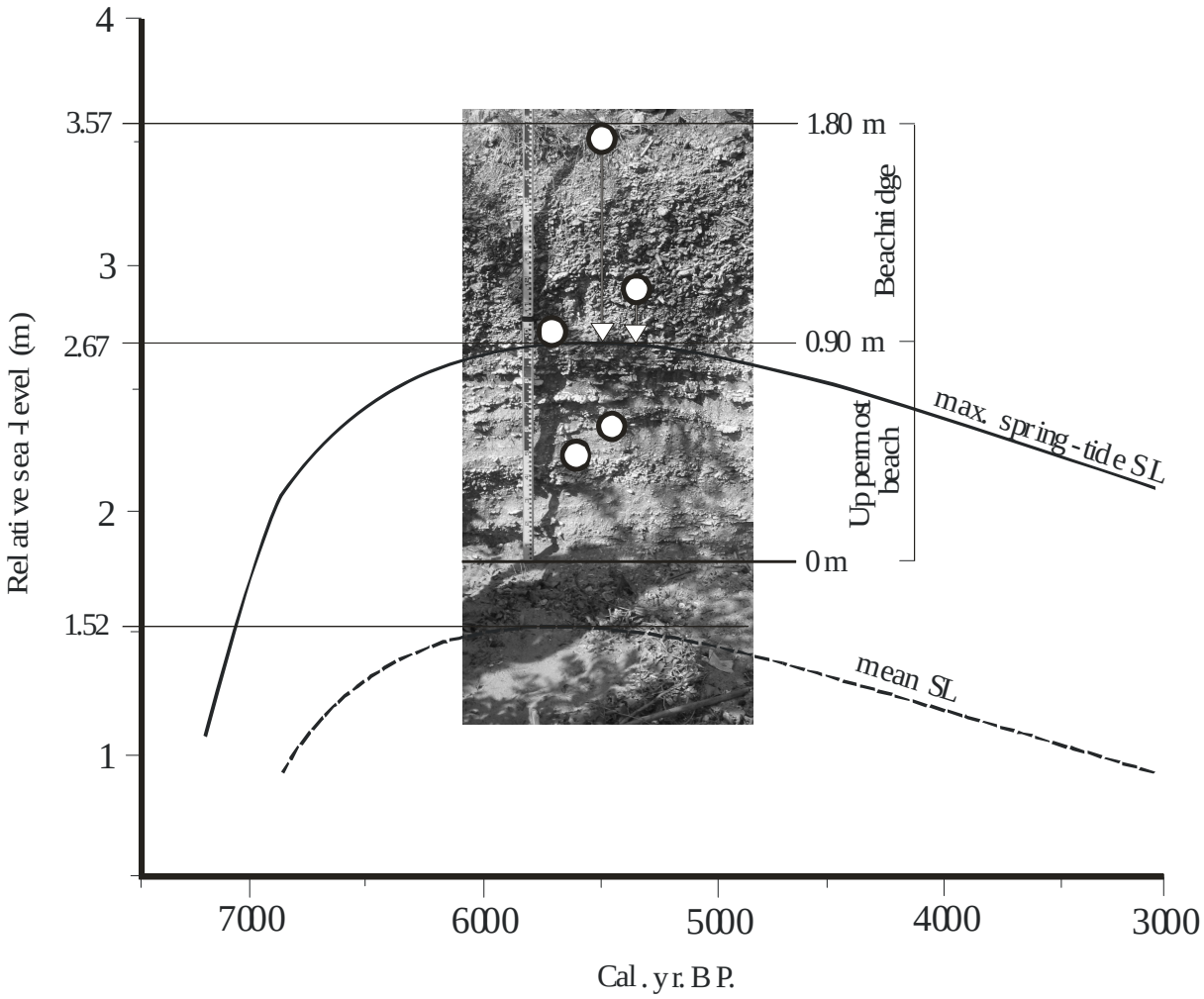

Fig. 4.8. Mid-Holocene sea-level highstand showing the top of the beachridge at 3.57 m, with the maximum spring-tidal sea level of 2.67 m and the mean sea level at 1.52 m put on the deposits` features. From 1.80 to 0.90 m is the beachridge deposit with three carbon datings indicating ages between 5687 to 5377 cal yr BP. The sequence between 0.90 to 0 m is below the beachridge, identified as the upper part of an ancient beach.

4.5. Discussion

With the aid of the beachrock and beachridge sea-level indicators, two different heights at highstand mean sea level could be measured: 1.52 m amsl was measured in beachridge, and the second height of 1.32 m amsl was calculated from the average of the maximum beachrock elevation with both resulting in a difference of 0.20 m. In fact, the small difference between both indicators is insignificant. Therefore, the scenery describes a sea-level highstand from 6721 to 5377 cal yr BP, preserved in beachrocks in the intertidal zone and beachridge in the supratidal zone (Fig. 4.5). The proposed scenery can also be supported by age results that go from older to younger beachrocks, directly overlying beachridge (Table 4.1).

However, this scenery is not ideal, because during beachrock lithification beachridge deposition did not occur, and vice versa. Thus, as no simultaneous formation of the two indicators was observed, and in order to avoid mistake interpretation of heights, it was assumed that the maximum mean sea level in southeast Vietnam for the mid-Holocene is measured in beachridge. Therefore, 1.52 m amsl and 2.67 m amsl denote the maximal spring-tidal sea level.

Once the maximal spring-tidal sea level between 5687 to 5377 cal yr BP had been identified, it was possible to calculate the mean sea level, assuming the same tidal range as observed at present. The mean sea level found in the mid-Holocene at 1.52 m amsl is a result of the subtraction of the present half spring tide at 1.15 m from the uppermost spring-tidal level below beachridge, measured at 2.67 m.

Different sea level positions from the mid-Holocene were corrected to a mean sea-level datum found in the vicinity of the sample stations. In this way, the topography of the working area corresponding to tidal influence is taken into account.

The beachridge above the mid-Holocene spring tide is a deposit originating from storm-surge event. The stratified lower part consists of sand and bioclastics belonging to the gravel beach, which preceded the formation of the beachridge deposit. It consists of medium to coarse sand as the most frequently occurring type of sand, being similar to the grain size of the present beach (Fig. 4.7; see also the beachrock study).

Beachridge deposits in SE-Vietnam as results of storm-surge events are suggested by its geomorphologic characteristics. Beachridge is deposited above spring tide, being composed exclusively of marine bioclastic fragments. Moreover, it seems to be arranged in a more or less continuous line parallel to the coastline. However, in this study beachrigde was only found at three locations, two in Ca Na and one in Phan Rang.

In addition, the bioclastic debris of beachridge indicates that the sediment deposits found on the inner continental shelf during the sea-level highstand were formed by a great number of

fragmentary coral reefs. This sedimentary characteristic might reveal some adverse climatic conditions that induced the death of these organisms during this time.

The rate of sea-level rise identified for the period from 7730 to 6700 cal yr BP amounts to 3.8 mm yr^{-1} was identified. Tanabe et al. (2003) elaborated in their Holocene sea-level history of the Red River Delta a rate of 6 mm yr^{-1}. Nonetheless, this rate is a result measured during the faster period of the Holocene sea-level rise between 9000 - 6000 cal yrs BP. Furthermore, Bird et al. (2007) found in Singapore a rate of sea-level rise of 3.3 mm y^{-1} from 7460 to 6530 cal yr BP.

Strong deceleration in sea-level rise was identified between the beachrock and the beachridge sea-level indicators within the period from 6700 to 5500 cal yr BP. Maybe this strong reduced rate of sea-level rise is the eustatic signal linked with a minor release of meltwater into the oceans from Arctic and Antarctic ice sheets (Fleming et al. 1998) due to the end of deglaciation, which was reached around 5 kyr. BP (Mitrovica & Milne, 2002).

Sea-level rise in SE-Vietnam seems not to have been influenced by local tectonic events (An, 1996). The tectonic activity in the region resulted in a last compression associated with the latest Pleistocene and continuing up to the Holocene in the regions of Phouc Dinh and Vinh Hai, northward of Nha Trang (Choi et al., 2005).

After the mid-Holocene sea-level highstand followed a slight drop between 5377 and 4500 cal yr BP. From 4500 cal yr BP to now the sea level fell more or less linearly to the present level. Secondary oscillations could not be observed since the differences of the mean sea level between the index points are restricted to the present intertidal fluctuation.

In comparison to other sea level studies from Vietnam, the Holocene sea-level history elaborated for SE-Vietnam has revealed significant differences to other regions of Vietnam. A maximal transgression between 6000 and 5000 yr BP for the southern region of the Mekong River Delta is evidenced by a coastal cliff (Nguyen et al. 2000, Ta et al. 2002) at approximately 4.5 m above the present mean sea level.

As regards the Red River - Song Hong Delta, Tanabe et al. (2003, 2006) elaborated a Holocene sea-level curve with ages derived from indicators such as marine notches, mangrove clay and shell midden and with additional dates from other authors. This sea-level curve has a mid-Holocene highstand at 2-3 m above the present sea level between 6000-4000 cal yr BP. The shape of this sea-level curve is similar to the spring-tidal curve for the SE-Vietnam coast established here (Fig. 4.9).

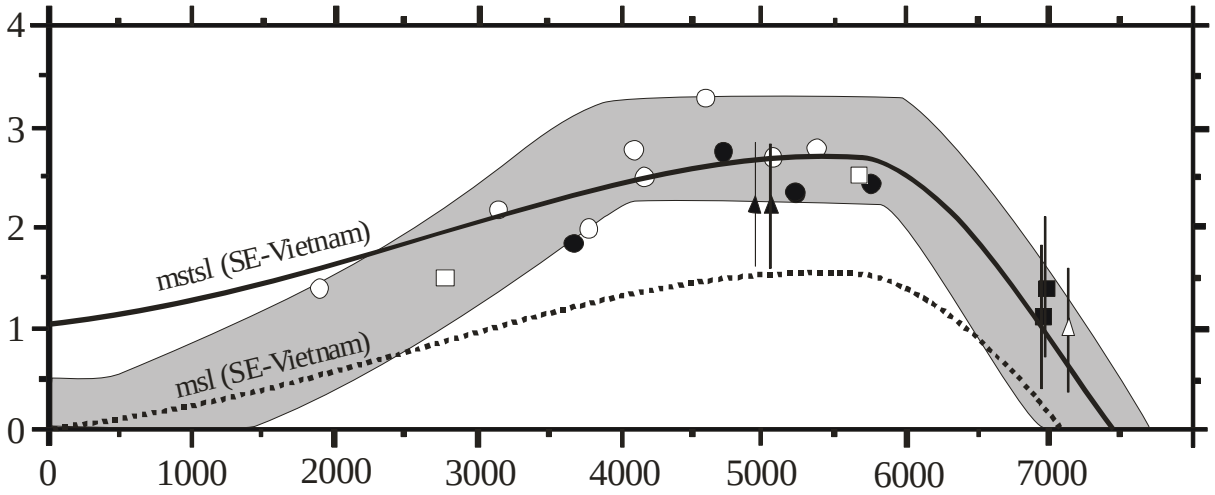

Fig. 4.9. The sea-level curve for the Red River - Song Hong Delta - (Tanabe et al., 2006) in North Vietnam compared with the SE-Vietnamese sea-level curve. The dashed line represents the mean sea level, the solid line the maximum spring-tidal sea level; similarly of the maximum spring-tidal on the sea level curve in southeast Vietnamese coast and the Red river sea-level envelope.

Boyd & Lam (2004) have proposed a sea-level curve using oyster datings from wave-cut notches found in Ha Long Bay. This curve indicates a sea-level highstand occurring in a similar age-interval to that presented in this study. However, the highstand is much higher. Maybe this occurred because the height was referenced by the Vietnamese national datum, whereas for the southeast sea-level curve a local mean sea level datum was used.

Furthermore, the above mentioned sea-level studies deal with islands in the vicinity of the Vietnamese coast. Korotky et al. (1995) presented datings sampled at scattered points around the islands. The mid-Holocene highstand is situated 4-5 m above the present sea level 5000 yrs BP. However, this work seems to be very complex, as it presents many index datings in several geomorphological deposits. Amongst others, beachrocks and the occurrence of a

marine terrace in high position are described. No information, though, about the sediment constituents of the marine terrace is given.

In order to reconstruct a Holocene sea-level curve, An (1996) used Korotky`s dates and interpolated them. However, this does not seem to be appropriate to reconstruct a sea-level curve, because it resulted in a sea-level curve with several highstand and lowstand positions.

In addition to the regional context, a comparison of the Holocene sea-level history in SE-Vietnam with other coastal regions of SE and E Asia had been done. These regions present records for highstand positions that agree with the Vietnamese sea-level highstand. This is mainly true for places where no tectonic processes occurred that could overprint the eustatic sea-level rise. In this case, the sea level is induced by a mantle rheology signal as a response to a glacio-isostatic process along with a hydro-isostatic process that will be discussed below.

A series of works were published about the coast of China northward of Vietnam, dealing with the reconstruction of the Holocene sea-level history. In many places the results did not show the mid-Holocene highstand (Zong, 2004; Chen & Stanley, 1998). The authors confirmed a rise of sea level above the present position with regard to the eustatic signal. However, Zong (2004) found out that the tectonic processes exceeded the eustatic signal on the East Chinese coast. Regarding the Hong Kong coast, Davis et al. (2000) described the highstand sea level attaining 1.7 m above the high-tidal level, dated from shell relict at 5140 cal yr BP; but this elevation was corrected too low after a re-examination by Yin & Hung (2002).

Opposite of the Vietnamese coast, the Philippine islands were investigated by Berdin et al. (2004). He found many places with Holocene sea level indicators on Palawan, Samar and Ilocos. The results suggest that sea-level elevations were caused by tectonic movements during the mid-Holocene period. However, Maeda et al. (2004) found a highstand 0.3 and 0.6 m amsl in Panglao and southwest Bohol, which is lower than in Vietnam. In contrast to

Berdin, Maeda suggests that the highstand is induced by an eustatic sea-level rise because the island is tectonically stable.

As regards the southward direction, scientific works have shown a higher mid-Holocene highstand. In beachridge on the Malay-Thai peninsula, Tjia (1996) showed a maximum sea level at 5 m above the modern sea level around 5 kyr BP. Horton et al. (2005) observed a mid-Holocene highstand sea-level at 3 and 4 m from 4850 to 4450 cal yr BP in a sedimentary sequence of assemblages dominated by pollen of mangroves and freshwater swamps from the Malay-Thai peninsula.

In the coastal region of the Thailand Gulf, Sinsakul (1992) identified a maximum sea-level highstand in beachridge deposits occurring at approx. 6 kys above 4 m of the present msl. However, Scoffin & Tisser (1998) described a sea-level highstand occurring at 6000 yrs for Phuket in the Andaman Sea in southwest Thailand showing an elevation of 1 m amsl from the flat coral reef.

As far as Singapore is concerned, Hesp et al. (1998) have presented a tentative sea-level curve from a fluvial and estuarine stream, reaching the maximum sea level around 6500 to 7000 yrs BP at approx. 3 m amsl. However, Bird et al. (2007) identified a sea-level highstand at approx. 7000 cal yr BP, elevated 1.5 m above msl in Singapore. This elevation is similar to the highstand sea level found in SE-Vietnam. In Java, Rimbaman (1992) measured a maximum msl of 3.5 m above the modern msl at 6 kyr BP in beachridge.

Most authors date the mid-Holocene highstand between 7000 and 5000 yrs, what is similar to the new data from SE-Vietnam. But some studies assume a higher elevation of sea level. The difference might be caused by the procedure used for identifying the uppermost sea level in the case of beachridge, which means that the above mentioned authors positioned the uppermost sea level on top of it. Hence, the sea-level highstand brought about elevations, which are some metres higher than those found in SE-Vietnam, where the thickness of beachridge was not taken into consideration because it was deposited in the supratidal zone.

In connection with the records presented before, the distribution of the mid-Holocene sea-level highstand is confirmed for the equatorial west Pacific coast. The mid-Holocene sea-level highstand was observed in every equatorial low-latitude setting. It is attributed to the last melting phase of ice-sheets, resulting in the postglacial sea-level rise. The succeeding sea level can be explained by glacio-isostatic effects adjusted for the rheological movements of the mantle and meltwater loading onto it.

The glacio-isostatic theory says that the elevated sea level was developed because of the migration of the mantle away from the central equatorial ocean basin interior towards the regions that had undergone maximum glaciations before. During the glacial period, the weight of the ice sheet caused a deformation of the crust, forcing the sublithospheric mantle to flow toward the equator, creating lithospheric forebulges adjacent to the ice sheet margins, and causing the development of a gravitational anomaly in the low latitudes. With the deglaciation, continents rebounded viscoelastically, causing the negative gravity anomaly to decay and forebulges to collapse. Additional oceanic space was created by this process in higher latitudes and water masses of the tropical ocean migrated towards the former forebulge regions. The sequence of these events is called “Equatorial Ocean Siphoning” and is based on the numerical models ICE-3G (Mitrovica & Peltier 1991) and ICE 4G (Peltier 1994, 1996).

The new sea-level curve reconstructed for SE-Vietnam supports this geophysical model However, the differences in timing and magnitude of highstands are presented as regards the places studied above, which had no tectonic influence, being a result of the differences in mantle rheology or in hydro-isostatic effect (Woodroffe, 1985, 1993; Woodroffe & Horton, 2005 and Compton, 2006). This means that the highstand might have started earlier in lower latitudes rather than in places of higher latitudes, as is described by Nakada (1986) and Nakada and Lambeck (1989).

Grossman et al. (1998) detected a mid-Holocene sea-level highstand throughout of the Central Pacific. Their approach was to use the highstand position of the sea level on several islands in

the Central Pacific with the amplitude plotted in relation to the latitudes. The result was a parabola crossing the equator with a higher sea-level highstand at the equator than in high latitudes, which is an effect of the forebulge oscillation during the glacial-isostatic adjustment. This parabola is considered by the authors as the best form to represent paleo-sea-level analyses. It was tried to establish a correlation between the Central Pacific data and the mean sea-level amplitude of 1.52 m measured in SE-Vietnam between 11° and 12° N. The plot is presented in figure 4.10. It can be noted that the sea-level highstand stays 50 cm below the descent of the parabola.

Finally, Caldas et al. (2006) elaborated a sea-level curve from beachrocks in a study recently accomplished, which deals with the coast of Rio Grande do Norte in northeast Brazil at approx. 5° 10` S // 36° 10` W. Their results are almost identical to the ones presented in this work. The mid-Holocene mean sea level in northeast Brazil was at 1.30 m above the modern sea level, which is 0.22 m lowers than in SE-Vietnam. The highstand at 5900 cal yr BP in northeast Brazil occurred 300 years earlier than in SE-Vietnam.

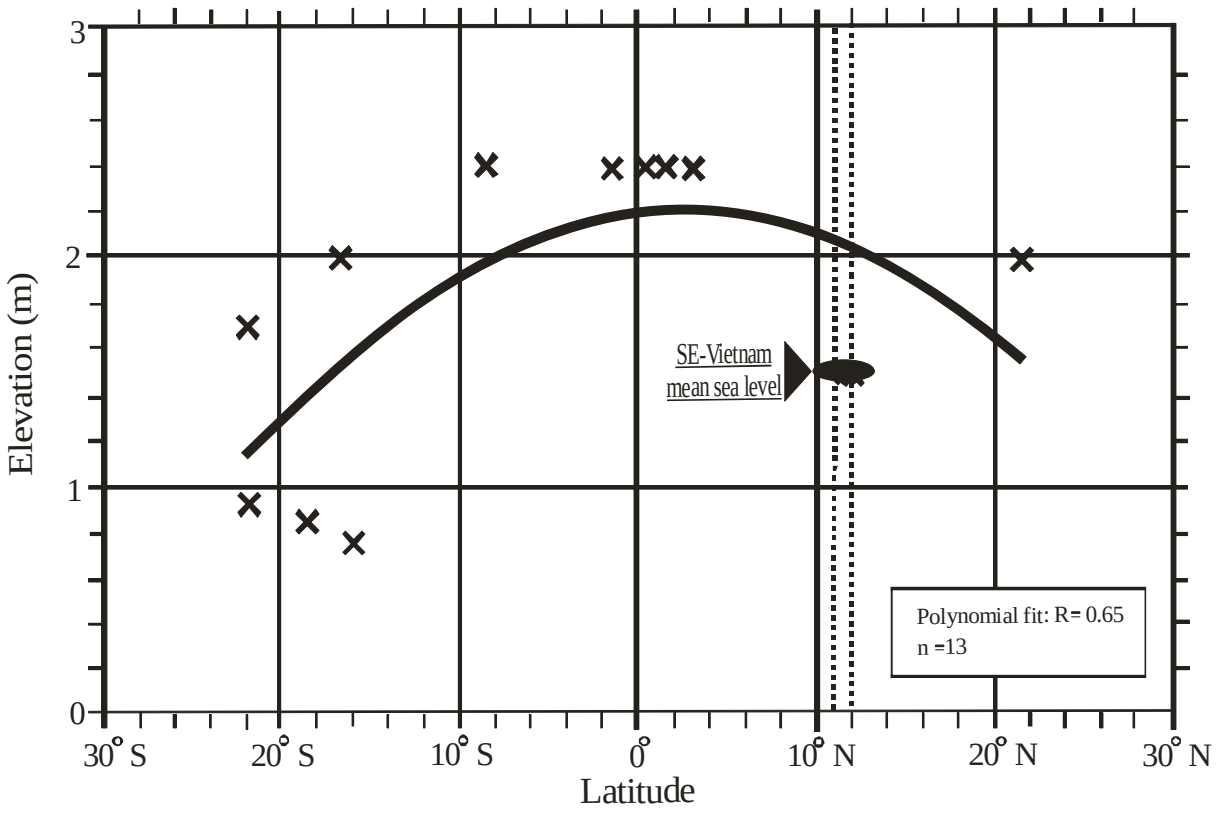

Fig. 4.10. The parabola shows the correlation between sea-level elevation and latitude indicating the rheological adjustment. The crosses mark primary data points selected by Grossmann et al. (1998) and the arrow marks the mean sea level measured on the Vietnamese coast between 11° and 12° N.

4.6. Conclusions

1. The identification of the sea-level highstand seems to be the most appropriate way of determining the Holocene sea-level changes in SE-Vietnam. This was followed by an accurate vertical reference to local tidal datum, respecting the morphological differences that influenced the tidal amplitude.
2. Former sea-level positions are indicated by beachrocks, which presented periods of sea-level stability, before and after the highstand sea level. Due to the study of their geological features, their geochemistry and chronology as well as their precise vertical height, it was possible to identify the marine origin of all investigated beachrocks.
3. Regarding beachridge, the decision to consider only its base as the maximum sea-level amplitude in the mid-Holocene proved to be correct.

4. The records of sea-level changes measured in SE-Vietnam were notably accurate. The maximum mid-Holocene spring tide was measured at 2.67 m, and the mean sea level at 1.52 m between 5687 and 5377 cal yr BP, assuming the same half-tidal range of 1.15 m as today. Moreover, the Holocene sea-level fluctuations occurring in SE-Vietnam indicate that tectonic movements did not take place during this time period.
5. The geophysical model of "Oceanic Syphoning" can explain Holocene eustatic sea-level history. However, the lack of more precise information about how the sea level in different regions of the equatorial strip was influenced impedes better knowledge about its variable amplitude throughout the equator.
6. Scientific works about the coastal region of Vietnam concerning coastal evolution in connection with sea-level fluctuation are scarce. The main works deal with both delta plains, with the northern Song Hong Delta as well as with the southern Mekong Delta, which shows the necessity for more investigation of the coastal region.

5. Coastal paleoceanography during the mid-Holocene sea-level highstand on the SE-Vietnam

Abstract:

Shallow coastal water temperatures in SE-Vietnam were evaluated for two different geological periods. In the mid-Holocene during sea-level highstand paleotemperature was reconstructed at 5605 - 5470 cal yr BP. The temperature indices were calculated by $\delta^{18}O_{PDB‰}$ from carbonate material sampled from the fossil shell *Spondylus sp* collected from the beachridge deposit near Ca Na in southeast Vietnam, which was identified as an indicator of sea-level highstand on the SE-Vietnamese coast.

Modern water temperature was taken from NOAA in the Climate Diagnostic Centre and linked with $\delta^{18}O_{PDB‰}$ from sclerochronologic growth of shells sampled in the coastal area of Nha Trang. The isotope indices were analysed of two specimens of *Meretrix lyrata* collected in a mixed environment and of one specimen of *Meretrix lusoria* sampled under the low tide line.

Due to the isotope variability identified in modern shells combined with the seasonal climatic variation in the locality where the shells grow, it becomes possible to identify the seasonal isotope variation conditioned by hydrological agents such as precipitation and evaporation. This gives way to calculate the salinity values that change by runoff freshwater and by rates of evaporation and precipitation. The salinity results confirmed a mixed environment in *Meretrix lyrata* specimens characterized by freshwater intrusion, where *Meretrix lusoria* was characterized by coastal sea water and a high evaporation rate.

Modern water temperatures were taken from two different positions because of coastal upwelling near of the southeastern coast. They were compared with the paleotemperature signal of $\delta^{18}O_{PDB‰}$ from *Spondylus sp*. The comparison showed that during summertime water temperature was approx. 1° C warmer in the mid-Holocene than today.

This warmer paleotemperature found in shallow water on the SE-Vietnamese coast during the mid-Holocene could be responsible for the great coral mortality in this period. This hypothesis is supported by the composition of beachridge which consists mainly of bioclastic detritus from marine organisms.

The higher temperatures during summer season are associated with the high light incidence in mid-Holocene times which was provoked by orbital changes.

5.1. Introduction

Stratigraphy studies on the Holocene (11,500 cal yr BP to the present) identified climatic cycles in many different places through the evaluation of proxies such as alkenone and oxygen isotope. The changes in climate occurred at intervals of approximately 2800-2000 and 1500 yr (Allen & Anderson, 1993; Bond et al., 2001; Mayewski et al., 1997; Noren, 2002; Stager et al., 1997; Stuiver and Braziunas, 1993; Denton & Karlén, 1973). These changes were induced by several forces such as volcanic aerosols, greenhouse gases and insolation variability.

The discoveries have related these rapid climate changes to the above mentioned natural effects. However, climate changes are mainly controlled by the orbital variation of the earth and the uneven solar variability (e.g.; Mayewski et al., 2004) of regular intervals at distinct times (Bush, 2005).

These rapid climate changes in the Holocene induced the variation of air-surface temperature. The same happened with water temperature: studies show that during the Holocene ocean temperature varied roughly with surface air temperature (Kim et al., 2004).

The different oceans had their particular water temperature indices. There was no synchronization during the investigated period over the last 7 kyr. There were regions of cooling water temperatures, whereas in other regions water temperatures increased (Kim et al., 2004). The absence of synchronization is a characteristic of rapid climate changes (Mayewski et al., 2004).

Apart from rapid climate change events, the Holocene is characterized by a long-term warming identified as the Holocene thermal Maximum, which occurred between 10,000 y BP to 5 kys BP. (Bush, 2001; Lorenz et al. 2006).

The Holocene climatic variability along the coast in Vietnam has not been much investigated. Most paleoclimatological studies evaluated South Asian and West Pacific tropical areas. These studies contain reconstructions of the paleoclimatic conditions during the Pleistocene and the Holocene, investigating mainly the monsoon regimes basically with regard to water circulation and paleohydrology in the South China Sea (e.g. Gong et al., 2005; Bush, 2001; Yafeng et al., 1993; Wang & Wang, 1990 and Wang & Sarnthein, 1999).

Paleoclimatological characteristics were recently investigated in the Song Hong (Red River) Delta of North Vietnam through sediment-core samples (Li et al., 2006a; 2006b). The paleoclimatic reconstructions are based on vegetation patterns from palynological records covering the last deglaciation throughout the Holocene until modern times. Results showed the variability between cold/wet and warm/dry periods.

During the Holocene, sea surface temperatures (SST) in the South China Sea were higher than the present annual temperatures (Rosenthal et al. 2003). The SST has been increased by 1.09° C over the last 7 kyr until today (Kim et al., 2004). Moreover, Jia et al. (2006) recorded temperature data similar to the modern annual temperature.

Information on paleotemperature in the present Vietnamese scenery is only available far from the Vietnamese coast, and unfortunately it shows several different values and only scarce results about shallow-water SST. Thus, the objective of this study is to compare the paleotemperature and the present temperature of shallow water in the coastal area of southeast Vietnam during two different periods between the mid-Holocene and modern times. The understanding of the climatic variability in the mid-Holocene is important in order to identify the effects of water temperature during the sea-level highstand in this period - see chapter 4.

Water paleotemperature will be reconstructed in the present study for the sea-level highstand at about 5605 - 5470 cal yr BP lasting from 5687 to 4850 cal yr BP in the mid-Holocene, and the results will be compared with present water-temperature records. Finally, the time indicated as sea-level highstand was presented as a period in which a rapid climate change

occurred (Mayewski et al. 2004), but concerning Vietnam no climatological information is available for this time (Li et al. 2006a; 2006b).

5.1.1 Bivalve shells

Studies using mollusc bivalves to reconstruct water temperature were done by Epstein & Mayeda (1953) with a revision in Epstein et al. (1953). Their works showed that the biomineralization process occurs in interaction with the water characteristics where the bivalves grow.

Hydrological conditions are archived in shells because mollusc bivalves build its skeletons in a distinct periodic accretion from the mantle-mediated to the shell margin, addicting $CaCO_3$. Periodic accretions characterize distinct growth patterns identified as “growth increments” (Clark, 1975; Jones, 1980; Schöne et al. 2002).

The variation of growth increments is strongly influenced by environmental factors such as the annual seasonal changes (e.g. Jones et al., 1989; Witbaard et al., 1994; Schöne et al., 2003), which stimulate the production of interval increments such as growth lines, with microscopic growth lines and macroscopic growth bands having approximately equal duration (Hall et al., 1974). Studies about these features are widely known as sclerochronology.

The interaction between environment and bivalve growth produces increments in a rhythmical pattern that during their secretion also bring forth biogeochemical elements over the whole life time of the mollusc (e.g. Elliot et al., 2003; Carré et al., 2005; Jones et al., 2005). The signature of these biogeochemical elements, assimilated during the formation of shell, contains rates of $\delta^{18}O$, a proxy used to exhibit hydrological parameters such as temperature and salinity.

Apart from $\delta^{18}O$, $\delta^{13}C$ proxy was analysed, which is a stable isotope with the signature of the dissolved inorganic carbon (DIC) in seawater (e.g. Mook & Vogel, 1968). It provides information about salinity, anthropogenic carbon and productivity. However, works with $\delta^{13}C$ have shown incorporation of the metabolic CO_2 respiratory process (e.g. McConnaughey,

1989 a, 1989b; Klein et al., 1996; McConnaughey et al., 1997; Lorrain et al., 2004; Gillikin et al., 2005).

The available $\delta^{18}O$ assimilated by mollusc shell with its fractionation into biogenic carbonate reflects a combination of both, temperature and oxygen isotope composition of water ($\delta^{18}O_w$) (Epstein et al., 1953). Furthermore, the $\delta^{18}O_w$ rate is highly linked to changes in salinity, reflecting local evaporation/precipitation and river runoff (e.g. Ingram et al., 1996). Thus, as was demonstrated by Epstein et al. (1953), Grossman & Ku (1986) and Böhm et al. (2000), $\delta^{18}O$ values were used to calculate sea-water temperature.

The biogenic carbonate $\delta^{18}O_{PDB‰}$, measured in bivalves, turned out to be an excellent instrument to understand temperatures variability in coastal and estuary regions (Gillikin, et al. (2005), because coastal areas are influenced by very different hydrographical factors such as gradients of salinity, temperature and productivity. This information is assimilated during the bivalves` continuous increment with high precision (Schöne et al., 2004). As a consequence, they are ideal for regions with rapid and great range of temperature and salinity.

5.2. Material and Methods

5.2.1. Working area

The working area is situated at the southeast coast of Vietnam between 11° 15` and 12° 17` N and of 108° 45` and 109° 15` E (Fig. 5.1). The fossil shell material was localized in Ca Na Town. In addition, the modern shells were collected from the beach in the region of Nha Trang Town, respectively approx. 200 km and 330 km east-northeast of Ho Chi Min City (Saigon).

The coastal zone of Nha Trang is characterized by a shallow embayment of 30 m of maximum water depth, which is open to the east. There is freshwater inflow by the discharge of the Cai River. The river is 75 km long at an altitude of 1475 m drains an area of approx. 2000 km^2. The input of freshwater to the Nha Trang Bay during the dry season is 5.6 $m^3\ s^{-1}$ and 78.1 $m^3\ s^{-1}$ during the wet season on average. The tide in the Nha Trang Bay is

characterized by a diurnal tidal regime with a tidal range of 1.7 m during high tide. The average precipitation in Nha Trang is 1359 mm yr^{-1}, with the maximum rainfall reaching 400 mm per month from September to December during the wet season. The maximum dry season occurs from February to May.

Hydrological conditions on the SE-Vietnamese coast were investigated by Rojana-anawat et al. (2000). In the Nha Trang region the SST is 28° C; in direction to the Mekong Delta the SST increases up to 29° C. Salinity is reduced to 31.5 – 32.0 psu due to the input of freshwater from the Mekong; near Nha Trang the grade of salinity rises to 33.5 and 34 psu. Furthermore, Tang et al. (2004) and Ho et al. (2000) proved evidence of coastal upwelling from 11° to 15° N westward to 110° E during the southwesterly monsoon winds.

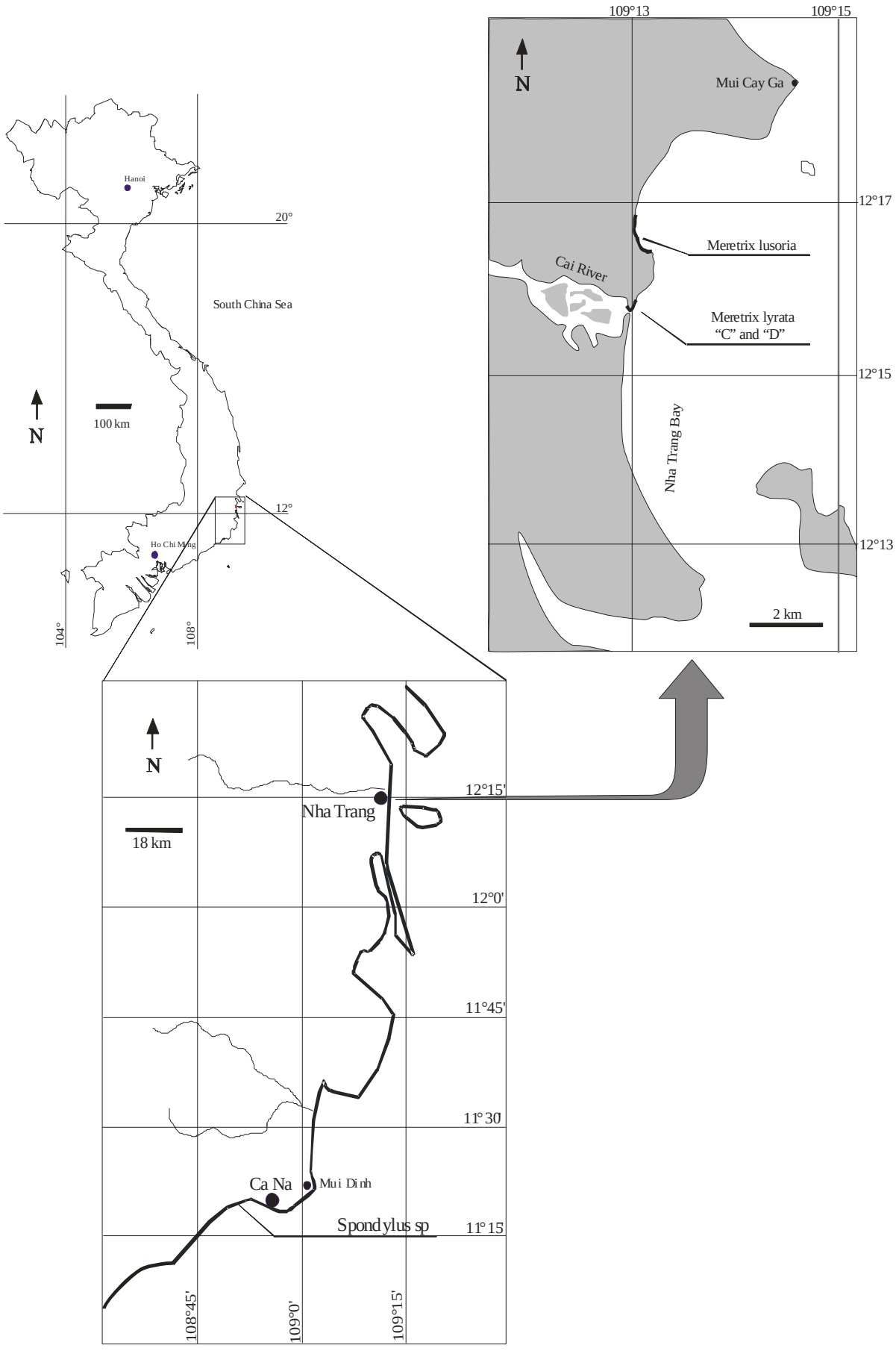

Fig. 5.1. Sample positions of shells collected in the working area between Ca Na and Nha Thang. Spondylus sp on the Ca Na coast and M. lusoria and M. lyrata C and D in the Nha Trang Bay.

5.2.2. Bivalve characterisation

The fossils were sampled from the beachridge deposit in Ca Na formed during the mid-Holocene sea-level highstand on the southeast Vietnamese coast in the time interval from 5687 to 4860 cal yr BP. This deposit in southeast Vietnam was found between 2.67 and 3.57 m (in Chapter 4) above the present mean sea level. The beachridge is composed of coral and shell skeletons.

Only well preserved shells specimens that did not show any significant signal of reworking were chosen for stable-isotope analyses. Thus, a specimen of the bivalve *Spondylus sp* was selected to take the carbonate powder from. The sample of *Spondylus sp* is identified as Vn11110306 collected on the beachridge top at the position of 11° 19,796` N and 108° 50,498` E, 4.95 km south-westward from Ca Na (Fig. 5.1). The observation of the fossil *Spondylus sp* belongs to the family Spondylidae. The living specimens of this family are mainly found in shallow water below low tide. The *Spondylus sp* preserved its original mineralogy with 100 % of aragonite. Further SEM observations showed cross-lamellar forms confirming aragonite which formed this specimen (Fig. 5.2c). The ^{14}C dating of this shell yielded an age of 5605 - 5470 cal yr BP.

Modern shells were sampled in Nha Trang Town. Two shells, sampled alive in the north of Nha Trang in the mouth of the Cai River, were identified as two specimens of *Meretrix lyrata*. The third shell, also collected alive at the extension of the Nha Trang Bay northward to the Mui Cay Ga region, was identified as *Meretrix lusoria* (Fig. 5.1). All samples were caught alive by a fisherman, bought on 12th of April 2005 and killed afterwards. The classification of fossil and modern shells was accomplished by Bui Quang Nghi, working as a scientist at the Nha Trang Oceanography Institute in Vietnam. The biological characteristics of each shell such as their behaviour and environment of growth are described in Kira (1965).

The *M. lusoria* (Roeding, 1798) belongs to the family of Veneridae an economically very important species. The species has symmetric triangular ovate valves. Their surface is covered

with a thin smooth and polished periostracum and is to colored white to chestnut-brown, usually with broad radial rays. They live in sandy bottoms in subtidal environments of about 10 m of waterdepth.

The *M. lyrata* (Sowerby, 1851) is characterized by solid and heavy symmetric valves of ovate shape, rounded interiorly and narrowing towards the posterior end. The surface shows concentric undulated growth. The species lives in shallow water below low tide.

After the shells had been investigated with regard to their mineralogical as well as their external shape, the method of carbonate extraction was applied. Transversal slices of the shells were sectioned, along their maximum growth axis using a low speed saw, starting on the umbo up to the rim. From each shell a slice was cut of approx. 1 cm thickness. Four slices were glued in sequence onto a millimetre-scale aluminium plate, for observations under the binocular.

The shells were put under a magnifying glass coupled to a drilling machine, and manually drilled along the umbo in direction to the rim, using a micro drill of 200 µm diameter. Followed a standard procedure described by e.g. Erlenkeuser & Wefer (1981); Jones et al. (1983); Krantz et al. (1987); and Mueller-Lupp et al. (2004).

The transect drill was extended along the growth axis under 0.5 mm from the shell surface to avoid contaminated material of the surface. The series of the holes had a spatial distance of ~ 1 mm between each hole. Where the growth increments were closer to each other, the spatial distance between each hole changed to ~ 0.5 mm (Fig. 5.2a).

Along the drilling profile, no growth increments were observed in *Spondylus sp* due to its low condition of preservation. In consequence, its profile sample displayed a spatial distance of 1 mm to the middle of the valve after passing to 0.5 mm. 135 powder samples were drilled along a profile of 110 mm length on *Spondylus sp* valve. The first 85 samples had a distance of 1 mm between each hole, whereas the last 50 samples had distances of 0.5 mm in between (Fig. 5.2b).

The slice of the *M. lusoria* valve, measuring 66.5 mm in length from the umbo to the rim, was drilled by 70 powder samples. The spatial distance for the first 41 holes was 1 mm, while the last 31 were drilled each 0.5 mm.

The *M. lyrata "C"* reached 53 mm in length from the umbo to the rim. The 52 collected samples were drilled, leaving space of 1 mm between each one.

The *M. lyrata "D"* reached 40 mm in length from the umbo to the rim and was drilled with 51 samples, with a spatial distance of 1 mm between the first 29 samples and 0.5 mm between the last 22 samples.

The distance between the holes revealed that the monthly grown shell contained calcium carbonate increment corresponding to 1 mm. However, in the direction of the shell rim the sampling distance was changed, as there was a very small distance between the growing rings.

5.2.3. Temperature estimation

The sampled powders were measured by fractionation of oxygen and carbon isotopes. The analyses were carried out by gas mass spectrometer in the Leibniz Laboratory in Kiel - isotopic device, Kiel University - sea chapter 2.

The background of $\delta^{18}O$ indicates that its fractionation provides important clues to the environmental conditions during shell formation. The isotopic composition in bivalves depends on two oceanographic conditions: $\delta^{18}O$ in seawater and the temperature of the environment where the animals live. In the coastal region the $\delta^{18}O$ of seawater ($\delta^{18}O_W$) changes its values due to precipitation/evaporation events as well as freshwater input by rivers, being agents that interfere with salinity concentration.

Meretrix lusoria

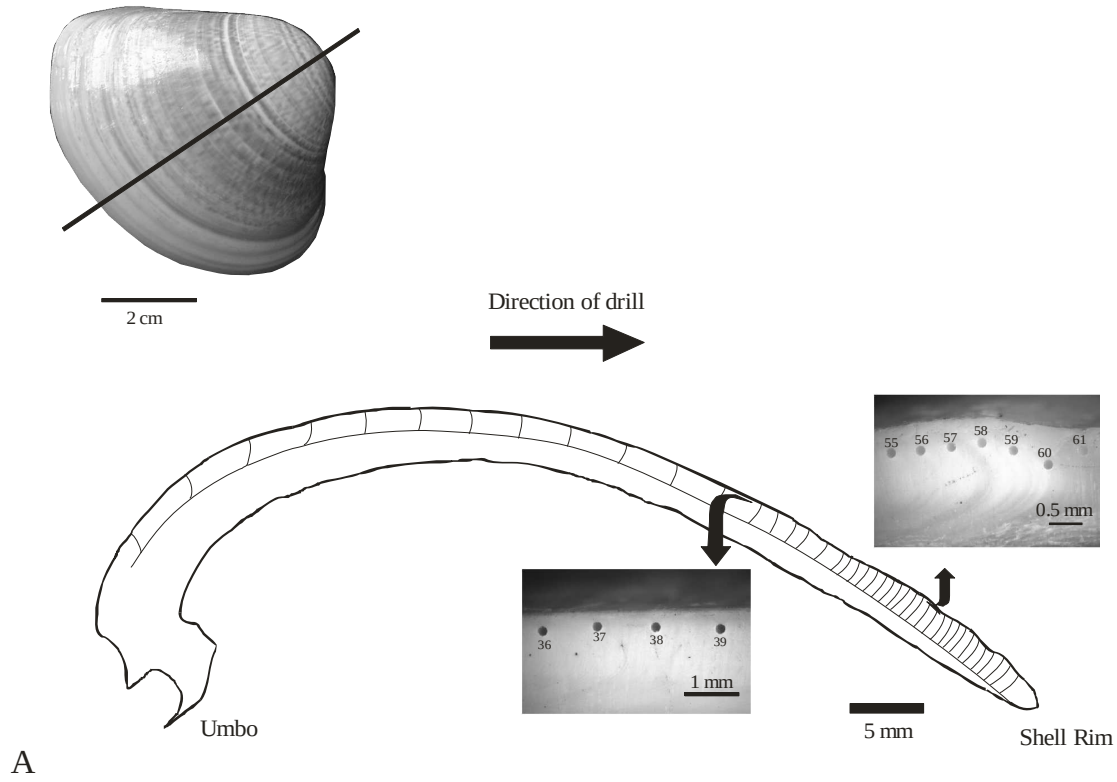

A

Spondylus sp

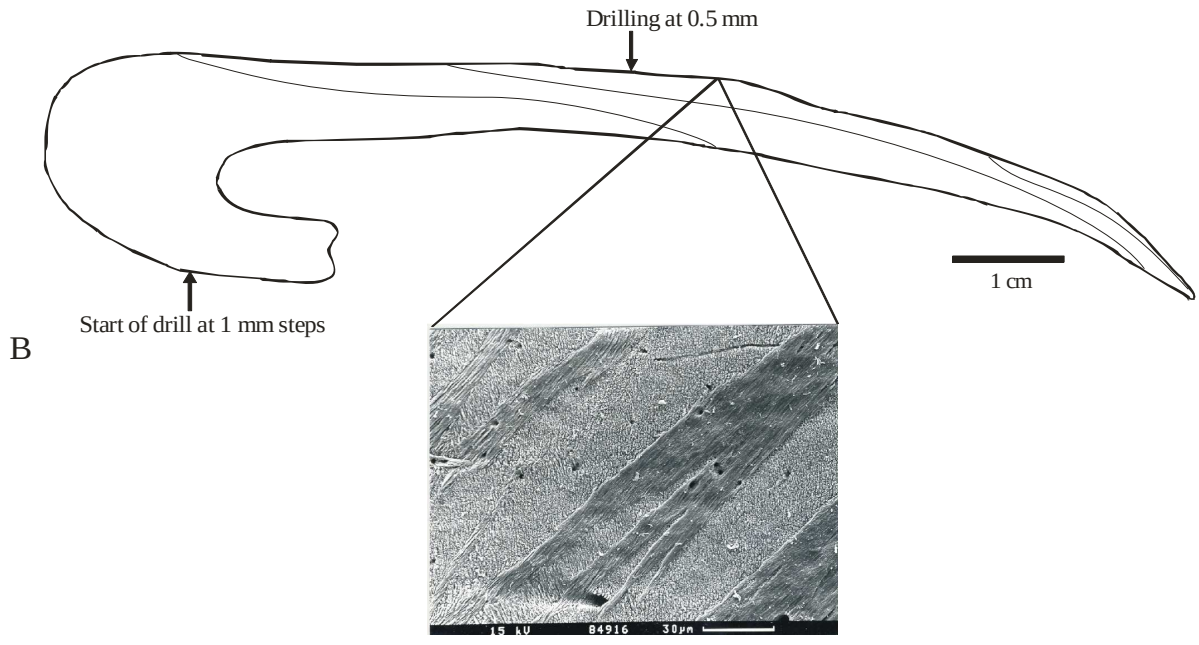

B

C

Fig. 5.2. Cutting and drilling of investigated shells. “A” presents the transverse section and the profile in M. lusoria with distances between the holes. “B” shows the profile of the fossil shell Spondylus sp. “C” is a picture of SEM, showing the cross-lamellar structure of aragonite.

In consequence, before calculating values of temperatures from $\delta^{18}O_{PDB‰}$, the variation of $\delta^{18}O_w$ linked with salinity should be known (e.g. Hong et al., 1995; Klein et al., 1996; Ingram et al., 1996; Auclair et al., 2003; Jones et al. 2005; Gillikin et al., 2005). In order to understand the relationship between salinity and $\delta^{18}O_w$, it is important to calculate temperatures by $\delta^{18}O_{PDB‰}$, especially for studies in coastal regions. This method is a very suitable model to obtain $\delta^{18}O_{PDB‰}$ temperature from bivalves, when no samples regarding daily growth increments are available.

According to Grossman and Ku`s (1986) the relationship between the temperatures and $\delta^{18}O_{PDB‰}$ can be expressed by below given equation (01). The water-temperature values derived from this equation are corrected to the SMOW (Standard Mean Ocean Water) scale,

$$T_{\delta 18O}\ (°C) = 21.8 - 4.69*(\delta^{18}O_{PDB‰} - (\delta^{18}O_{w‰} - 0.2\ ‰)) \qquad \text{(Equa.01)}$$

where $\delta^{18}O_{PDB‰}$ is related to the PDB ‰ measured from the aragonite constitution of shell and where $\delta^{18}O_W$ is measured relative to $\delta^{18}O$ in water. Thus, it is assumed that the $\delta^{18}O_w$ is constant and that each shift of 1‰ in $^{18}O_{PDB‰}$ reflects a temperature change of the ambient seawater of 4.69° C.

5.3. Vital effect

As has been demonstrated, shell building minerals secreted in a quantity of taxa (mainly molluscs) show that the composition of oxygen isotope reflect in part the temperature of the water in which the mollusc lives. However, the signals of the biogenic mineral are in particular related to biological processes influenced by the environmental conditions. These results are known as “physiological effect” or are also called “vital effect” (Weiner and Dove, 2003). Additionally, according to Epstein et al. (1951) the those taxonomic groups, in which not all biogenic minerals are deposited in equilibrium with the environment, are represented by echinoderms, corals and plants as coralline algae.

With the increase of studies to reconstruction paleoenvironmental conditions from the isotope records embedded in skeletons, scientists have observed the necessity to obtain more knowledge about the "vital effect". Studies on the "vital effect" were intensified and consequently divided in two categories known as kinetic effect and taxonomic effect.

- Kinetic effect: investigates the isotopic disequilibrium deposited in biogenic mineral linked with the environment. This condition is induced by physical modification that alters the velocity of isotopic assimilation (e.g. McConnaughey, 1989 a, b; Ziveri et al., 2003; Zhou & Zheng, 2003).
- Taxonomic effect: recognizes, which phyla, genera and species deposit their skeletal material in isotopic equilibrium with the environment (e.g. Urey et al. 1951; Craig, 1953; Carpenter & Lohmann, 1995; Filippi, et al. 1997).

5. 4. Results

5.4.1. Oxygen and carbon isotopes

Records of $\delta^{18}O_{PDB‰}$ are very similar for specimens of *M. lyrata "C"* and *M. lyrata "D"*. The *M. lyrata "C"* obtained by statistic estimation a mean of -3.67 ‰ ± 0.5 (n=52), ranging from -5.17 to -2.51 ‰ (Tab. 5.1). These values are similar to the oxygen isotope found in the *M. lyrata "D"* that shows a mean of -3.43 ‰ ± 0.6 (n=51) from -5.59 to -2.35 ‰. In this connection, the similarity might be traced back to the fact that the samples were collected at the same place.

The isotope values of *M. lusoria* have a mean of -2.49 ‰ ± 0.3 (n=70), ranging from -3.38 to -1.89 ‰. In this case, the shells show heavier isotope values compared with both species of lyrata. The $\delta^{18}O_{PDB‰}$ of fossil *Spondylus sp* shows a mean of -1.58 ‰ ± 0.5 (n=135), ranging from -2.60 to -0.07 ‰ and presenting isotopic fractionation, which is heavier than that for modern shells.

Like the records of $\delta^{18}O_{PDB‰}$, the results of $\delta^{13}C_{PDB‰}$ were fairly similar for specimens of *M. lyrata*. The statistics for *M. lyrata "C"* yielded a mean of -1.65 ‰ ± 0.3 (n=52), corresponding to a range from -2.52 to -1.01 ‰.

M. lyrata "D" showed a mean of -1.63 ‰ ± 0.4 (n=51), ranging from -3.46 to -0.62 ‰. The third examined shell, *M. lusoria*, presented a mean of 0.50 ‰ ± 0.3 within a range from -0.21 ‰ to 1.40 ‰. In this case, positive values were noted, in contrast to the other two shells that presented negative indices of isotope carbon.

Analysing the results on the growing axis in fossil shell, isotope values more enriched than those demonstrated in the present shells were observed. *Spondylus sp* carbon records were ranging from 0.14 to 2.52 ‰ with a mean of 1.43 ‰ ± 0.4 (n=136) also having positive carbon values like in *M. lusoria* (Tab. 5.1).

Shell Species	Mean (‰)	Min.	Max.	Range	n
M. lyrata "C" (O)	-3.67 ±0.5	-5.17	-2.51	2.66	52
M. lyrata "D" (O)	-3.43 ±0.6	-5.59	-2.35	3.24	51
M. lusoria (O)	-2.49 ±0.3	-3.38	-1.89	1.49	70
Spondylus sp (O)	-1.58 ±0.5	-2.60	-0.07	2.53	135
M. lyrata "C" (C)	-1.65 ±0.3	-2.52	-1.01	1.51	52
M. lyrata "D" (C)	-1.63 ±0.4	-3.46	-0.62	2.84	51
M. lusoria (C)	0.50±0.3	-0.21	1.40	1.61	70
Spondylus sp (C)	1.43±0.4	0.14	2.52	2.38	135

Table 5.1. The statistical results of $\delta^{18}O_{PDB‰}$ (O) and $\delta^{13}C_{PDB‰}$ (C) were analysed in species shells from Vietnam.

The lighter values showed in both specimens of *M. lyrata* significant influence of freshwater, which confirms the fact that these specimens lived in an environment characterized by shallow marine water influenced by freshwater input. Thus, maximum values of $\delta^{18}O$ reached -2.51 and -2.35 ‰, whereas in a normal marine environment the water values are higher -1.3 ‰ (Wang and Tsai, 1993; Wang et al. 1994). The equivalent is observed for $\delta^{13}C$ with negative values in marine water environment (Tab. 5.1); where marine carbon-13 isotope is fractionated in mainly positive values.

The measured isotope values indicate a freshwater influence (Fig. 5.3). In fact the considering marine conditions influenced by freshwater from a river month of the northern of Nha Trang Bay is characterized by freshwater from the Cai River estuary.

In *M. lusoria* the values of $\delta^{18}O$ present a minimum equal to -3.38 ‰ and a maximum of -1.89 ‰ (Tab. 5.1). This isotopic fractionation indicates the influence of freshwater and marine water, but on the cross-plot isotope values showed tendency towards marine influence (Fig. 5.3). Also, *M. Lusoria*`s place of sampling showed no significant freshwater influence. Therefore, these lighter $\delta^{18}O$ values might be linked with the seasonal hydrological conditions such as the salinity variations in the shell's environment.

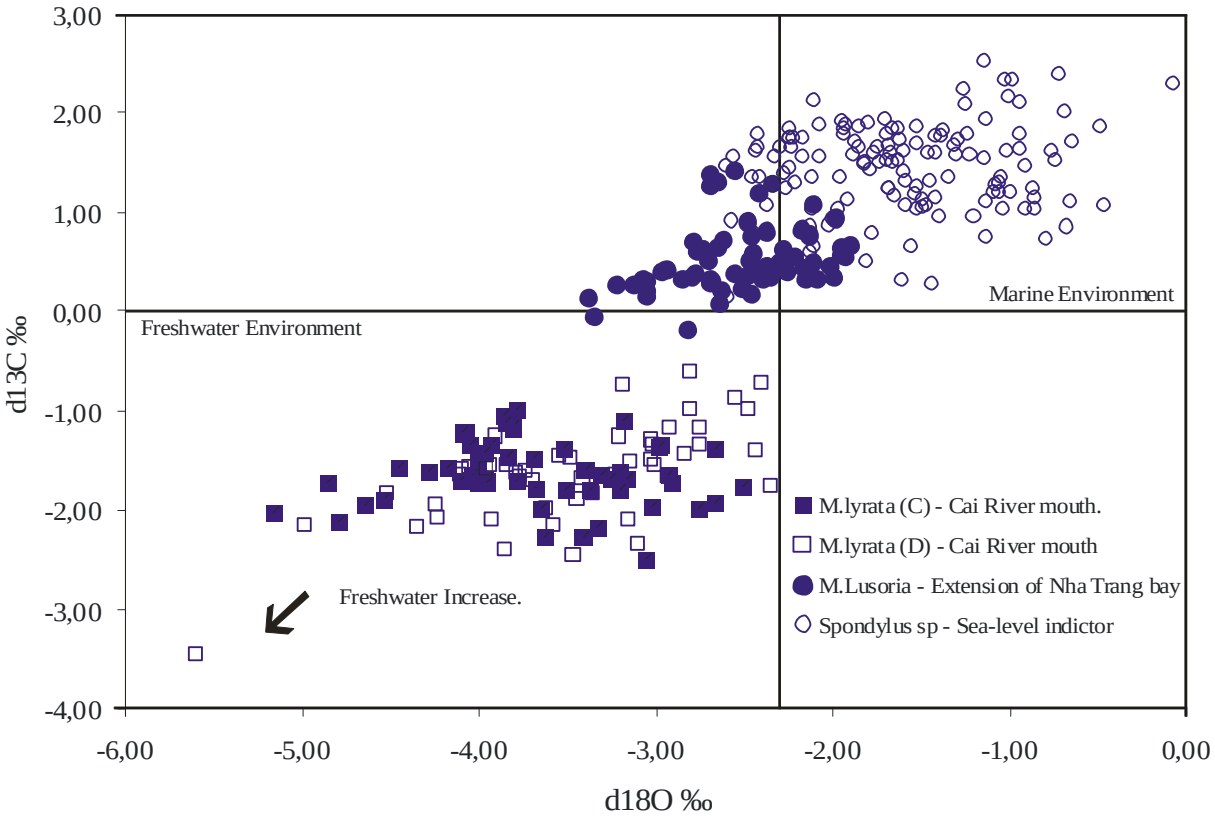

Fig. 5.3. Cross-plot $\delta^{13}C$ vs.$\delta^{18}O$ of mollusc shells from SE-Vietnam shows the distribution range from marine to freshwater fields of modern and fossil shells.

The *Spondylus sp* shell indicates marine water signature in its isotopic values. The noted enrichment of $\delta^{18}O_{PDB‰}$ at -1.58 ‰ on average showed that *Spondylus sp* lived only in marine environment, which is confirmed by $\delta^{13}C_{PDB‰}$ values, indicating the complete absence of freshwater influence (Tab. 5.1). However, the cross-plot $\delta^{18}O$ vs. $\delta^{13}C$ reflects a tendency in

Spondylus sp isotopes towards a lighter fraction (Fig. 5.3). This tendency goes along with a hydrological variation in shallow water controlled by precipitation and evaporation events during different seasonal periods (Israelson et al., 1994). A similar tendency was observed for *M. Lusoria*.

5.4.2. Isotopic profiles

The isotopic fractions along each growth axis of the shell were investigated for the evolution of the intra-shell isotopic behaviour accompanied by seasonal changes as well as for the probable growth time of shells (Fig. 5.4).

a) Inter-annual $\delta^{18}O_{PDB‰}$

Fractionations of $\delta^{18}O_{PDB‰}$ from the carbonate increment of shells make it possible to recognize the local seasonal cycle (Williams et al., 1982; Jones et al., 1983; Krantz et al. 1987). As already mentioned, the $\delta^{18}O_{PDB‰}$ is correlated to the life time of shells, which is controlled by seasonal hydrological conditions such as temperature and $\delta^{18}O_w$ seawater composition. Actually, lighter or more negative values of $\delta^{18}O$ indicate warmer temperatures and heavier or more positive values are connected to colder temperatures (e.g. Krantz et al., 1987; Marchitto et al., 2000; Müller-Lupp & Bauch, 2005).

Knowing the variation of oxygen isotopes within the shells, the seasonal fluctuations could be determined. $\delta^{18}O_{PDB‰}$ is basically categorized into lighter values for warm periods and heavier values for cold periods (Fig. 5.4). Following this standard, the spring-summer period in each shell before April 2005 was identified.

The countdown of the $\delta^{18}O_{PDB‰}$ profile from April 2005 in *M. lyrata "C"*, *"D"*, and *M. lusoria* demonstrated two or three periods of continuing lighter values. In detail, this means that the modern shell's cycle is characterized by period S1 representing the first spring-summer, period S2, showing the second spring-summer, and period S3, displaying the third spring-summer (Fig. 5.4).

The life cycles of *M. lyrata "C"* and *M. lusoria* underwent three warm periods before April 2005, indicated by S1 for 2002, by S2 for 2003 and by S3 for 2004, alternating with heavier values of $\delta^{18}O$ that represented a colder seasons in between. In *M. lyrata "D"* only two periods of lighter $\delta^{18}O$ values could be identified pointing to warmer periods. As a result, *M. lyrata "D"* experience the first warmer period in 2003, as shown in S1, and the second warmer period in 2004, as demonstrated in S1 (Fig. 5.4).

The variability of oxygen isotopes in *Spondylus sp* profiles showed five periods with lighter values, identifying roughly warmer periods (Fig. 5.4). Isotope values in *Spondylus sp* were analyzed from 36 to 104 mm of the shell, because this interval exhibited a clear series of different seasons (Fig. 5.4). Moreover, identifying the great amplitudes in oxygen-isotope values, suggested that the animal had a free-swimming life in very shallow waters, an environment that favoured an immense variability of $\delta^{18}O$ due to the changes in precipitation and evaporation.

b) Inter-annual $\delta^{13}C$

According to definition, the $\delta^{13}C_{PDB‰}$ formed in marine water stays in isotopic equilibrium with the atmosphere in values between 0 and 4 ‰. Negative values are typically found in coastal and in estuarine areas where the water surface is influenced by the recycling of carbonate from organic matter and by dissolved carbonate of terrestrial origin (Mook & Vogel, 1968; Israelson et al., 1994).

The total dissolved inorganic carbon (DIC) of the water is controlled primarily, by bicarbonate which is influenced by metabolic phytoplankton which can enhance or deplete of the $\delta^{13}C$ (Krantz et al., 1987, 1988). Consequently, interpretation of environment or even interaction of temperature with $\delta^{13}C$ is considered to be very difficult (e.g. Tanaka et al., 1986; Romanek et al., 1992, McConnaughey et al., 1997; Lorrain et al., 2004).

Values depleted in $\delta^{13}C$, in both *M. lyrata* are linked with a freshwater intrusion into the marine system, inducing change in salinity (Erlenkeuser, 1995). In addition, depleted $\delta^{13}C$

hints also to another process in coastal areas which is induced by the recycling of organic matter and the oxidation of phytoplankton that decreases dissolved inorganic carbonate in water. In contrast to this enriched values of $\delta^{13}C$ were found in *M. Lusoria*, being probably values in equilibrium with marine water, which is also true for enriched *Spondylus sp* values (Fig. 5.4).

Contrary to $\delta^{18}O$, the variation of $\delta^{13}C$ in the present shells is more homogeneous for *M. lusoria* than for both *M. lyrata* (Tab. 5.1). The similar fluctuation of $\delta^{13}C$ in *M. lusoria* as well as in fossil *Spondylus sp* may be associated with the variation of salinity during the annual season in shallow coastal water.

Furthermore, an interesting drop of the $\delta^{13}C$ profile was observed, showing a trend away from the umbo - see *M. lusoria* and *M. lyrata "C"* (Fig. 5.4). Normally, this drop is explained by the ontogenetic effect. It is categorized as a physical change related to the transformation from a fast-growing juvenile stage to a slower-growing adult stage in which metabolic energy is primarily diverted to gametogenesis which is manifested in light shell $\delta^{13}C$ values. This mechanism involves a shift to lighter $\delta^{13}C$ values by the inclusion of more metabolically derived CO_2 into the bicarbonate pool used in calcification (Krantz et al., 1987; Wefer & Berger, 1991; Klein et al., 1996).

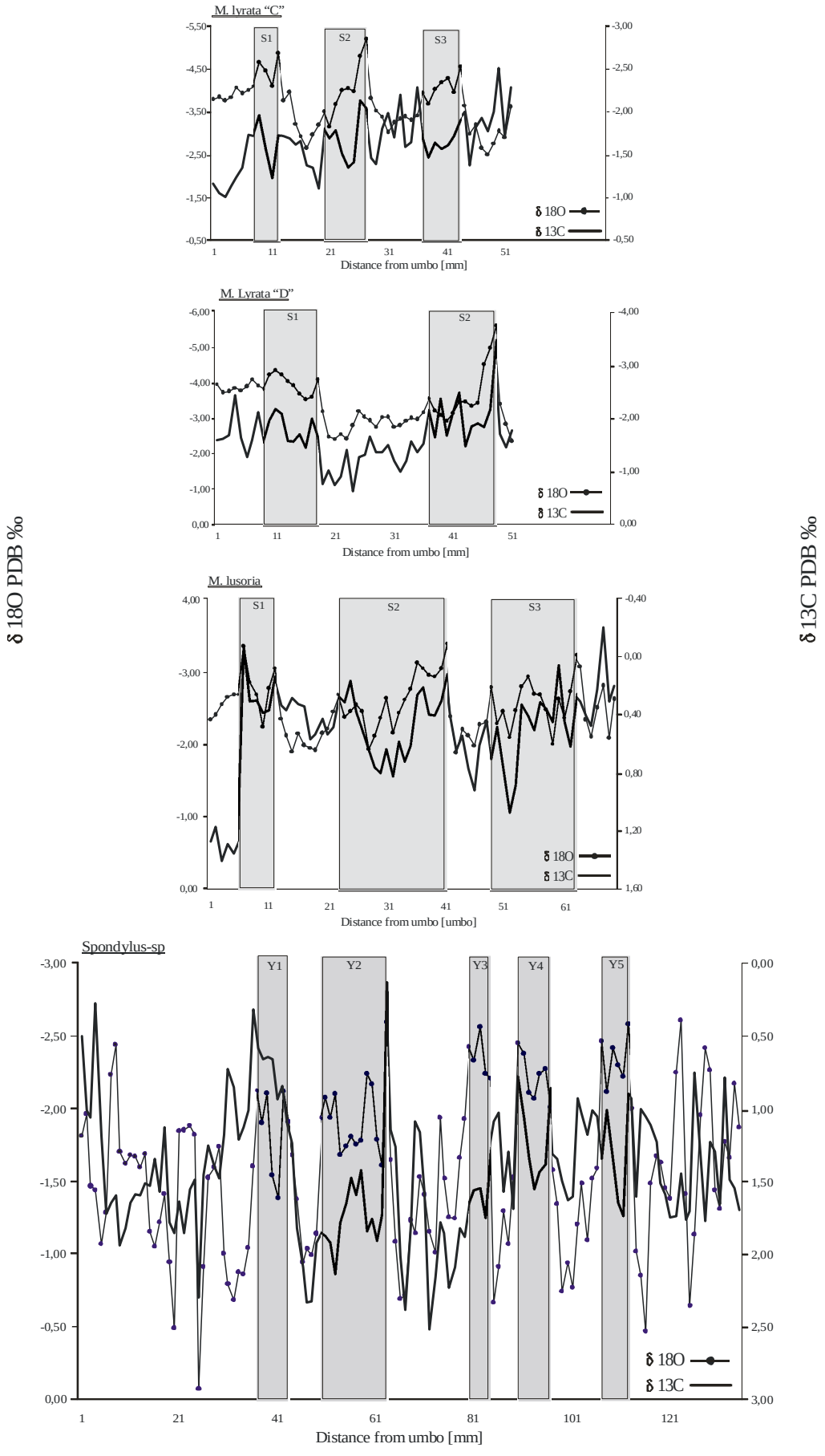

Fig. 5.4. Stable isotope profiles measured on the shells. Grey areas are the light $\delta^{18}O$ values, represented by S1, S2 and S3 in modern shells and Y1 to Y5 in fossil shell.

5.4.3. Calibration of $\delta^{18}O_{PDB‰}$ by precipitation and temperature

The oxygen isotope record in shells showed seasonal variation, which confirmed their potential as archives of temperature records. Therefore, the fractionation values of oxygen isotope are connected with the seasonal variability of the growing place. However, in order to identify the variability of $\delta^{18}O_{PDB‰}$ within the system and the local water temperature it is necessary to accomplish a calibration between the two agents.

The calibration was elaborated using records of precipitation and SST of the north of the Nha Trang coast at the latitude 12° 24` N and between 108° 48` and 110° 36`E longitude. The monthly climatological records were connected to $\delta^{18}O_{PDB‰}$ values in the shell profiles, which revealed a seasonal variation during their lifetime as regards the time span from April of 2005 (the date of collection) until July 2002.

The indices of precipitation and SST were provided by the NOAA Climate Diagnostics Centre in the Earth System Research Laboratory (ESRL), a section of the Physical Sciences Division in (http://www.cdc.noaa.gov/cgi-bin/Timeseries/). The data set contains the monthly average temperature and rainfall rates from 2001 to 2005 of north the Nha Trang coast (Fig. 5.5).

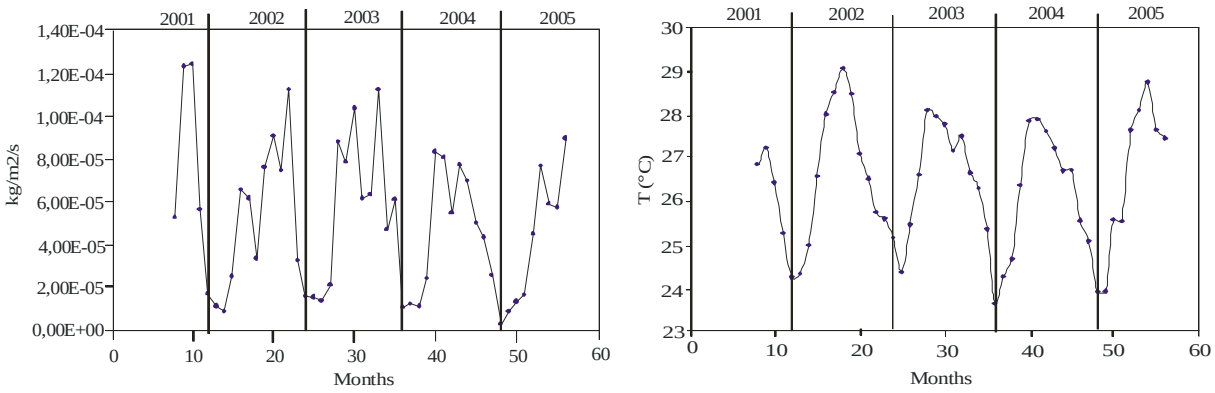

Fig. 5.5. Precipitation and temperature values from the Nha Trang coast from August 2001 to August 2005, used to calibrate $\delta^{18}O_{PDB‰}$ fractions from shells.

It was not possible to establish a correlation between $\delta^{18}O_{PDB‰}$ fractions and temperature because when comparing seasonal temperature and precipitation with variation of $\delta^{18}O_{PDB‰}$,

it was noticeable that many light peaks in $\delta^{18}O_{PDB‰}$ were related to high rainfall rates (Fig. 5.6). The $\delta^{18}O_{PDB‰}$ related to rainfall in the region of the Nha Trang coast is well connected with the growth of the rhythms of shells; thereby the lighter oxygen isotopes in modern shells provide evidence of the increase of rainfall during warm temperatures in spring-summer seasons.

Concerning fig. 5.6, the correlation between precipitation and $\delta^{18}O_{PDB‰}$ from each shell is accomplished. The growth-rhythms of the examined shells are strongly connected with local precipitation, creating a direct connection between the rainfall peaks and $\delta^{18}O_{PDB‰}$ peaks measured in shells. The calibration shows a connection between the original extreme values of rainfall and a corresponding point for $\delta^{18}O_{PDB‰}$.

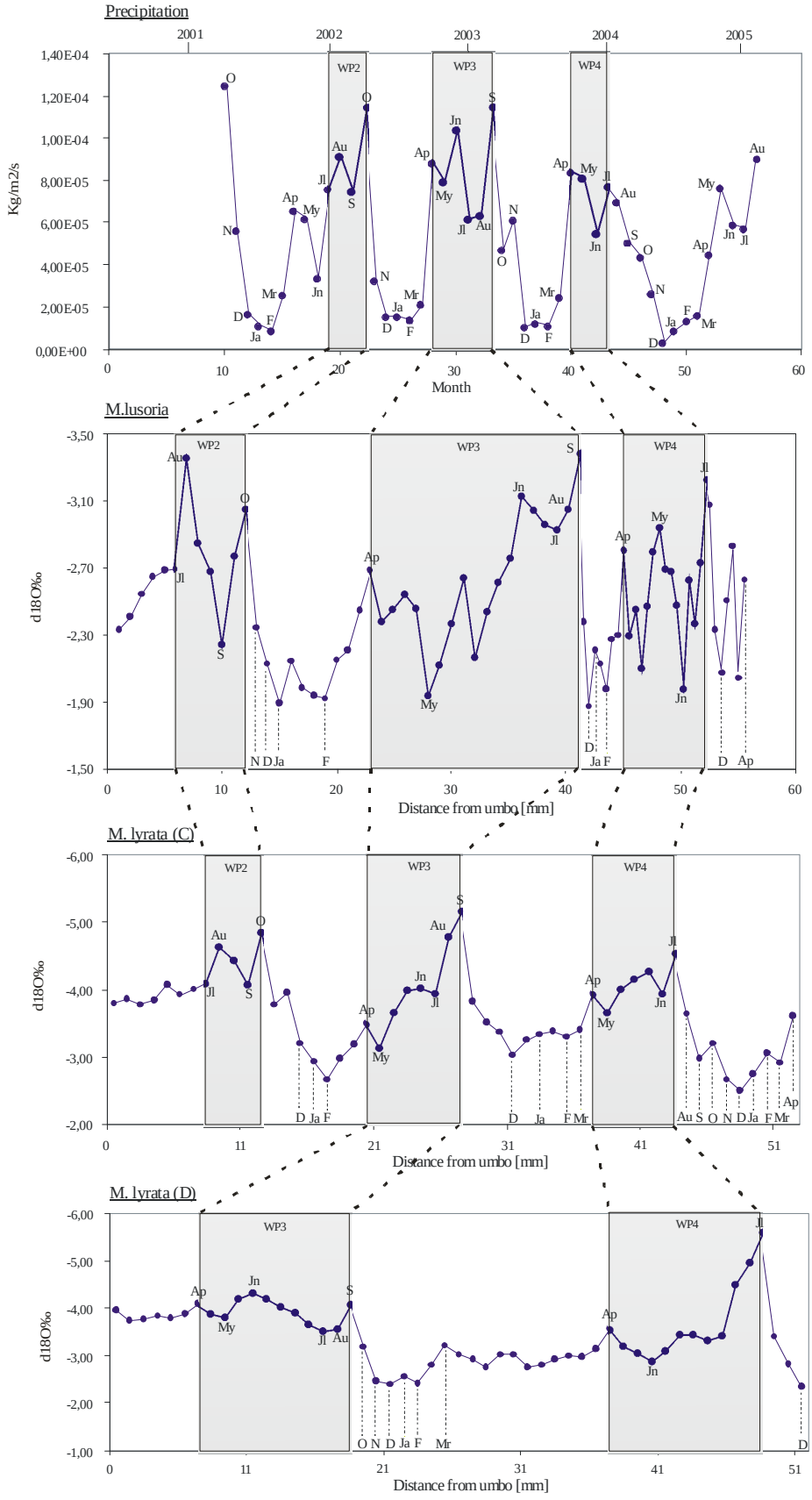

Fig. 5.6. Calibration between shell profiles of $\delta^{18}O_{PDB‰}$ with precipitation data from the Nha Trang Bay. The upper graph shows the precipitation variability from October 2001 to August 2005 with warm periods (WP), provided by NOAA/CIRRES; the points represent monthly average. The lower graphs contain $\delta^{18}O_{PDB‰}$ from modern shells. The exact months are directly linked with $\delta^{18}O_{PDB‰}$, while those that represent the probable months are indicated by dashed lines.

Through the connection of rainfall values with $\delta^{18}O_{PDB‰}$ the indices of water temperature could be determined, because for each month of rainfall records there was a corresponding temperature value (Fig. 5.5). On the basis of these water temperatures linked to each $\delta^{18}O_{PDB‰}$, it was possible to calculate the scale of SMOW ‰. Furthermore, the water-temperature indices that were not directly related to $\delta^{18}O_{PDB‰}$, values were extrapolated between two known temperature indices.

5.4.4. SMOW ‰ estimation

For calculating the $\delta^{18}O_w$ scale, the paleotemperature equation (Equa. 1) was applied; the values of $\delta^{18}O_w$ were calculated by an inversion of equation 1, using the known SST calibrated with $\delta^{18}O_{PDB‰}$ (Equa. 2),

$$\delta^{18}O_w = - (((T\ °C - 21, 8)/-4, 69) - \delta^{18}O\ PDB‰) \qquad \text{Equa. 2}$$

apart from the $\delta^{18}O_w$ scale in shells, the hydrological balance between freshwater and seawater was identified, as well as determination of the salinity variations in the environment, where the modern shells lived (Tab. 5.2). The salinity was estimated using a simple mass balance equation based on theoretical marine water (34.5 psu = 0.3 ‰) and freshwater (0 psu = - 9 ‰) endmembers.

Previous values of $\delta^{18}O_w$ were measured in four water samples taken outside Nha Trang Bay at 12° 15.950` N and 109° 16.200` E during the FS-Sonne cruise 187-3 on 25th of April, 2006. Water samples from in 1 and 2 m depth yielded -0.06 ‰ vs. SMOW ‰ on average with a salinity of 33.6 psu. This is very similar to SMOW ‰ already analysed April 1999 in subsurface waters of South China Sea with -0.05 ‰ and a salinity of 33.3 psu (Lin, 1999).

After the temperatures in $\delta^{18}O_{PBD‰}$ in calcium carbonate had been determined, it was necessary to bring these water-temperature records into line with the seasonal variation.

Owing to the lifetime of modern shells, there is no sclerochronological development agreeing with the seasonal period.

Greater increments of carbonate material are growing in spring-summer seasons, smaller increments occur in autumn-winter seasons. Thus, the shells` growth was normalized to calendar months with the basis of seasonal SST (Fig. 5.7).

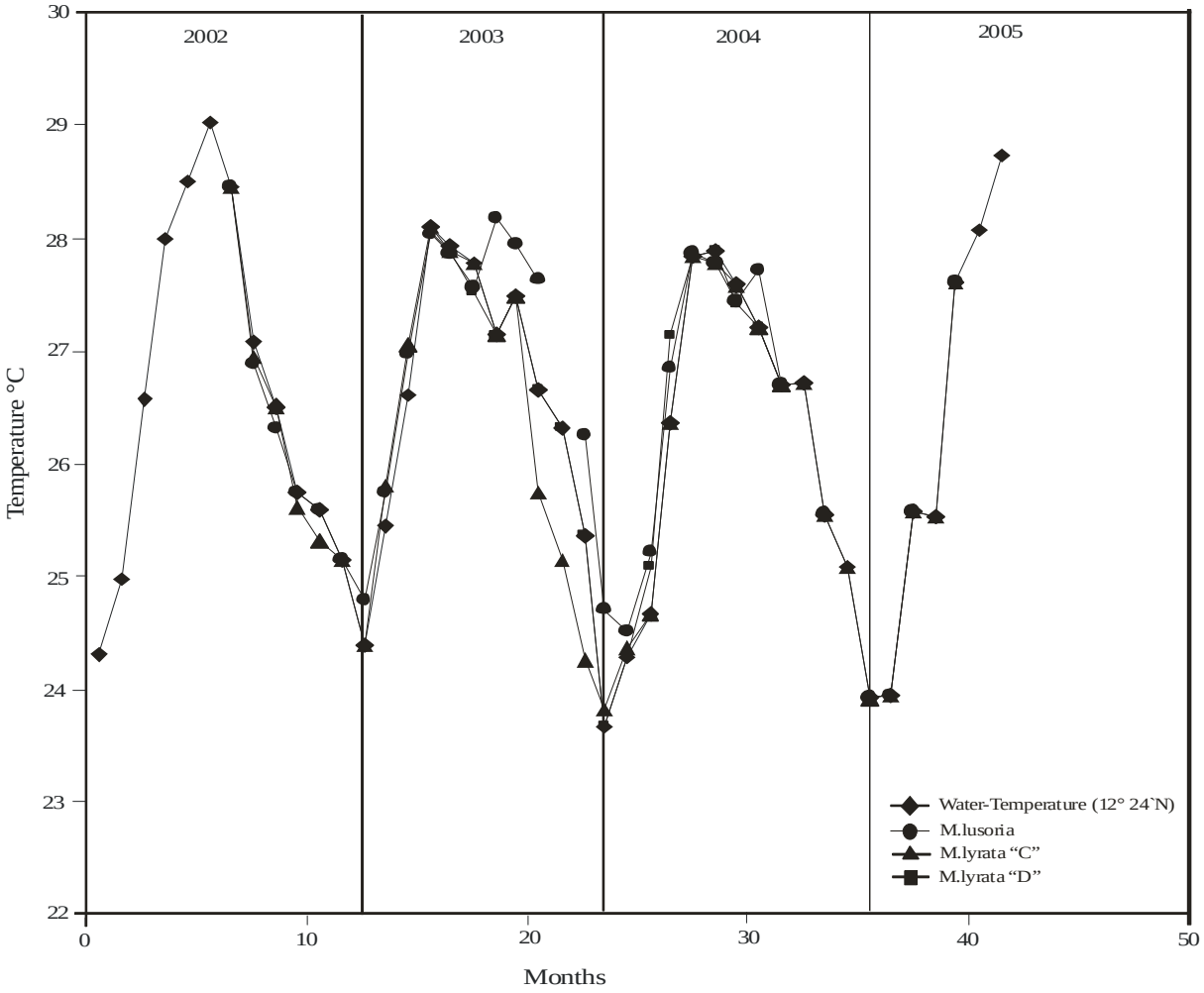

Fig. 5.7. Monthly variation of SST from January 2002 to June 2005 with the respective temperature $\delta^{18}O_{PDB‰}$ of shells; the normalization of points measured in the shell to calendar months is required to equalize the seasonal temperature variation with the shell` growth.

The normalized profile available in *M. lusoria* presents $\delta^{18}O_w$ indices ranging from -0.89 ‰ to -2.14 ‰ and indicating temperature values between 23.9 and 28.4° C with 26.4° C on average. Salinity records calculated from $\delta^{18}O_w$ range between 25.1 psu and 30.1 psu with 28.2 psu on average. The not normalized salinity dates measured in *M. lusoria* are linked with $\delta^{18}O_{PDB‰}$ records in form of a linear regression in $R^2 = 0.505$ (n= 64) (Fig. 5.8)

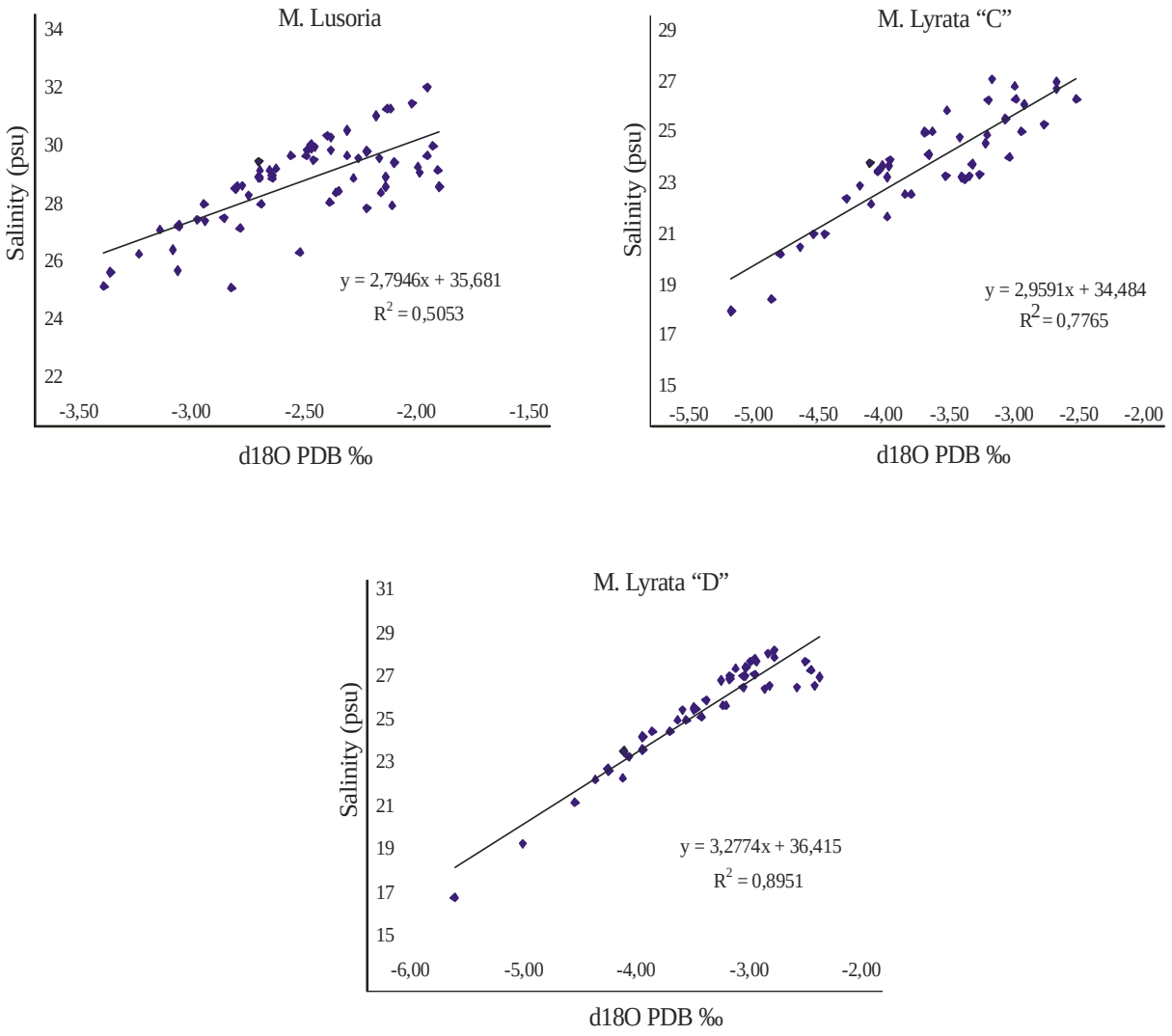

Fig. 5.8. Linear regressions between salinity values and δ^{18}O PDB ‰ measured in modern shells.

The indices of salinity calculated from $\delta^{18}O_w$ yielded higher values indicating high salinity in winter months than in summer months, indicating more precipitation rates. Linear regression between salinity rates and $\delta^{18}O_{PDB‰}$ shows low relationship, being an indicator of evaporation events caused by the absence of freshwater input, which characterises the place where the *M. lusoria* was found at.

The *M. lyrata "C"* $\delta^{18}O_{PDB‰}$ profile has $\delta^{18}O_w$ values ranging from -1.74 to -3.38 ‰ which are related to water temperature values ranging from 23.8 to 28.4° C with 26° C on average; salinity values show a range of 20.1 to 26.7 psu with a mean of 23.9 psu (Tab. 5.2). The relationship between salinity dates and $\delta^{18}O_{PDB‰}$ can be calculated by linear regression with

R^2 = 0.776 (n=44), indicting that salinity variation is linked to the different periods of precipitation, in which the $CaCO_3$ precipitated in *M. lyrata "C"* was influenced by freshwater input from the Cai River. In summer, with the increasing rainfall rate, water becomes lighter in $\delta^{18}O_w$ due to the decreasing salinity concentration (Tab. 5.2).

The indices of water temperatures in *M. lyrata "D"* range from 23.6 to 28° C with a mean of 26.4° C. From these values a profile of SMOW ‰ ranging from -1.52 to -4.24 ‰ was calculated. The salinity concentration varies widely with indices from 16.6 to 27.6 psu with 24.9 psu on average. The relationship between salinity and $\delta^{18}O_{PDB‰}$ revealed R^2 = 0,895 (n=44), which is in accordance with the seasonal standard of rainfall rates, showing periods more or less saline as observed in *M. lyrata "C"* (Tab. 5.2).

Month	Distance from umbo (mm)	$\delta^{18}O$ [PDB ‰]	$\delta^{13}C$ [PDB ‰]	Water temperature (°C)	SMOW ‰	Salinity [psu]
M. lusoria						
July (2002)	6	-2.69	1.25	28.4	-1.07	29.4
August	9	-2.96	0.18	26.9	-1.67	26.9
September	11	-2.51	0.37	26.3	-1.35	28.2
October	12	-3.05	0.14	25.7	-2.01	25.6
November	13	-2.35	0.33	25.5	-1.34	28.3
December	14	-2.13	0.36	25.1	-1.21	28.8
January (2003)	18	-1.99	0.37	24.7	-1.16	29.0
February	20	-2.04	0.48	25.7	-1.00	29.7
March	22	-2.33	0.51	26.9	-1.02	29.5
April	27	-2.51	0.32	28.0	-0.98	29.7
May	35	-2.57	0.69	27.8	-0.89	30.1
June	38	-3.04	0.29	27.5	-1.62	27.2
July	39	-2.93	0.40	28.1	-1.59	27.3
August	40	-3.05	0.29	27.9	-1.64	27.1
September	41	-3.38	0.12	27.6	-2.14	25.1
October	41.5	-2.38	0.41	26.2	-1.43	27.9
November	*					
December	42	-1.89	0.65	24.7	-1.29	28.5
January (2004)	43	-2.17	0.66	24.5	-1.39	28.1
February	44	-2.12	0.76	25.2	-1.19	29.9
March	44.5	-2.30	0.45	26.8	-1.02	29.6
April	47.5	-2.49	0.70	27.8	-0.99	29.7
May	49.5	-2.70	0.38	27.7	-1.22	28.7
June	51.5	-2.44	0.39	27.4	-1.03	29.5
July	52	-3.22	0.25	26.7	-1.87	26.1
August	52.5	-3.07	0.31	26.7	-1.83	26.3
September	*					
October	53	-2.33	0.41	25.5	-1.33	28.3
November	*					
December	54	-2.30	0.35	23.9	-1.65	27.0
January (2005)	54.5	-2.81	-0.20	23.9	-2.15	26.4
February	55	-2.09	0.31	25.5	-1.09	29.3
March	*					
April	55.5	-2.63	0.20	27.6	-1.19	28.9
M. lyrata „C“						
July (2002)	8	-4.10	-1.72	28.4	-2.48	23.7
August	10	-4.45	-1.77	26.9	-3.24	20.6
September	11	-4.09	-1.24	26.5	-2.88	22.1
October	13	-4.32	-1.72	25.6	-3.30	20.4
November	14	-3.96	-1.69	25.3	-3.01	21.6
December	15	-3.21	-1.62	25.1	-2.29	24.4
January (2003)	16	-2.93	-1.66	24.3	-2.18	24.9
February	18	-2.86	-1.36	25.8	-1.77	26.6
March	19	-3.19	-1.11	27.0	-1.87	26.1
April	20	-3.50	-1.80	28.0	-1.96	25.8
May	23	-3.61	-1.67	27.8	-2.12	25.2
June	24	-4.04	-1.35	27.7	-2.57	23.3
July	25	-3.96	-1.42	27.1	-2.62	23.1
August	26	-4.79	-2.13	27.4	-3.38	20.1
September	28	-4.50	-1.75	26.2	-3.36	20.2
October	29	-3.52	-1.38	25.1	-2.60	23.2
November	30	-3.37	-1.81	24.2	-2.65	23.0
December	32	-3.14	-1.84	23.8	-2.51	23.6
January (2004)	34	-3.36	-1.89	24.3	-2.61	23.2
February	35	-3.31	-1.65	24.6	-2.50	23.6
March	36	-3.41	-2.29	26.3	-2.23	24.7
April	37	-3.95	-1.70	27.8	-2.46	23.8

May	41	-4.04	-1.58	27.7	-2.57	23.3
June	42	-3.95	-1.72	27.5	-2.52	24.6
July	43	-4.54	-1.90	27.2	-2.18	20.9
August	44	-3.65	-1.99	26.7	-2.40	24.0
September	45	-2.98	-1.37	26.7	-1.74	26.7
October	46	-3.20	-1.81	25.5	-2.20	24.8
November	47	-2.66	-1.94	25.0	-1.76	26.6
December	48	-2.51	-1.77	23.9	-1.86	26.2
January (2005)	49	-2.76	-2.00	23.9	-2,10	25.6
February	50	-3.06	-2.52	25.5	-2.05	25.5
March	51	-2.91	-1.72	25.5	-1.91	26.1
April	52	-3.62	-2.29	27.6	-2.18	25.0
M. lyrata „D“						
April (2003)	8	-4.00	-1.85	28.0	-2.47	23.7
May	10	-4.03	-1.76	27.8	-2.53	23.5
June	15	-4.04	-1.83	27.5	-2.62	23.1
July	16	-3.54	-1.46	27.1	-2.20	24.8
August	17	-3.61	-2.00	27.4	-2.20	24.8
September	18	-4.10	-1.66	26.6	-2.86	22.2
October	19	-3.19	-0.75	26.3	-2.03	25.5
November	20	-2.48	-1.01	25.3	-1.52	27.6
December	21	-2.40	-0.74	23.6	-1.80	26.4
January (2004)	22	-2.55	-0.88	24.2	-1.82	26.3
February	24	-2.61	-1.01	25.0	-1.71	27.8
March	32.5	-2.96	-1.36	27.1	-1.62	27.1
April	33.5	-3.39	-1.91	27.8	-1.90	26.0
May	34	-3.10	-2.37	27.8	-1.60	27.2
June	38	-3.66	-1.94	27.4	-2.26	24.1
July	38.5	-5.59	-3.46	27.2	-4.24	16.6
August	39	-3.41	-1.70	26.7	-2.16	25.0
September	*					
October	39.5	-2.84	-1.45	25.5	-1.84	26.3
November	*					
December	40	-2.35	-1.77	23.9	-1.70	26.8

* No information

Table. 5.2. Shell profiles normalized to calendar months with monthly isotope values and water temperature of the Nha Trang region.

The profile of $\delta^{18}O_{PDB‰}$ for the mid-Holocene *Spondylus sp* 5537 ±55 cal yr BP is shown in Tab. 5.3. From a total of 139 powder samples collected from the shell, 87 samples were used to calculate the paleotemperature.

The investigation of $\delta^{18}O$ isotopic variation in the graph of Fig. 5.4, *Spondylus sp* revealed that isotope values are linked to hydrological conditions. This clear isotopic variation was observed mainly between 36 and 104 mm (Tab. 5.3) where periods of light and heavy values from -2.60 to -0.47 $\delta^{18}O_{PDB‰}$ respectively were found.

Due to the large variability indicating seasonality, records of temperature were calculated using a scale of SMOW values because the isotope dates suggested a seasonal precipitation influx, although the clam had assimilated isotopes in marine conditions (Fig. 5.3). Through the equation 1 applied to estimate the paleotemperature by a $\delta^{18}O_w$ scale ranging from 0 ‰, linked at - 0.47 PDB ‰ of *Spondylus sp*, to - 0.5 ‰ linked at - 2.60 PDB ‰, the results of water temperature were obtained ranging from 23.1 to 30.7° C with a mean of 27.5° C to 5605 - 5470 cal yr BP.

Furthermore, water temperatures were calculated on the basis of constant respective SMOW ‰ values of 0 and - 0.5 ‰. These results showed a difference of 2.4° C water temperature, which represent the influence of precipitation rates during the different seasons (Tab 5.3).

Distance from umbo (mm)	$\delta^{18}O$ [PDB ‰]	$\delta^{13}C$ [PDB ‰]	$\delta^{18}O_w$ from 0 to -0.5 ‰	T° C from 0 to - 0.5 ‰	T° C at 0 ‰ $\delta^{18}O_w$	T° C at - 0.5 ‰ $\delta^{18}O_w$
36	-1,60	0,32	-0.22	27.3	28.4	26.0
37	-2,12	0,59	-0.38	29.0	30.8	28.5
38	-1,91	0,67	-0.30	28.3	29.9	27.5
39	-2,11	0,65	-0.36	29.0	30.7	28.4
40	-1,55	0,66	-0.21	27.1	28.1	25.8
41	-1,39	0,94	-0.15	26.6	27.4	25.0
42	-2,12	0,84	-0.38	29.0	30.8	28.5
43	-1,91	1,11	-0.31	28.7	29.8	27.5
44	-1,68	1,23	-0.26	27.5	28.7	26.4
45	-1,37	1,82	-0.14	26.6	27.3	25.0
46	-0,94	2,09	-0.05	25.0	25.3	22.9
47	-1,04	2,33	-0.07	25.4	25.7	23.4
48	-0,99	2,33	-0.05	25.2	25.5	23.1
49	-1,14	1,92	-0.10	25.7	26.2	23.9
50	-1,93	1,84	-0.32	28.4	29.9	27.6
51	-2,08	1,87	-0.35	28.9	30.6	28.3
52	-1,94	1,91	-0.33	28.4	30.0	27.6
53	-2,10	2,13	-0.36	29.0	30.7	28.4
54	-1,69	1,78	-0.26	27.5	28.8	26.4
55	-1,74	1,65	-0.27	27.8	29.0	26.7
56	-1,81	1,47	-0.29	27.9	29.4	27.0
57	-1,76	1,59	-0.27	27.8	29.1	26.8
58	-1,78	1,42	-0.28	27.9	29.2	26.9
59	-2,24	1,84	-0.45	29.4	31.4	29.0
60	-2,17	1,75	-0.39	29.2	31,0	28.7
61	-1,79	1,90	-0.29	27.9	29.3	26.9
62	-1,61	1,72	-0.23	27.3	28.4	26.1
63	-2.59	0.14	-0.49	30.7	33.0	30.7
64	-1.65	1.14	-0.24	27.4	28.6	26.3
65	-1.08	1,27	-0.08	25.5	25.9	23.6
66	-0.69	2.01	-0.01	24.0	24.1	21.7
67	-0.72	2.38	-0.02	24.1	24.2	21.9
68	-1.23	1.77	-0.11	26.1	26.6	23.4
69	-1.14	1.09	-0.09	25.7	26.2	23.9
70	-1.53	1.17	-0.20	27.1	28.0	25.7

71	-1.41	1.58	-0.16	26.7	27.5	25.1
72	-1.15	2.52	-0.10	25.8	26.3	23.9
73	-1.01	2.16	-0.06	25.3	25.6	23.3
74	-1.93	1.79	-0.32	28.4	29.9	27.6
75	-1.52	1.85	-0.19	27.1	28.0	25.6
76	-1.25	2.23	-0.12	26.1	26.7	24.4
77	-1.24	2.09	-0.12	26.1	26.7	24.3
78	-1.66	1.83	-0.24	27.5	28.6	26.3
79	-1.92	1.88	-0.31	28.4	29.9	27.5
80	-2.42	1.65	-0.47	30.0	32.2	29.9
81	-2.33	1.56	-0.44	29.7	31.8	29.4
82	-2.56	1.54	-0.48	30.6	32.9	30.5
83	-2.24	1.75	-0.41	29.4	31.4	29.0
84	-2.20	1.29	-0.40	29.3	31.2	28.9
85	-0.66	1.09	-0.01	23.9	24.0	21.6
85.5	-0.91	1.03	-0.04	24.9	25.1	22.8
86	-1.29	1.57	-0.13	26.3	26.9	24.6
86.5	-1.07	1.29	-0.07	25.5	25.9	23.5
87	-1.52	1.69	-0.20	27.0	28.0	25.7
87.5	-2.45	0.78	-0.47	30.1	32.3	30.0
88	-2.37	1.06	-0.45	29.8	32.0	29.6
88.5	-2.11	1.34	-0.34	29.0	30.8	28.4
89	-2.07	1.55	-0.35	29.9	30.6	28.2
89.5	-2.24	1.43	-0.41	29.4	31.4	29.0
90	-2.27	1.38	-0.43	29.4	31.5	29.2
90.5	-2.01	0.86	-0.34	28.7	30.3	28.0
91	-1.58	1.31	-0.21	27.2	28.3	25.9
91.5	-1.34	1.34	-0.14	26.5	27.1	24.8
92	-0.74	1.51	-0.02	24.2	24.3	22.0
92.5	-0.94	1.64	-0.04	25.1	25.3	22.9
93	-0.77	1.61	-0.03	24.3	24.5	22.1
93.5	-1.20	0.93	-0.11	26.0	26.5	24.2
94	-1.48	1.03	-0.18	26.9	27.8	25.5
94.5	-1.10	1.18	-0.08	25.6	26.0	23.7
95	-1.52	1.02	-0.19	27.1	28.0	25.6
95.5	-1.59	1.06	-0.22	27.2	23.8	26.0
96	-2.46	1.34	-0.48	30.1	32.4	30.0
96.5	-2.12	1.01	-0.37	29.0	30.8	28.4
97	-2.41	1.35	-0.46	30.0	32.2	29.8
97.5	-2.30	1.64	-0.44	29.5	31.6	29.3
98	-2.22	1.73	-0.40	29.3	31.3	28.9
98.5	-2.58	0.90	-0.49	30.6	32.9	30.6
99	-2.00	0.93	-0.34	28.6	30.2	27.9
99.5	-1.02	1.61	-0.06	25.3	25.6	23.3
100	-0.85	1.01	-0.03	24.7	24.9	22.5
100.5	-0.47	1.05	0.00	23.1	23.1	20.7
101	-1.49	1.11	-0.18	26.9	27.8	25.5
101.5	-1.67	1.23	-0.25	27.5	28.7	26.4
102	-1.63	1.51	-0.23	27.4	28.5	26.2
102.5	-1.45	1.59	-0.17	26.8	27,7	25.3
103	-1.38	1.75	-0.52	26.6	27.3	25.0
103.5	-2.24	1.74	-0.42	29.3	31.4	29.0
104	-2.60	1.45	-0.50	30.7	33.1	30.7

Table 5.3. Isotope profiles and temperature values were estimated from the fossil shell *Spondylus sp* 5537 ± 55 cal yr BP.

5.5. Discussion

5.5.1. Shell growth

$\delta^{18}O_{PDB‰}$ measurements gave important information about the growth of modern shells in connection with the local environment, which show different hydrological conditions. The isotopic records in the shells demonstrate concordance between temperature and rainfall rates, where local seasonality was evaluated by $\delta^{18}O_{PDB‰}$ precipitated in shell-carbonate (Fig. 5.6). In this way, distinct carbonate increments suggest that different seasons of the year provide the pattern of shell growth.

Once a pattern of shell growth was accomplished, it was possible to demonstrate that a great increment of carbonate grew during spring and summer season. This great increment of carbonate is changed by cooler temperatures in autumn and winter and therefore decreases. Observations on the growing time in every clam identified maximum ages of 34 months.

The *M. lusoria* lived 34 months, presenting a rate of ontogenic growth of 1.63 mm/month. However, during the spring-summer months of the second year, the growing rate increased to 3.1 mm/month (Fig. 5.6), while during the warmer period of the third year, the growing rate decreased to 2 mm/month. In WP4, there is a lower rainfall rate than in WP3, which explains the lower growing rate of the shell during the last warm period. It should be mentioned that the growing rate observed in WP3 in *M. lusoria* corresponds to the observations of Wang and Peng (1990).

The growing rate of *M. lyrata "C"* was evaluated at 1.52 mm/month after 34 months of life time with the last two similar warm periods archived in the shell (Fig. 5.6). In WP3 the shell had grown 1.33 mm/month, whereas in WP4 the growth was evaluated at 1.75 mm/month. The WP4 period shows that more carbonate was developed in four months time. Also, heavier isotopic values were caused by a lower rainfall rate.

The growth of *M. lyrata "D"* was evaluated after 21 months of life time. It is characterized by a long interval with an increment rate of 1.90 mm/month, whereas the rate in WP3 and WP4

constitutes 2 mm/month and 4 mm/month respectively (Fig. 5.6). Additionally, its profile has a drilling series reaching back to December 2004 because further drilling was impossible because of the fact that the rim of the shell was broken.

M. lyrata "C" and "D" do not show similar growth based on isotope records, although they lived in the same environment. In September of WP3 the isotope value in *M. lyrata "C"* is 0.40 $\delta^{18}O_{PDB‰}$ lighter than in *M. lyrata "D"* and in July of WP4 it is 1.05 $\delta^{18}O_{PDB‰}$ lighter in *M. lyrata "D"* than in July in *M. lyrata "C"* (Table 5.2). As the shells grew in the same place, the isotopic difference may be due to physiological differences between specimens as described below.

The recognition of the vital effect on the shells is necessary because of the different species of shells. It was tried to identify the difference of the growing rate expressed by isotopic fractions without taking into account hydrological conditions.

Linear regression analysis between $\delta^{13}C$ vs. $\delta^{18}O$ in order to observe the kinetic effect suggests, that *Spondylus sp*, *M. lusoria* and *M. lyrata "C"* have aragonite precipitates in equilibrium with the environment through the low correlation between $\delta^{13}C$ vs. $\delta^{18}O$ (McConnaughey et al., 1997; McConnaughey, 1989a, 1989b; Carré et al., 2005). A marked difference is observed in *M. lyrata "D"* in the linear regression at R^2= 0.44, showing a smooth equilibrium between carbonate and oxygen isotopes (Fig. 5.9).

The different between species affirm the "vital effect", shifting isotopic assimilation among the shells during the ontogenetic development (Buchardt, 1977). Due to the fact that a difference was only recognized in $\delta^{18}O_{PDB‰}$ without their SMOW ‰ values, it can be ascertained as a result, that isotope precipitation among the shells represents a physiological variation of each specimen.

Therefore, it was tried to observe the "vital effect" by the difference between each shell in $\delta^{18}O_{PDB‰}$ assimilated during the shell mineralization; after subtracted their respective amount of SMOW ‰ was ranging between -0.95 ‰ to -1.10 ‰, exhibiting a difference of 0.15 ‰ in

$\delta^{18}O_{PDB‰}$. This deviation could represent a variation of $\delta^{18}O_{PDB‰}$ in different species of clams, but there is a difference between both *M. lyrata* sampled in the same environment. Moreover, in *M. lyrata "D"* a vital effect for the equilibrium between the isotopes, influenced by the kinetic effect, was already noted. Thereby, the probable factor ascribed to the vital effect is 0.1 ‰ $\delta^{18}O_{PDB‰}$ found between *M. lyrata "C"* and *M. lusoria*, which grew in distinct environments. On the other hand, when it comes to the comparison with *Spondylus sp* the difference increases to 0.2 $\delta^{18}O_{PDB‰}$, which might be linked to distinct temperatures between the periods.

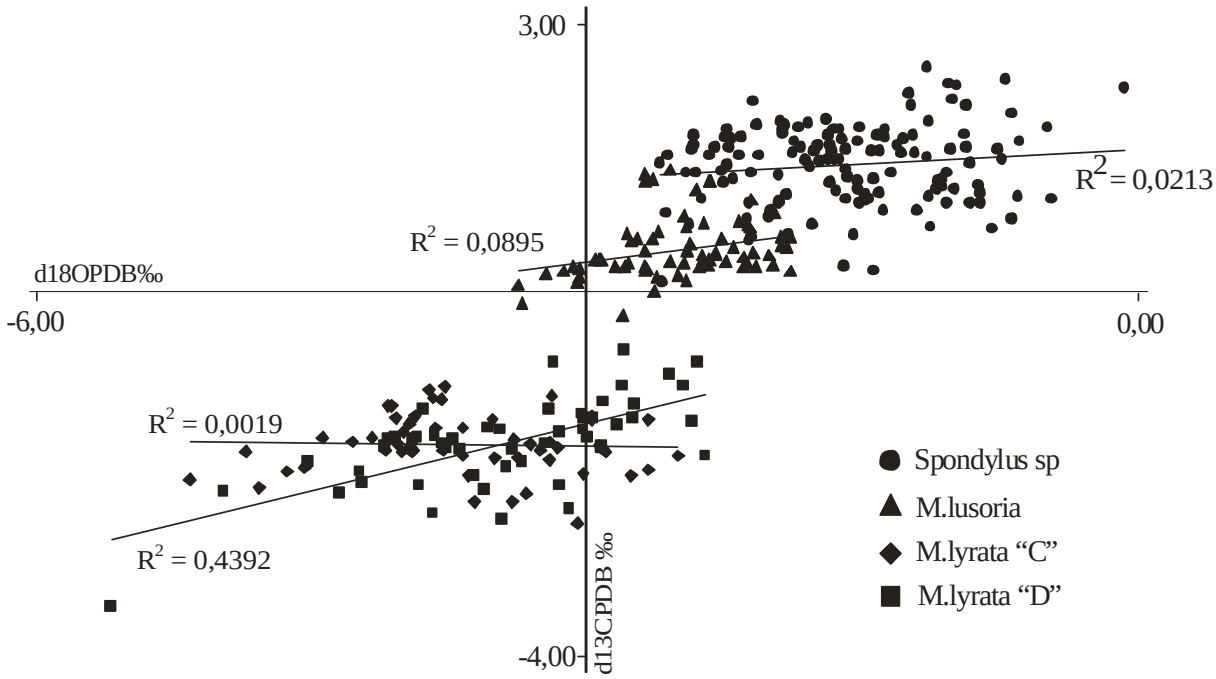

Fig. 5.9. $\delta^{13}C$ vs. $\delta^{18}O$ values in linear regression from a series of shell samples used to evaluate the kinetic effect.

5.5.2. Evaluation of modern temperatures and paleotemperatures

Modern water temperature examined at the latitude of 12° 24` N was linked to the lifetime of recent shells and was afterwards normalized to monthly variation (Fig. 5.7). The water temperature presented an annual mean of 26.4° C, ranging from 23.7 to 28.5° C. Recent works on the modern coastal surface temperature in the studied region revealed values from 24 to 30.3° C (Rojana-anawat et al., 2000), measured by a CTD taken at a maximal depth of 5 m during April and May of 1999. In addition, Tang et al. (2004) provided a standard for winter-temperature at 25° C and summer-temperatures higher than 28° C.

The results of the measurement of paleotemperature from the axial growth in the specie *Spondylus sp* showed that during sea-level highstand in the mid-Holocene the water-temperature values ranged from 23.1° C ($\delta^{18}O_w$ = 0 ‰) to 30.7° C ($\delta^{18}O_w$ - 0.5 ‰) with an average of 27.5° C (Fig. 5.9). These temperature values for the mid-Holocene are very similar to the values that were found recently by Wei et al. (2007) in the coastal area of Sanya on Hainan, island localized in the northern South China Sea. They have reconstructed a temperature interval from 23.9 winter to 30.5° C summer with an average of 27.2° C, based in coral records during the period 6271 - 6175 cal yr BP.

Comparing the values of modern water temperature and paleotemperatures ($\delta^{18}O_w$ from 0 to - 0.5 ‰), their mean presents a difference by 1.2° C, with the mean of modern $\delta^{18}O_{PDB‰}$ temperature being 26.3° C, whereas the mean of paleotemperature is 27.5° C. However, when values of modern water temperatures are plotted with paleotemperatures$_{\delta 18OPDB‰}$, a considerable difference within the evaluated period is observed. This applies mainly to summer season, because during the mid-Holocene the water temperature was warmer in summer than at the present time, in maximal 2.2° C, whereas the temperature in winter reached roughly 24° C in both periods (Fig. 5.10).

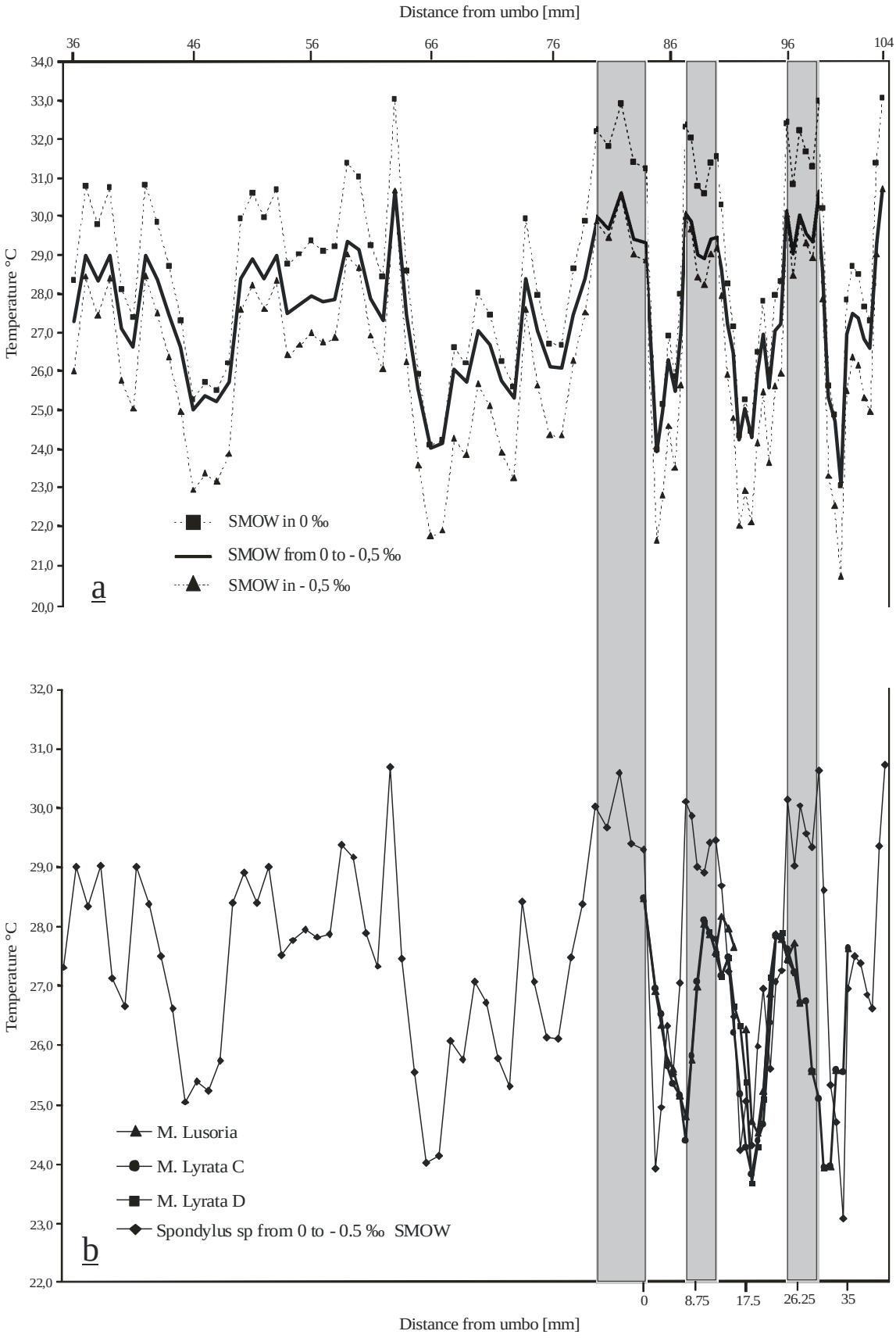

Fig. 5.10. The plot shows two profiles: in "a" the probable paleotemperature$_{\delta 18OPDB‰}$ records concern the distance on the shell from 36 to 104 mm with $\delta^{18}O_w$ varying from 0 to 0.5 ‰ (continued line) and the values of temperatures just at 0 ‰ and - 0.5 ‰, showing the hydrologic balance between low and high precipitation rates respectively (dashed line). In "b" the temperature of modern shells is compared with paleo-water-temperature, calculated on smow from 0 to 0.5 ‰.

In order, to verify the difference between modern and paleotemperature during summer, arithmetic mean values in mid-Holocene and modern summer periods were compared. This procedure established a modern summer water temperature with a mean of 27.9° C and a paleo-summer-temperature with a mean reaching 29.7° C and several records rising above 30° C. The temperature difference amounts to 1.8° C, indicating that the mid-Holocene summer seasons were warmer than summer seasons of at present time.

However, upwelling event only take place in summer in the studied area. This regional upwelling in SE-Vietnam is formed during the southwesterly monsoon between 11° and 15° N and west of 110° E (Fig. 5.11).

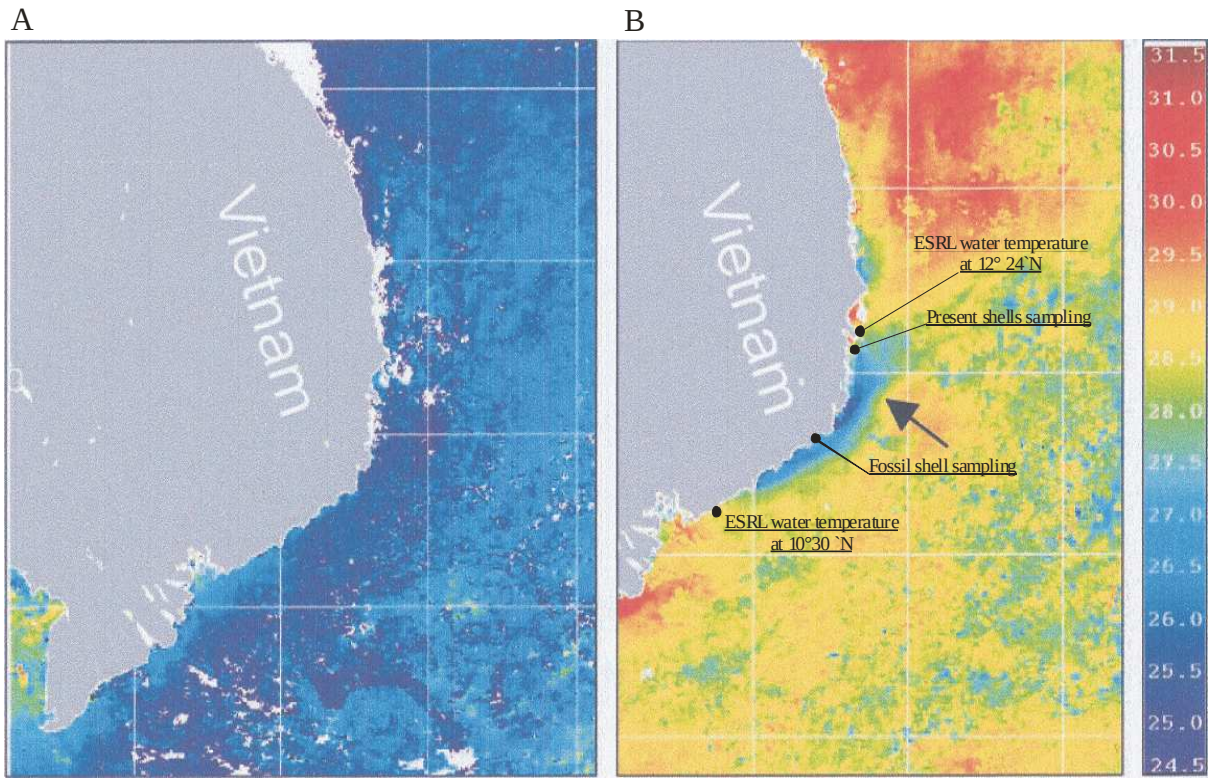

Fig. 5.11. “A” shows the SST of Feb. 1999; “B” shows the SST in the summer season of July 1999. Arrow indicates cold water upwelling from the coast towards the open ocean. The shell samples as well as the ESRL water temperature in 12° 24` N were collected in the area of upwelling, whereas the ESRL water temperature at 10° 30` N is outside of the upwelling area.

Therefore, the difference between the seasonal water temperature at 5605 - 5470 cal yr BP and the present time (Fig. 5.9) can be misinterpreted because the present water temperature in summer is influenced by cold upwelling water, which provokes the great temperature

difference between the two studied periods. Thus, another comparison with water-temperature records outside of the upwelling area, southward near the Mekong Delta with records at 10° 30` N and 108° 48` to 110° 36` E is proposed.

The comparison presented in Fig. 5.13 shows higher temperature outside of the upwelling area (Fig. 5.12). For this reason, the water-temperature indices from this region compared with the mid-Holocene temperature presented no significant difference on average. However, paleotemperature indices of summer seasons are approx. 1° C warmer than modern water temperature 10°.30` N

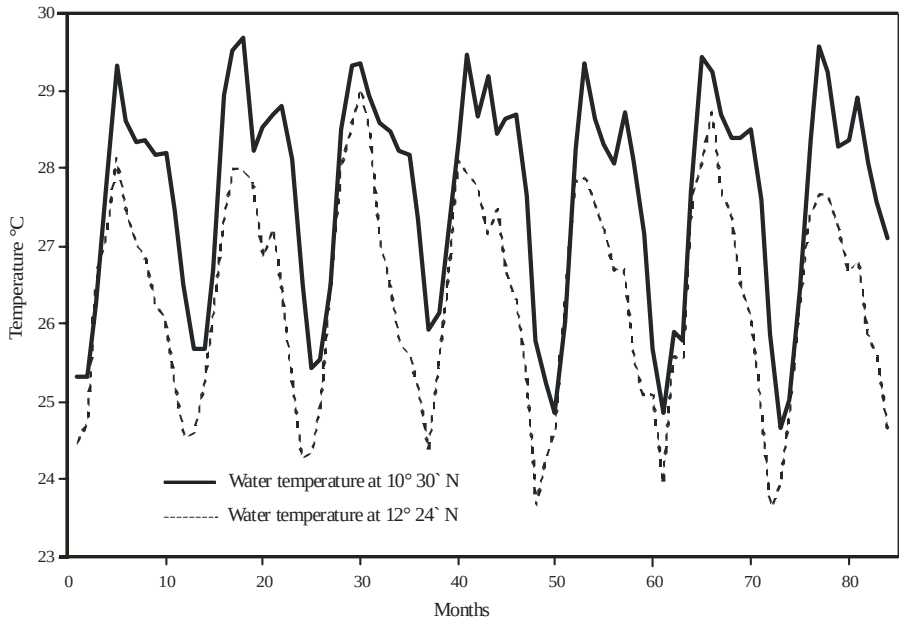

Fig. 5.12. The water-temperature records sought to ESRL are presented in two positions. The temperature at 10° 30` N is warmer than at 12° 24` N, being a result linked to different isotherms.

Consequently, all the results of the water temperature found between the studied periods, the assumption that the water temperature was 1° C warmer during summer periods in the mid-Holocene to 5605 - 5470 cal yr BP became fairly realistic. Furthermore, the water temperature records indicate strong seasonality, defined as a greater difference between summer and winter periods, in mid-Holocene.

Jones et al. (2005), who worked with oxygen isotopes from shells, suggest a higher seasonality for the northeastern coast of Florida during the mid-Holocene, which Hodell et al.

(1991) identified for the Caribbean region. Furthermore, Hodell et al. (1991) suggests a Holocene climate model with a high rate of evaporation and precipitation during each annual cycle. Normally, the increase of evaporation and precipitation rates is controlled by insolation that is manipulated by orbital forcing. As regards the Holocene, Hodell et al. (1991) describe a long-term insolation evoked by orbital changes, which might be the reason for the seasonality observed in the paleotemperatures on the southeast Vietnamese coast.

This orbital forcing is generally controlled by precession and obliquity cycles, increasing the amplitude of season. Obliquity alters the season distribution of insolation so that the amplitude of the season cycles is enhanced. Precession became important during the early mid-Holocene because it placed perihelion in the boreal summertime. Furthermore, it is able to cause a shift in the occurrence of the maximum insolation throughout the years with the highest insolation in the equatorial regions (Bush, 2001; Bush, 2005; Lorenz et al., 2006). Additionally, this warm period has been identified as the Holocene Thermal Maximum. It started around 10,000 y BP and ended around 5000 y BP, when insolation declined towards the present (Haug, 2001).

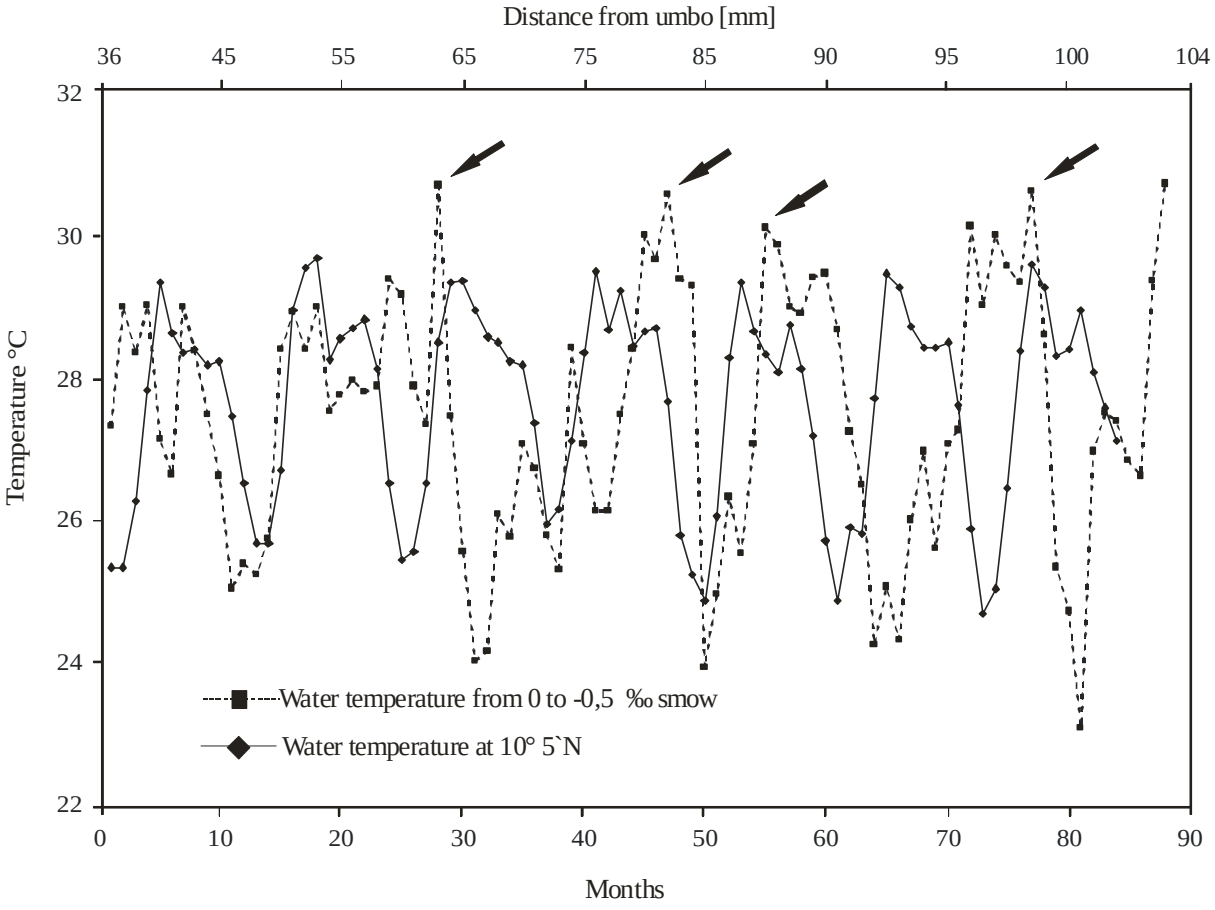

Fig. 5.13. Comparison between water paleotemperatures ($\delta^{18}O_w$ from 0 to -0.5 ‰) sampled in the dorsal position from 36 to 104 mm of Spondylus sp and water temperatures ERSL indices at the latitude of 10° 30` N from January 2000 to December 2006. The arrows show warmer temperature in summer than today. Colder water temperature during winter the mid-Holocene might be linked to the warmer isothermal at 10° 30` N.

5.5.3. Paleotemperature implications

The present water-temperature variation compared with the $\delta^{18}O_{PDB‰}$ paleotemperature during the mid-Holocene showed a seasonal difference in summer of approx. 1° C. This seasonal difference can be observed in graph 5.13, with the warmer peaks being above the 30° C in almost all summers in the mid-Holocene. Thus, this value suggests that the shallow water temperature of the coast was warmer than the present water temperature.

The warmer period indicated by the water temperature during the mid-Holocene for the southeast Vietnamese coast might be a part of the warmer period already described as the Holocene Thermal Maximum period (Hypsithermal). In this connection, effects of rapid climate changes could not be observed in this work. The Hypsithermal period is an episode, in which the magnitude of insolation increased by the orbital variation of the earth between

10,000 cal yrs BP and approx. 5000 cal yrs BP. Studies show that during this period the maximum occurred between 8000 and 7000 cal yr BP (Duplessy et al., 2001 and Haug et al., 2001). Nevertheless, Thompson et al. (1995) suggested that the maximum occurred between 6500 and 5200 yr BP.

Concerning the regional discussion, Röthlisberger (1986) found warmer temperatures during the mid-Holocene in New Zealand, and Gagan et al. (1998) identified temperatures about 1° C higher than it is today around 5350 cal yr BP in Australia. In the North Pacific region, water temperature has been studied for the last 7000 yrs, showing an increase of 1.09° C up to the present for the South China Sea (Kim et al., 2004). However, these data are mentioned for the period from the mid-Holocene until today, assuming that the water temperature of the entire South China Sea does not affect coastal areas, where warm temperatures in the studied interval are a result of insolation that increased during the mid-Holocene.

In northern Vietnam, paleoclimatic reconstructions were carried out in the Song Hong Delta (Red River). Li et al. (2006a; 2006b) reconstructed changes in vegetation through palynological study. Firstly, these works investigated the climate variation since the last deglaciation until the present time at the Song Hong Delta. Secondly, the climate change with anthropogenic impact during the Holocene was presented. For the period studied here, the above mentioned palynological records between 6500 - 5200 cal yrs BP indicated a cooling climate, which is in contrast to what is presented here as well as to what was described for northern Vietnam (Wei et al., 2007).

Additionally, evidence of elevated mid-Holocene temperatures was derived from the deposit where the *Spondylus sp* had been. The deposit was completely composed by coral and mollusc fragments dated between 5686 to 4835 cal yr BP, indicating its time of formation. This attribute of beachridge, consisting of a great quantity of coral fragments, indicates that during the period of sea-level highstand a significant death rate of these organisms occurred. Coral bleaching occurs on three levels, all of them based on rising water temperature, when

the average temperature reaches 1 and 2° C above the mean water temperature in tropical regions or when temperatures exceed 30° C (Glynn, 1993, 1996; and Buchheim, 1998).

5.6 Conclusions

1. Modern $\delta^{18}O_{PDB‰}$ and $\delta^{13}C_{PDB‰}$ isotope values identified in shells corresponded to hydrological conditions where they were collected. This is mainly true for the salinity results that showed variable conditions of the coastal system: freshwater intrusion for the two *M. lyrata* specimens and evaporation/precipitation rates for *M. lusoria*.
2. Due to the O-isotope measurement in the three growth profiles of shells, it was possible to elaborate a seasonal standard between isotopes and precipitation/temperature on the Nha Trang coast. Furthermore, with the knowledge of $\delta^{18}O_{PDB‰}$ fluctuation within the system, it was possible to calculate precise values of $\delta^{18}O_w$.
3. Through the high quality of isotopes measured on the modern shells it was possible to identify a precise seasonality for shallow coastal water.
4. Water-paleotemperatures were calculated within the period 5605 - 5470 cal yr BP from one AMS-radiocarbon dated shell of *Spondylus sp*.
5. These mid-Holocene paleo-water-temperatures record revealed warmer coastal waters than today.
6. In more detail, estimations showed that during the maximum sea-level highstand the water was approx. 1° C warmer in the summer season than modern summer water temperatures from oceanographic measurements and recalculated from modern shells (cf. point 3). This indicates more pronounced seasonality in the mid-Holocene.
7. Ca Na beachridge sea-level highstand indicators in SE-Vietnam are mainly coral fragments. The death of this high amount of coral might have been induced by an increase of water temperature.

8. Finally, warmer water paleotemperature in shallow water identified on the SE-Vietnamese coast during the mid-Holocene 5604-5470 cal yr BP was probably connected with the “Holocene Thermal Maximum” in its later phase.

6. General discussion

Different coastal sediment deposits such as beachrocks, beachridges, washover and backbeach were used as sea-level indicators to reconstruct the Holocene sea-level curve for SE-Vietnam. Holocene coastal evolution is characterized by a mid-Holocene sea-level highstand reaching 1.52 m above the modern mean sea-level in the period 5690 to 5380 cal yr BP.

Furthermore, paleotemperature in coastal water during the mid-Holocene sea-level highstand was investigated. The results were compared with modern water temperatures, which proved that during the sea-level highstand between 5687 to 5377 cal yr BP the coastal water had more seasonality than today with regard to summer season (Fig 5.10). The period in the mid-Holocene characterized by a warmer water temperature might have provoked a significant death of constructor organisms, as coral fragments are the principal components deposited in beachridge. Despite the important premises already described in the present study for coastal evolution and paleoceanographic conditions some questions still remain unsolved.

The first question which has to be raised is why there is a low occurrence of beachrocks along the SE-Vietnamese coast.

Based on personal information and the information provided by authors as Korotky et al. (1995) and Tam (1991), the development of beachrocks was reported throughout the coast of Vietnam, but their occurrence is insignificant because of some hydrographic characteristics of the studied coast.

The southeast Vietnamese coast displays several characteristics that make one expect the formation of even more beachrock, such as: supersaturation of $CaCO_3$ dissolved in water, high water temperature and a mesotidal regime generating a wet-dry cycle at the shoreline being a favourable environment for the precipitation of calcium carbonate. However, these favourable conditions for beachrock formation are contrasted by some noteworthy characteristics of the SE-Vietnamese coast that impede their formation.

The storage of sediment perhaps is reduced on the SE-Vietnamese coast due to the different landforms, including mountains being located near the water and thus hampering the deposition of sediment at the coast due to the step slop. Moreover, the lack of sedimentation can also occur due to the regime of coastal currents that do not prevent sediment deposition, but transport it off the coast. The fact that beachrocks are always found in sheltered position, as in embayment or opposite of platform reefs, representing a low-energy environment, supports this interpretation (Fig. 3.1).

The second important question is how beachridge is deposited in the coastal region. Is it only one deposit or is it fragmented in several places along the coast?

Studies about beachridge on the SE-Vietnamese coast showed that it has the same characteristics proposed by Hesp et al. (2005), being deposits found above the maximum spring tide and provoked by storm-surge events.

The deposits were found at three stations on the Vietnamese coast with approx. 34.8 km, of maximal distance between them. Two locations were in the vicinity of Ca Na town and the third was in Phan Rang, all showing very similar characteristics: sediment consisting almost exclusively of carbonate skeleton, buried in the relief and approx. 2.67 m above the present mean sea level in the stations of Ca Na. The location in Phan Rang, the height of beachridge, could not be taken into consideration because the place where the beachridge was found was heavily affected by anthropogenic activity.

From these characteristics connected with the definition by Hesp et al. (2005), it could be inferred that the beachridge deposit may be only one formation, which is buried but runs parallel on the SE-Vietnamese coast. This argument was already discussed in chapter 4, but it has to be pointed out that the development of beachridge is a relevant issue concerning the coastal evolution in SE-Vietnam.

The third question to be solved is: Why was no beachrock cementation process observed within the interval of beachridge formation?

The beachrocks in the studied area are outstanding sea-level indicators enabling to reconstruct a sea-level curve from the early mid-Holocene in two phases. The first phase is between 6721 to 5869 cal yr BP, elevated at 1.32 m amsl; the second phase recognizes the final drop as well as the start of the sea-level stabilization, occurring between 3760 to 640 cal yr BP. However, during the period of beachridge formation from 5687 to 4836 cal yr BP, no beachrock cementation event could have been detected (Fig. 4.5).

The absence of a cementation process maybe is linked with some environmental changes because beachrock cementation needs a combination of stable substrate (regular grain size) and a slow sedimentation rate (e.g. Scoffin, 1987 and Moore, 1989). In this way, an unfavourable environment for beachrock cementation can be induced by weather conditions.

During the sea-level highstand in the mid-Holocene, when the beachridge was formed, the temperature of the water was warmer than at present (Fig. 5.10). Through the identification of warmer water temperature, it can be concluded that the climate conditions in the mid-Holocene provided a sea-surface temperature that was warmer than it is in the present time.

Several studies about climate conditions show that the increase of the sea-surface temperature has an immense impact on the weather conditions in so far as it turns their events more intense. As a result, the velocity of the wind, the storm frequency, and hurricane events are increased (e. g. Emanuel, 2005). The strengthening of these events is directly linked to an increase of the water current circulation as well as to storm-surge events. Thereby, an increase of the water force arriving on the SE-Vietnamese coast changed the characteristics of the beach substrate, preventing the cementation of beachrocks.

In addition, a fourth question could be answered with regard to this scenery: How was the fragmentary up to pebble-size deposited into the beachrigde.

Beachridge deposit consists of great amount of miscellaneous carbonate skeleton (see Fig. 4.4 and 4.6a, b), consisting of organisms having died due to the warmer water temperature during the studied period. The deposition of this material above the maximum spring-tide level in the

mid-Holocene indicated that the waves as well as storm-surge regimes during this period was much stronger than today, caused also by intensification of storms, which was provoked by an increasing temperature.

7. Final conclusions and suggestions

An exhaustive study and precise data have revealed that the coastal evolution in SE-Vietnam since the mid-Holocene has been strongly influenced by the sea-level highstand and the warming of the shallow sea during the mid-Holocene.

On the southern Vietnamese coast, three examples of beachrocks were found at two locations in Ca Ná and Son Hai towns. They were found exclusively in the intertidal zone. The research indicated that their lithification took place in the intertidal zone and that afterwards this marine characteristic changed due to the influx of freshwater from the vadose environment. Furthermore, the beachrocks` ages suggested three intervals of lithification, which are linked to different stages of sea-level.

The sea-level history in SE-Vietnam could be reconstructed with the help of beachrocks and beachridge. Through the beachrocks the sea-level rise as well as the sea level decline could be reconstructed. The sea-level highstand position was determined by investigating beachridge and underlying upperbeach deposits.

Regarding the period of the sea-level highstand between 5690 - 5380 cal yr BP, the reconstruction of the water temperature for the time interval 5605 - 5470 cal yr BP showed warmer temperatures in summer season by 1° C than the present seasonal variation measured between 2002 to 2005. This warmer water-temperature in summer during the mid-Holocene might have provoked the bleaching of reef-corals, which could be destroyed and deposited in beachridge by storm-surges or other episodes induced by extreme weather conditions.

As far as the evolution of the SE-Vietnamese coast is concerned, it was noted during this work that the SE-Vietnamese coast is less studied in comparison with other places in Vietnam as for instance the northern and southern deltas. Therefore, the demand for further study concerning this coastal area in order to better understand the coastal processes during sea-level fluctuation in SE-Vietnam is high. The findings presented in this study already indicate that dates from the coastal areas of Vietnam can provide precise evidence for their evolution.

Thus, objectives of future works could focus on the investigation of the circumstances of transport and deposition of sediment by means of beachrock formation; geophysical records on the coastal area could be used to identify the real distribution of beachridge; coastal water-temperature reconstructions covering a large time frame could enhance the knowledge about the sea-level highstand period.

8. References

Admiralty Chart n° 3883, Point Lagan to Cap Varella, 1:200000 (1971).

Alexandersson, T., 1972. Mediterranean Beachrock cementation: Marine precipitation of Mg-Calcite. In: Stanley, D. J. (Editor). The Mediterranean Sea: A Natural Sedimentation Laboratory. Dowden Hutchison & Ross, Pennsylvania, pp: 203-223.

Allen B.D., Anderson, R.Y., 1993. Evidence from western North America for rapid shifts in climate during the last glacial maximum. Science 260, pp: 1920-1923.

An, L.D., 1999. Discussion on the Process Forming the Co Lour of the Phan Thiet Red Sands. Journal of Geology, Series A V. 1-2, pp: 36-40.

An, L.D., 1996. The Fluctuation Holocene Sea Level in the Vietnamese Coastal Zone. Journal of Earth Science 18(4), pp: 365-367.

Auclair, A.-C., Joachimski, M.M., Lécuyer, C., 2003. Deciphering kinetic, metabolic and environmental controls on stable isotopic fractionations between seawater and the shell of *Terebratalia trasversa* (Brachiopoda). Chemical Geology 202, pp: 59-78.

Badyukov, D.D., 1986. Ancient shorelines as indicators of sea level. Journal of Coastal Research 2(2), pp:147-157.

Bathurst, R.G.C., 1971. Carbonate sediments and their diagenesis. Developments in Sedimentology 12. Elsevier Sciences, Amsterdam, 658 p.

Berdin, D.R., Siringan, P.F., Maeda, Y., 2004. Holocene sea-level highstand and its implications for the vertical stability of Panglao Island, Southwest Bohol, Philippines. Quaternary International 115-116, pp: 27-37.

Bernier, P., Dalongeville, R., 1996. Mediterranean coastal changes in beach-rock cementation. Z. Geomorphol. N.F:, Suppl. Bd. 102, pp: 185-198.

Bernier, P., Bonvallot, J., Dalongeville, R., Prieur, A., 1990. Le beach-rock de Temae (Ile de Moorea Polynésie française). Signification géomorphologique et processus diagenetiques. Zeitschrift für Geomorphologie N. F. 34 (4), pp: 435-450.

Bezerra, F.H.R., Lima-Filho, F.P., Amaral, R.F., Caldas, L.H.O. and Costa-Neto, L.X., 1998. Holocene coastal tectonic in NE Brazil. In: I. Stewart, C. Vital-Finzi (Ed.) Coastal Tectonics: Geological Society, London. 146, pp: 279-293.

Beier, J.A., 1985. Diagenesis of Quaternary Bahamian beach-rock: petrographic and isotopic evidence. Journal Sedimentary. Petrology 55, pp: 755-761.

Bird, M.I., Fifield, L.K., Teh, T.S., Chang, C.H., Shirlaw, N., Lambeck, K., 2007. An inflection in the rate of early mid-Holocene eustatic sea-level rise: A new sea-level curve from Singapore. Estuarine, Coastal and Shelf Science. 71, pp: 523-536.

Böhm, F., Joachimski, M.M., Dullo, W.-C., Eisenhauer, A., Lehnert, H., 2000. Oxygen isotope fractionation in marine aragonite of coralline sponges. Geochimica et Cosmochimica Acta. V. 64 N°. 10, pp: 1695-1703.

Bond, G., Kromer, B., Beer, J., Muscheler, R., Evans, M.N., Showers, W., Hoffmann, S., Lotti-Bond, R., Haydas, I., Bonani, G., 2001. Persistent solar influence on North Atlantic climate during the Holocene. Science 294, pp: 2130-2133.

Boyd, W.E., Lam D.D., 2004. Holocene Elevated Sea Levels on the North Coastal of Vietnam. Australian Geographical Studies 42 (1), pp: 77-88.

Buchardt, B., 1977. Oxygen isotope ratios from shell material from the Danish middle Palaeocene (Selandian) deposits and their interpretation as paleotemperature indicators. Palaeogeography, Palaeoclimatology, Palaeoecology 22, pp: 209-230.

Buchheim, J., 1998. Coral reef bleaching. Odyssey expeditions-Marine Biology Learning Centre Publications.

Bush, A.B.G., 2001. Pacific sea surface temperature forcing dominates orbital forcing of the early Holocene monsoon. Quaternary Research 55, pp: 25-32.

Bush, A.B.G., 2005 CO_2/H_2O and orbitally driven climate variability over central Asia through the Holocene. Quaternary International 136, pp: 15-23.

Caldas, L.H.O., 2002. Late quaternary coastal evolution of the northern Rio Grande do Norte coast, NE-Brazil. Doctor Thesis. Christian Albrecht University of Kiel 2002. 100 p.

Caldas, L.H.O., Stattegger, K., Vital, H., 2006 Holocene sea-level history from coastal sediments of the northern Rio Grande do Norte coast, NE Brazil. Marine Geology 228 pp: 39-53.

Calvet, F.; Cabrera, M.C.; Carracedo, J.C.; Mangas, J.; Pérez-Torrado, F.J.; Recio, C.; Travé, A., 2003. Beachrock from the island of La Palma (Canary Islands, Spain). Marine Geology 197, pp: 75-93.

Carpenter, S.J. Lohmann K.C., 1995. $\delta^{18}O$ and $\delta^{13}C$ values of modern brachiopod shells. Geochimica et Cosmochimica Acta 59 pp: 3749-3764.

Carré M., Bentaleb, I., Blamart, D., Ogle, N., Cardenas, F., Zevallos, S., Kalin, R.M., Ortlieb, L., Fontugne, M., 2005. Stable isotopes and sclerochronology of the bivalve *Mesoderma donacium*: potential application to Peruvian paleoceanographic reconstructions. Palaeogeography, Palaeoclimatology, Palaeoecology 228, pp: 4-25.

Chacón, E., Berrendero, E., Pichel, G.F., 2006. Biogeological signatures of microboring cyanobacterial communities in marine carbonates from Cabo Rojo, Puerto Rico. Sedimentary geology 185, pp: 215-228.

Chen, Z., Stanley, D.J., 1998. Sea-Level Rise on Easter China's Yangtze Delta. Journal of Coastal Research 14 N°1, pp: 360-366.

Choi, S.J., Chwae, U., Hoc Bui, Thanh Hai Tran, Thi Mai Pham, 2005. Preliminary Neotectonic study on southeastern coast of Vietnam. Geological Society of America, abstracts V.37, N°. 7, 73 p.

Clack II, G.R., 1975. Periodic growth and biological rhythms in experimentally growth bivalve. In: Rosenberg, G.D., Runcorn, S.K. (Eds.), Growth Rhythms and the History of the Earth's Rotation. Wiley, London, pp: 103-117.

Compton, S.J., 2006. The mid-Holocene sea-level highstand at Bogenfelds Pan on the southwest coast of Namibia. Quaternary Research 66, pp: 303-310.

Cooper, J.A.G., 1991. Beachrock formation in low latitudes: implications for coastal evolutionary models. Marine Geology 98, pp: 145-154.

Coudray, J., Montaggioni, L., 1986. The diagenetic products of marine carbonate as sea level indicators. In: O.v.d. Plassche (Editor), Sea-level research: a manual for the collection and evaluation of data. Geo Books, Norwich, pp: 311-360.

Craig, H., 1953. The geochemistry of the stable carbon isotopes. Geochimica et Cosmochimica Acta 3, pp: 53-92.

Dang, P.X., Mitsuguchi, T., Kitagawa, H., Shibata, Y., Kobayashi, T., 2004. Marine reservoir correction in the south of Vietnam estimated from an annually-banded coral. Radiocarbon 46, pp: 657-660.

Darwin, C., 1841. On a remarkable bar of sandstone off Pernambuco on the Coastal of Brazil. London Edinburgh Dublin Phil. Mag. J. Sci. 19, pp: 257-261.

Davis, A.M., Aitchison, J.C., Flood, P.G. Morton, P.G., Baker, R.G.V., Haworth, R.J., 2000. Late Holocene higher sea-level indicators from the South China coast. Marine Geology 171, pp: 1-5.

Denton, G.H., Kalén, W. 1973. Holocene climatic variation – Their pattern and possible cause. Quaternary Research 3, pp: 155-205.

Donnelly, P.J., Butler, J., Roll, S., Wengren, M., Webb III, T., 2004. A backbarrier overwash records of intense storms from Brigantine, New Jersey. Marine Geology 210, pp: 107-121.

Duplessy, J.-C., Ivanova, E., Murdmaa, I., Paterne, M., Labeyrie, L., 2001. Holocene paleoceanography of the northern Barents Sea and variations of the northward heat transport by the Atlantic Ocean. Boreas 30, pp: 2-16.

Elliot, M., deMenocal, P.B., Linsley, B.K., Howe, S.S., 2003. Environmental controls on the isotopic composition of *Mercenaria mercenaria*: Potential application to paleoenvironmental studies. Geochemistry Geophysics Geosystems V. 4 N° 7.

Emanuel, K., 2005. Increasing destructiveness of tropical cyclones over the past 30 years. Nature V. 436 (4), pp: 683-688.

Emrich, K., Ehhalt, D.H., Vogel, J.C., 1970 Carbon isotope fractionation during the precipitation of calcium carbonate. Earth and Planetary Science Letters 8, 363-371.

Epstein, S., Mayeda, T., 1953. Variation of O^{18} content of waters from natural Sources. Geochimica et Cosmochimica Acta 1953 Vol. 4, pp: 213-224. Pergamon Press, London.

Epstein, S., Buchsbaum, R., Lowenstam, H.A., and Urey, H.C., 1953. Revised carbonate-water isotopic temperature scale. Bull. Geol. Soc., Am 64, pp: 1315-1325.

Epstein, S., Buchsbaum, R., Lowenstam, H.A., and Urey, H.C., 1951. Carbonate-water isotopic temperature scale. Bull. Geol. Soc., Am 62, pp: 417-426.

Erlenkeuser, H., 1995. Stable carbon isotope ratios in the waters of the Laptve Sea/Sept. 94. In: Kassens, H., Pienpenburg, D., Thiede, J., Timokhov, L., Hubberten, H.-W., Priamikov, S. (Eds.): Russian-Germany cooperation: Laptve Sea System. Report on polar Research 176 pp: 170-177.

Erlenkeuser, H., Wefer, G., 1981. Seasonal growth of bivalves from Bermuda recorded in their ^{18}O profiles. Proceedings of the Fourth International Coral Reef Symposium, Manila, 1988 V. 2.

Fang, W., Fang, G., Shi, P., Huang, Q., Xei, Q., 2002. Seasonal structures of upper layer circulation in southern South China Sea From in situ observation. Journal geophysical Research, 107(C11), pp: 3202-3212.

Fairbridge, R.W., 1986, Monsoons and Paleomonsoons. Episodes 9, pp: 143-149.

Fleming, K., Johnston, P., Zwartz, D., Yokoyama, Y., Lambeck, K., Chappell, J., 1998. Refining the eustatic sea-level curve since the Last Glacial Maximum using far-and intermediate-field sites. Earth and Planetary Science Letters 163, pp: 327-342.

Filippi, M.L., Moscariello A., Hunziker J., 1997. Stable isotope in Lake Geneva carbonate sediments and molluscs: review and new data. Eclog. Geol. Helv. 90, pp: 199-210.

Folk, R.L., 1974. The nature history of crystalline calcium carbonate: effect of magnesium content and salinity, Journal Sedimentology Petrology 44, pp: 40-53.

Folk, R.L., 1993. SEM scanning of bacteria and nannobacterias in carbonate sediments and rocks. Journal of Sedimentary Petrology 63(5), pp: 990-999.

Font, Y., Calvet, F., 1997. Beachrocks, Holocenos de la Isla de La Reunión Océano Indico. Cuadernos de Geología Ibérica 22, pp: 81-102. (in Spanish).

Fontaine, H., Workman, D.R., 1997, Vietnam. In Moores, E.M. and Fairbridge, R.W. (eds), Encyclopedia of European and Asia regional geology, pp: 774-782. Chapman & Hall, London, United Kingdom.

Friedman, G.M., Sanders, J.E., 1978. Principles of Sedimentology. John Wiley & Sons New York. pp: 144-179.

Gagan, M.K., Ayliffe, L.K., Hopley, D., Cali, J.A., Mortimer G.E., Chappell, J., McCulloch, M.T., Head, M.J., 1998. Temperature and sea-surface water balance of the mid-Holocene tropical Western Pacific. Science 279, pp: 1014-1018.

Guerra, C.N., Kiang, H.C., Sial, N.A., 2005. Carbonate cement in contemporaneous beachrocks, Jaguaribe beach, Itamaracá island, northeastern Brazil: petrographic, geochemical and isotopic aspects. Anais da Academia Brasileira de Ciencais 77(2), pp: 343-352.

Gillikin, D.P., Ridder, F.D., Ulens, H., Elskens, M., Keppns, E., Baeyens, W., Dehairs, F., 2005. Assessing the reproducibility and reliability of estuarine bivalve shells (*Saxidomus giganteus*) for sea surface temperature reconstruction: Implications for paleoclimate studies. Palaeogeography Palaeoclimatology Palaeoecology 228, pp: 70-85.

Ginsburg, R.N., 1953. Beachrock in south Florida. Journal Sedimentary Petrology 23, pp: 85-92.

Gischler, E., Lomando, A.J., 1997. Holocene cemented beach deposits in Belize. Sedimentary Geology 110, pp: 277-297.

Given, R.K., Wilkinson, B.H., 1985a. Kinetic control of morphology, composition and mineralogy of abiotic sedimentary carbonates. Journal Sedimentary Petrology 55, pp: 109-119.

Glynn, P.W., 1993. Coral reef bleaching: ecological perspectives *Reports*. Coral Reefs 12, pp: 1-17.

Glynn, P.W., 1996 Coral reef bleaching: facts, Hypotheses and implications. Global Change Biology 2, pp: 495-509.

Gong, S.Y., Mii, H.S., Wei, K.Y., Horng, C.S., You, C.F., Huang, F.W., Chi,W.R., Yui,T.F., Torng, P.K., Huang S.T., Wang, S.W., Wu, C.J., Yang, M.K., 2005. Dry climate near the Western Pacific Warm Pool: Pleistocene caliches of the Nansha Island, South China Sea. Palaeogeography Palaeoclimatology Palaeoecology 226, p: 205-213.

Grossman, E.L., Ku, T.-L., 1986. Oxygen and carbon isotope fractionation in biogenic aragonite: Temperature effects. Chemical Geology (Isotope Geoscience Section) 59, pp: 59-74.

Grossman, E.E., Fletcher III, C.H., Richmond, M.B., 1998. The Holocene sea-level highstand in the equatorial Pacific: analysis of the insular paleosea-level database. Coral Reef 17, pp: 309-327.

Hall Jr. C., Dollase, W.A., Corbató, C.E., 1974. Shell growth in *Tivela stultorum* (Mawe, 1823) and *Callista chione* (Linnaeus, 1758) (Bivalve): annual periodicity, latitudinal differences, and diminution with age. Palaeogeography Palaeoclimatology Palaeoecology 15, pp: 33-61.

Hanebuth, J.J.T., Stattegger, K., Grootes, M.P., 2000 Rapid Flooding of the Sunda Shelf: A Late-Glacial Sea-level Records. Science 288, pp: 1033-1035.

Hanor, J.S., 1978. Precipitation of beachrock cements: mixing of marine and meteoric waters vs. CO_2 degassing. Journal of Sedimentary Petrology 48, pp: 489-502.

Haug, G.H., Hughen, K.A., Sigman, D.M., Peterson, L.C., Röhl, U., 2001. Southward migration of the intertropical convergence zone through the Holocene. Nature 293, pp: 1304-1307.

Hattin, E.D., Dodd, R., 1978. Holocene cementation of Carbonate sediments in the Florida Keys. Journal of Sedimentary Petrology 48(1), pp: 307-312.

Hesp, A. P., Hung, C.C., Hilton, M., Ming, L.C., Turner, M.I., 1998. A first Tentative Holocene Sea-level Curve for Singapore. Journal of Coastal Research 14 (1), pp: 308-314.

Hesp, H. Dillenburg, R.S., Barbosa, G.E., Tomazzelli, J.L., Ayup-Zouain, N.R., Esteves, L.S., Gruber, S.L.N., Toldo-Jr.,E.E., Tabajara, L.L.C.A. and Clerot, L.C.P., 2005. Beach Ridges, foredunes or transgressive dunefields? Definition and an examination of the Torres to Tramandai barrier system, Southern Brazil. Anais da Academia Brasileira de Ciencias 77(3), pp: 493-508.

Ho, C.R., Zheng, Q., Soong, Y.S., Kuo, N.J., Ho, J.H., 2000. Seasonal variability of sea surface height in the South Chine Sea observed with TOPE/POSEIDON altimeter data. Jounal Geophys Research 105(C6), pp: 13981-13990.

Hodell, D.A., Curtis, J.H., Jones, G.A., Higuera-Gundy, A., Brenner, M., Binford, M.W., Dorsey, K.T., 1991. Reconstrution of Caribbean climate changes over the past 10. 500 years. Nature 352, pp: 790-793.

Hong, W., Keppens, E., Nielsen, P., Riet, A.V., 1995. Oxygen and Carbon Isotope study of the Holocene Oyster reefs and Paleoenvironmental Reconstruction on the northwest coastal of Bohai Bay, China. Marine Geology 124, pp: 289-302.

Holail, H., Rasched, M., 1992. Stable isotopic composition of carbonate-cement recent beachrock along the Mediterranean and the Red Sea coasts of Egypt. Marine Geology 106, pp: 141-148.

Hopley, D., 1986. Beachrock as a sea-level indicator. In: O.v.d. Plassche (Editor), Sea level research: A manual for collection and evaluation of data. Geo books, Norwich, pp: 157- 173.

Horton, B.P., Gibbard, P.L., Mine, G.M., Morley, R.J., Purintavaragul, C., Stargardt, M.J., 2005. Holocene sea levels and paleoenvironments, Malay-Thai Peninsula, Southeast Asia. The Holocene 15(8), pp: 1199-1213.

Hu, J., Kawamura, H., Hong, H., Qi, Y., 2000. A Review on the currents in the South China Sea: Seasonal circulation, South China Sea Warm Current and Kuroshio intrusion. Journal Oceanography 56, pp: 607-624.

Huang, Q.-Z., Wang, W.-Z., Chen, J.-C., 1994. Tides, tidal currents and storm-surge set-up of South China Sea. In: Zhou, D., Liang, Y., & Zeng, C. (eds.), Oceanography of China Seas, Vol.1, Kluwer Academic Publishers, pp: 113-122. Dordrecht.

Hudson, J.D., 1977. Stable isotopic and limestone lithification: Journal of the Geological Society of London 133, pp: 637-660.

Ingram, B.L., Conrad, M.E., Ingle, J.C., 1996. Stable isotope and salinity systematics in estuarine waters and carbonates: San Francisco Bay. Geochimica et Cosmochimica Acta V. 60 N°. 3, pp: 455-467.

Israelson, C., Buchardt, B., Funder, S., Hubberten, H.W., 1994. Oxygen and carbon isotope composition of Quaternary bivalve shell as a water mass indicator: Last interglacial and Holocene, East Greenland. Palaeogeography Palaeoclimatology Palaeoecology 111, pp: 119-134.

James, N.P., Choquette, P.W., 1983. Limestone - The sea floor diagenetic environment. Geosciences Canada 10, pp: 162-179.

James, N.P., Choquette, P.W., 1984. Diagenesis limestones-The meteoric diagenetic environmental. Geosciences Canada 11, pp: 161-194.

James, N.P., Choquette, P.W., 1990. The sea-floor diagenetic environment. In: I.A. Mcreath and D.W. Morrow (Eds.), Diagenesis, Ottawa, Ontario, Canada, Geological Association of Canada, pp: 13-34.

James, N.P., Ginsburg, R.N., 1979. The seaward margin of Belize barrier and atoll reefs. International Association of Sedimentology, Special publication 3, 179 p.

Jia, G., Xie, H., Peng, P`an., 2006. Contrast in surface water $\delta^{18}O$ distributions between the Last Glacial Maximum and the Holocene in the Southern South Chine Sea. Quaternary Science Reviews 25, pp: 1053-1064.

Jones, B., Rosean, M.R., Renaut, R.W., 1997. Silica-Cemented beachrock from Lake Taupo, North Island, New Zealand. Journal of Sedimentary Research 67 (5), pp: 805-814.

Jones, D.S., 1980. Annual cycle of shell growth increment formation in two continental shelf bivalves and its paleoecologic significance. Paleobiology 6(3), pp: 331-140.

Jones, D.S., 1983. Sclerochronology: reading the record of the molluscan shell. American Scientist 71, pp: 384-391.

Jones, D.S., Williams, D.F., Arthur, M.A., 1983. Growth history and ecology of the Atlantic surf clam, *Spisula solidissima* (Dillwyn), as revealed by stable isotope and annual shell increments. Journal Exp. Marine Biology Ecology 73, pp: 225-242.

Jones, D.S., Arthur, M.A., Allard, D.J., 1989. Sclerochronological records of temperature and growth from shells of *Mercenaria mercenaria* from Narragansett, Rhode Island. Marine Biology 102, pp: 225-234.

Jones, D.S., Quitmyer, R.I., Andrus, C.F.T., 2005. Oxygen isotopic evidence for greater seasonality in Holocene shells of *Donax variabilis* from Florida. Palaeogeography Palaeoclimatology Palaeoecology 228, pp: 96-108.

Kelletat, D., 1989. Biosphere and man as agents in coastal geomorphology and ecology. Geoökodynamik Band 10, pp: 215-252.

Kelletat, D., 2006. Beachrock as sea-level indicator? Remarks from a Geomorphological point of view. Journal of Coastal Research 22 (6), pp: 1558-1564

Khadkikar, A.S., Rajshekhar, C., 2003. Microbial cement in Holocene beachrocks of South Andaman Islands, Bay of Bengal. Research Communication, Current Science, V. 84 N° 7, pp: 933-936.

Kim, J.-H., Rimbu, N., Lorenz, S.J., Lohmann, G., Schounten, S., Nam S.-I., Rühlemann, C., and Schneider, R.R., 2004. North Pacific and North Atlantic sea-surface temperature variability during the Holocene. Quaternary Science Reviews 23, pp: 2141-2154.

Kindler, P and Bain, R.J., 1993. Submerged Upper Holocene beachrock on San Salvador Island, Bahamas: Implications for a recent sea-level history. Geologische Rundschau 82, pp: 241-247.

Kinsman, J.J.D., 1969. Interpretation of SR^{+2} concentration in carbonate mineral and rocks. Journal Sedimentary Petrology 39, pp: 486-508.

Kira T., 1962. Shells of the Western Pacific in colours. V.1. 224 p.

Klein R.T., Lohmann, K.C., Thayer, C.W., 1996. Bivalve skeletons record sea-surface temperature and $\delta^{18}O$ via Mg/Ca and $^{18}O/^{16}O$ ratios. Geology V. 24 N°. 5, pp: 415-418.

Kneale, D., Viles, H.A., 2000. Beach cement: incipient $CaCo_3$-cemented beachrock development in the upper inter-tidal zone, North Uist, Scotland. Sedimentary Geology 132 (3-4), pp: 165-170.

Korotky, M.A., Razjigaeva, N.G., Ganzey, L.A.., Volkov, V.G., Grebennikova, T.A., Bazarova V.B., and Kovalukh N.N., 1995. Late Pleistocene-Holocene coastal development of islands off Vietnam. Journal Southeast Asian Earth Sciences 11 (4), pp: 301-308.

Krantz, D.E., Kronick, A.T., Williams, D.F., 1988. A model for interpreting continental-shelf hydrographic processes from the stable isotope and cadmium: calcium profiles of scallop shells. Palaeogeography Palaeoclimatology Palaeoecology 64, pp: 123-140.

Krantz, D.E., Williams, D.F., Jones, D.S., 1987. Ecological and paleoenvironmental information using stable isotope profiles from living and fossil molluscs. Palaeogeography Palaeoclimatology Palaeoecology 58, pp: 249-266.

Krumbein, W.E., 1979. Photolithotropic and Chemoorganotrophic Activity of Bacteria and Algae as Related to Beachrock Formation and Degradation (Gulf of Aqaba, Sinai). Geomicrobiology Journal V. 1 N° 2, pp: 139-203.

Lam, D.D., Boyd, W.E., 2000 Holocene coastal stratigraphc and a model from sedimentary development of the Hai Phong area in the Red River Delta, north Viet Nam. Journal of Geology (Vietnam) Series B, 15-16, 18-28.

Lanh, V.V. (ed.), 1997. Atlas of Natural Condition, Ecology and Bioproduction of Strong Upwelling Sea Region in Southern central Vietnam. National Centre of Natural Science and Technology of Vietnam, Institut of Oceanography, Hanoi. 125 p.

Land, L.S., Goreau, F.T., 1969. Submarine lithification of Jamaican reefs. Journal Sedimentary Petrology 12, pp: 457-462.

Land, L.S., Moore, C.H. Jr., 1980. Lithification, micritization, and syndepositional diagenesis of biolithites on the Jamaican island slope. Journal Sedimentary Petrology 50, pp: 357-369.

Lambeck, K., Johnston, P., 1998. The viscosity of the mantle: evidence from analyse of glacial rebound phenomena. In: Jackson, I. (Ed.), The Earth's Mantle. Cambridge University Press, Cambridge, pp: 461-502.

Li, Z., Saito, Y., Matsumoto, E., Wang, Y., Haruyama, S., Hori, K., Doanh, L.Q. 2006 a. Palynological record of climate change during the last deglaciation from the Song Hong (Red River) delta; Vietnam. Palaeogeography Palaeoclimatology Palaeoecology 235, pp: 406-430.

Li, Z., Saito, Y., Matsumoto, E., Wang, Y., Tanabe S., Vu, L.Q. 2006 b. Climate change and human impact on the Song Hong (Red River) Delta, Vietnam, During the Holocene. Quaternary International 144, pp: 4-28.

Lin, Ching-Fen, 1999. Oxygen Isotope Composition of Seawaters from the South China Sea and Luzon Strait. Master's Thesis, Taiwan. 80 p. (in Chinese, abstract in English). http://etd.lib.nsysu.edu.tw/ETD-db/ETD-search/view_etd?URN=etd-0719100-112551.

Long, A., 2001. Mid-Holocene sea-level change and coastal evolution. Progress in Physical Geography 25(3), pp: 399-408.

Longman, M. W., 1980. Carbonate diagenetic texture from near surface diagenetic environments. The American Association of Petroleum Geologists Bulletin 64(4), pp: 461-487.

Lorenz J.S., Kim, J.-H., Rimbu, N., Schneider, R.R., Lohmann, G., 2006. Orbitally driven insolation forcing on Holocene climate trends: Evidence from alkenone data and climate modelling. Paleoceanography 21, PA1002.

Lorrain, A., Paulet, Y.-M., Chauvaud, L., Dunbar, R., Mascciarone, D., Fontugne, M., 2004. $\delta^{13}C$ variation in scallop shells: Increasing metabolic carbon contribution with body size? Geochimica et Cosmochimica Acta V. 68 N°. 17, pp: 3509-3519.

Mabesone, J.M., 1964. Origin and age of the sandstone reefs of Pernambuco (North-eastern Brazil). Journal Sedimentary Petrology 35, pp: 715-726.

Macintyre, I.G., 1977. Distribution of submarine cements in a modern Caribbean Fringing reef, Galeta Point, Panama. Journal Sedimentary Petrology 47, pp: 503-516

Macintyre, I.G., 1985. Submarine cements – The Peloidal Question. In: Carbonate cements (Eds.) Schneidermann N. & Harris P.M. Society of Economic Palaeontologists and Mineralogists, 379 p.

MacLean, R.F., 1974. Geologic significance of bioerosion of beachrock. Proc. Int. Coral Reef Symp., Vol.2. Great Barrier Reef Comm., Brisbane, pp: 401-408.

Maeda, Y., Siringan, F., Omura, A., Berdin, R., Hosono, Y., Atsumi, S., Nakamura, T., 2004. Higher-than-present Holocene mean sea level in Ilocos, Palawan and Samar, Philippines. Quaternary International 115-116, pp: 15-26.

Magaritz, M., Gavish, E., Bakler, N. and Kafri, U., 1979. Carbon and oxygen isotope composition indicators of cementation environment in recent, Holocene, and Pleistocene sediments along the coast of Israel. Journal of Sedimentary Petrology 49(2), pp: 401-412.

Marchitto Jr., T.M., Jones, G.A., Goodfriend, G.A., Weidman, C.R., 2000. Precise temporal correlation of Holocene mollusk shells using Sclerochronology. Quaternary Research 53, pp: 236- 246.

Margaritz, M., 1983. Carbon and oxygen isotope composition of recent and ancient coated grains. In: T.M. Peryt (Editor), Coated grains. Springer Verlag, Berlin, pp: 27-37.

Mathers, S.J., Zalasiewicz, J.A. 1999. Holocene sedimentary architecture of the red river delta Vietnam. Journal of Coastal Reasearch 15, pp: 314-325.

Mayewski, P.A., Rohling, E.E., Stager, J.C., Karlén, W., Maash, A.K., Meeker, L.D. Meyerson, E.A., Gasse, F., Kreveld, S.v. Holmgren, K., Lee-Thorp, J., Rosqvist, G., Rack, F., Staubwasser, M., Scheneider, R.R., Steig, E.J., 2004. Holocene climate variability. Quaternary Research 62, pp: 243-255.

Mayewski, P.A., Meeker, L.D., Twickler, M.S., Whitlow, S., Yang, Q., Lyons, W.B., Prentice, M., 1997. Major features and forcing of high-latitude northern hemispheric circulation using a 110.000-year long glaciochemical series. Journal of Geophysical Research 102, pp: 26345-26366.

McConnaughey, T., 1989a. ^{13}C and ^{18}O isotopic disequilibrium in biological carbonates: I. Patterns. Geochimica et Cosmochimica Acta V 53 pp: 151-162.

McConnaughey, T., 1989b. 13C and 18O isotopic disequilibrium in biological carbonates: II. *In vitro* simulation of kinetic isotope effects. Geochimica et Cosmochimica Acta V 53, pp: 163-171.

McConnaughey, T.A., Burdett, J., Whelan, J.F., Paull, K.C., 1997. Carbon isotopic in Biological carbonates: Respiration and Photosynthesis. Geochimica et Cosmochimica Acta V 61 N° 3, pp: 611-622.

Meyers H.J., 1987. Marine vadose beachrock cementation by cryptocrystalline magnesium Calcite-Maui, Hawaii Journal Sedimentary Petrology V 57 (3), pp: 558-570.

Mien, N. Q., Phon, L. K., 2000. Some results of ^{14}C dating in investigations on Quaternary geology and geomorphology in Nam Dinh-Ninh Binh area, Viet Nam. Journal of Geology (Vietnam) Series B 15, pp: 106-109.

Milliman, J.D., 1974. Marine Carbonates. Part I: Recent sedimentary carbonates. Springer Verlag, Berlin. 379 p.

Milliman, J.D. 1977, Role of Calcareous Alge in Atlantic Continual Margin Sedimentation In: Flügel, E., Fossil Alge 232-247. Berlin –Heidelberg (Spring).

Mitrovica, J.X., Peltier, W.R., 1991. On postglacial geoid subsidence over the equatorial oceans. Journal Geophysics Research 96 (B12) pp: 20053-20071.

Mitrovica, X.J., and Milne, G.A., 2002. On the origin of late Holocene sea-level highstands within equatorial ocean basins. Quaternary Science Reviews 21, pp: 2179-2190.

Mook, W.G., Vogel, J.C., 1968. Isotopic equilibrium between shells and environment. Science 159, pp: 874-875.

Moore, C.H., 2004. Carbonate reservoirs – Porosity evolution and diagenesis in a sequence stratigraphic framework. Developments in sedimentology 55. Elsevier, 444 p.
Moore, C.H., 1989. Carbonate Diagenesis and Porosity. Dev. Sedimant N° 46. Elsevier, Amsterdam, 338 p.

Moore, C.H. Jr., and Billings, G.K., 1971. Preliminary model of beachrock cementation, Grand Cayman island, B.W.I. In Bricker, O.P.(Ed), carbonate cements. Johns Hopkins Press, Baltimore, MD, pp: 40-43.

Moore, C.H. Jr. 1973. Intertidal Carbonated cementation, Grand Cayman, West Indies Journal Sedimentary Petrology 43, pp: 591-602.

Morse, J.W., Mackenzie, F.T., 1990. Geochemistry of Sedimentary Carbonates. Developments in Sedimentology 48. Elsevier Sciences, Amsterdam, 707 p.

Müller-Lupp, T., Bauch, H., 2005. Linkage of Artic atmospheric circulation and Siberian shelf hydrography: A proxy validation using $\delta^{18}O$ records of bivalve shells. Global and Planetary Changes 48, pp: 175-186.

Mueller-Lupp, T., Bauch, H.A., Erlenkeuser, H., 2004. Holocene hydrographical changes of the eastern Laptev Sea (Siberian Arctic) recorded in $\delta^{18}O$ profiles of bivalve shells. Quaternary Research 61, pp: 32-41.

Nadeau, M-J., Schleicher, M., Grootes, P.M., Erlenkeuser, H., Gottang, A., Mous, D.J.W., Sarntheim, M., and Willkomm, H., 1997. The Leibniz-Labor AMS facility at the Christian-Albrechts University, Kiel, Germany. Nuclear Instruments and Methods in Physics Research 123, pp: 22-30.

Nakada, M., 1986. Holocene sea-level in oceanic island: Implications for the rheological structure of the Earth's mantle. Tectonophysics 121, pp: 263-276.

Nakada, M., Lambeck, K., 1989. Late Pleistocene and Holocene sea-level changes in Australia region and mantle rheology. Geophysical Journal International 96, pp: 497-517.

Neumeier, U., 1999. Experimental modelling of beachrock cementation under microbial influence. Sedimentary Geology 126, pp: 35-46.

Nghi, T., Di Ch Dy, N., Thuan, D.V., Vinh, V.V., Cong Ko, M., Ti NH, T.N.N.T., 1998. Environmental and forming mechanism of Phan Thiet red sands. Journal of Geology, Series A, V 245(3-4), pp: 10-20.

Nguyen, V.L., Ta, T.K.O., Tateishi, M., 2000. Late Holocene depositional environments and coastal evolution of Mekong River Delta, Southern Vietnam. Journal of Asian Earth Sciences 18, 427-439.

Noren, A.J., Bierman, P.R., Steig, E.J., Lini, A., Southon, J.A., 2002. Millennial-scale storminess in variability in the Northeastern United States during the Holocene. Nature 419, pp: 821-824.

Oliveira, M.I.M.D., Bagnoli, E., Farias, C.C., Nobrega, A.M.B. and Santiago, M., 1990. Consideracoes sobre a geometria, petrografia, sedimentologia, diagenese e idade doe beachrocks do RioGrande do Norte. In: XXXVI Congresso Brasileiro de Geologia. V 2. Sociedade Brasileira de Geologia, Natal. pp: 621-634.

Odin, G.S., 1988, Green Marine Clays. Elsevier, Amsterdam, 445 p.

Odin, G.S., Matter, A., 1981, De glauconiarum origine. Sedimentology 28, pp: 611-641.

Omoto, K., 2001. Radiocarbon ages of beach rocks and late Holocene sea-level changes in the southern part of the Nansei Island, Southwest of Japan. Radiocarbon 43(2B), pp: 887-898.

Omoto, K., 2004. Radiocarbon ages and isotope fractionations of beachrock samples collection from the Nansei island, southwestern Japan. Radiocarbon 46 (2), pp: 539-550.

Pedone, A.V. & Folk, L.R., 1996. Formation of aragonite cement by nannobacterias in the Great Salt Lake, Utah. Geology V.7 N° 8, pp: 763-765.

Peltier, W.R.,1994. Ice Age Paleotopography. Science 256, pp: 195-201.

Peltier, W.R., 1996. Mantle viscosity and ice-age ice-sheet topography. Science 273, pp: 1359-1364.

Peltier, W.R., 2002. On eustatic sea-level history: Last Glacial Maximum to Holocene. Quaternary Science Reviews 21, pp: 377-396.

Perry, J.J., Stanly, T.J., 1997. Microbiology: dynamics and diversity. Saunders College Publishing. Florida, USA, 911 p.

Pirazzoli, P.A., 1991. World Atlas of Holocene Sea-level Changes. Oceanography series V 58. Elsevier, Amsterdam, 300 p.

Purser, B.H., 1980. Sédimentation et diagenèse des carbonates néritiques récents. Les éléments de la sédimentation et de la diagenèse. Éditions Technip. Institut Français du Pétrole, Paris. Tome 1, pp: 213-257, (in French).

Pyökäri, M., 1982. Beachrock on Pattaya Beach in southeastern Thailand. Zeitschrift für Geomorphologie 26(3), pp: 375-388. Berlin and Stuttgart.

Ramsay, P.J., 1995. 9000 years of sea-level changes along the Southern African Coastline. Quaternary International 31, pp: 71-75.

Ramsay, P. J., Cooper, J. A. G., 2002. Late Quaternary sea-level changes in South Africa. Quaternary Research 57, pp: 82-90.

Rey, D., Rubio, B., Bernabeu, A.M., Vilas, F., 2004. Formation, exposure, and evolution of a high-latitude beachrock in the intertidal zone of the Corrubedo complex (Rio de Arousa, Galicia, NW Spain).

Rimbaman, I., 1992. The role of sea-level changes on the coastal environment of northern West Java (case study of Eretan, Losarang and Indramayu). Journal of Southeast Asian Earth Sciences 7(1), pp: 71-77.

Rojana-anawat, P., Pradit, S., Sukramongkol, N., Siriraksophon, S., 2000. Temperature, Salinity, Dissolved Oxygen and Water Masses of Vietnamese Waters. Proceedings of the SEAFDEC Seminar on Fisheries Resources in the South China Sea, Area IV: Vietnamese Waters. Southeast Asian Fisheries Development Center, Thailand. pp: 346-355.

Romanek, C.S., Grossman, E.L., Morse, J.W., 1992. Carbon isotopic fractionation in synthetic aragonite and calcite – effects of temperature and precipitation rate. Geochimica et Cosmochimica Acta 56, pp: 419-430.

Rosenthal, Y., Oppo, D.W., Linsley, B.K., 2003. The amplitude and phasing of the climate change during the last deglaciation in the Sulu Sea, Western Equatorial Pacific. Geophysical Research Letter 30 (8) 1428.

Röthlisberger, F., 1986. 10.000 Jahre Gletschergeschichte der Erde: Ein Vergleich zwischen Nord-und Südehemisphäre. Aarau, Verlag, Sauerländer, 416 p.

Russell, R.J., 1959. Origin of Beachrocks. Zeitschrift für Geomorphologie NF 3, pp: 227-236.

Schleicher, M., Gootes, P.M., Nadeau, M.-J. and Scoon, A., 1998. The carbonate ^{14}C background and its components at the Leibniz AMS facility. Radiocarbon 40(1), pp: 85-93.

Schmalz, R.F., 1971. Formation of beachrock at Eniwetok Atoll. In: Bricker, O.P. (Ed.), Carbonate Cements. Johns Hopkins Press, Baltimore, pp: 17-24.

Schroeder, J.H., 1979. Carbonate diagenesis in Quaternary beachrock of Uyombo, Kenya: sequence of processes and coexistence of heterogenic products. Journal Sedimentary Petrology 68(3), pp: 894-919.

Schroeder, J.H., 1973. Submarine and vadose cements in Pleistocene Bermuda reef rock. Sedimentary Geology 10, pp: 179-204.

Scoffin, T.P., 1970. Conglomeratic Beachrock in Bimini, Bahams. Journal of Sedimentary Petrology 40, pp: 756-758.

Scoffin, T.P., 1987. An Introduction to Carbonates Sediments and Rocks. Blackie, Glasgow, 274 p.

Scoffin, T.P., Le Tissier, M.D.A., 1998. Late Holocene sea level and reef-flat progradation, Phuket, South Thailand. Coral Reefs 17, pp: 273-276.

Schöne, R. B., Castro, A. D. F., Fierbig, J. Houk, S.D., Oschmann, W., Kröncke, I., 2004. Sea surface water temperatures over the period 1884-1983 reconstructed from oxygen isotope ratios of a bivalve mollusc shell (*Arctica islamica*, southern North Sea). Palaeogeography Palaeoclimatology Palaeoecology 212, pp: 215-232.

Schöne, B.R., Lega, J., Flessa, K.W., Goodwin, D.H., Dettman, D.L., 2002. Reconstructing daily temperatures from growth rates of the intertidal bivalve mollusc *Chione cortezi* (Northern Gulf of California, Mexico). Palaeogeography Palaeoclimatology Palaeoecology 184, pp: 131-146.

Schöne, B.R., Tanabe, K., Dettman, D.L., Sato, S., 2003. Environmental controls on shell growth rates and $\delta^{18}O$ of the shallow-marine bivalve mollusc *Phacosoma japonicum* in Japan. Marine Biology 143, pp: 473-485.

Sellwood, B.W., 1994. Principles of carbonate diagenesis. In: Parker A., Sellwood, B (Eds.), Quantitative Diagenesis: Recent Developments and Applications to Reservoir Geology. NATO ASI Series. Series C, Mathematical and Physical Sciences V 435, pp: 1-32.

Semeniuk, V., Searle, J.D., 1987. Beach Rock Ridges/Bands along a High-Energy Coastal in Southwestern Australia-Their Significance and Use in Coastal History. Journal Coastal Research 3(3), pp: 331-342.

Shaw, P.-T., Chao, S.-Y., 1994. Surface circulation in the South China Sea. Deep-Sea Research I. V. 41, N°11/12, pp: 1663-1683.

Siesser, W.G., 1974. Relict and recent beachrock from southern Africa. Geol. Soc. Am. Bull. 85, pp: 1849-1854.

Sinsakul, S., 1992. Evidence of Quaternary sea level change in the coastal areas of Thailand: a review. Journal of Southeast Asian Earth Sciences 7(1), pp: 23-37.

Software WXTide32 version 4.0, 2004. Copyright 1998-2004, Michael Hopper.

Spurgeon, D., Davis, A.R. Jr., Shinnu, A.E., 2003. Formation of ´Beach Rock` at Siesta Key, Florida and its influence on barrier island development. Marine Geology 200, pp: 19-29.

Stager, C.J., Cumming, B., Meeker, L.D. 1997. A high-resolution 11.400-yr diatom record from Lake Victoria; East Africa. Quaternary Research 47, pp: 81-89.

Stoddart, D.R. and Cann, J.R., 1965. Nature and origin of beach rocks. Journal of Sedimentary Petrology 35, pp: 243-273.

Strasser, A., Davaud, E. and Jedoui, Y., 1989. Carbonate cements in Holocene beachrock: example from Bahiret el Biban, Southeastern Tunisia. Sedimentary Geology 62, pp: 89-100.

Stuiver, M., Braziunas, T.F., 1993. Sun, ocean, climate and atmospheric $^{14}CO_2$: an evaluation of casual and spectral relationships. Holocene 3, pp: 289-305.

Stuiver, M. and Reimer, P.J., 1993. Extended ^{14}C database and revised CALIB radiocarbon calibration program. Radiocarbon 35, pp: 215-230.

Ta, T.K.O., Van Lap Nguyen, Tateishi, M., Kobayashi, I., Tanabe, S., Saito, Y., 2002. Holocene delta evolution and sediment discharge of the Mekong River, south Vietnam. Quaternary Science Reviews 21, pp: 1807-1819.

Tam, D.N., 1991. Coastal Evolution: Changes of Environmental in the Coastal Regions of Viet Nam and Problems of Management and Exploration. Mineral Resource Development Series Vol. 60. United National, New York, pp: 109-114.

Tamura, T., Saito, Y., Sieng, S., Ben, B., Kong, M., Choup, S., Tsukawaki, S., 2007. Depositional faces and radiocarbon ages of drill core from the Mekong River lowland near Phnom Penh, Cambodia: Evidence for tidal sedimentation at the time of Holocene maximum flooding. Journal of Asian Earth Science 29, pp: 585-592.

Tanabe, S., Hori, K., Saito, Y., Haruyama, S., Van Phai Vu, Kitamura, A., 2003. Song Hong (Red River) delta evolution related to millennium-scale Holocene sea-level changes. Quaternary Science Reviews 22, pp: 2345-2361.

Tanabe, S., Saito, Y., Quang Lan Vu, Hanebuth, J.J.T., Quang Lan Ngo, Kitamura, A., 2006. Holocene evolution of the Song Hong (Red River) delta system, northern Vietnam. Sedimentary Geology 187, pp: 29-61.

Tanaka, N., Monaghan, M.C., Rye, D.M., 1986. Contribution of metabolic carbon to mollusc and barnacle shell carbonate. Nature 320, pp: 520-523.

Tang, D., Kawamura, H., Dien, V.T., Lee, M., 2004. Offshore phytoplankton biomass increase and its oceanographic causes in the South Chine Sea. Marine Ecology Progress Series 268, pp: 31-41.

Taylor, J.C.M. and Illing, L.V., 1969. Holocene intertidal calcium carbonated cementation, Qatar, Persian Gulf. Sedimentology, 12, pp: 69-107.

Thong, B.X., Toan, N.D., Tuong, N.T., 2000. Climatological Regime and Weather Conditions Occurred on the Expedition (May, 1999) on Vietnam Continental Shelf. In: Southeast Asian Fisheries Development Center (ed) Proceeding of the SEAFDEC seminar on the fishery resources in the South China Sea, area IV: Vietnamese water. Southeast Asian Fisheries Developmental Centre, Bangkok, pp: 356-364.

Thompson, G.L., Mosley-Thompson, E., Davis, M.E., Lin, P.-N., Henderson, K.A., Cole-Dai, J., Bolzan, J.F., Liu, K.-b., 1995. Late Glacial Stage and Holocene Tropical Ice core Records from Huascarán, Peru. Science 296 pp: 46-50.

Thuy, N.T.B., Satir, M., Siebel, W., Vennemann, T., Long, T.V., 2004. Geochemical and isotopic constraints on the petrogenesis of granitoids from the Delat zone, southern Vietnam. Journal of Asian Earth Sciences 23, pp: 467-482.

Tjia, H.D, 1996. Sea-Level Changes in the Tectonically Stable Malay-Thai Peninsula. Quaternary International 31 pp: 95-101.

Tucker, E., 1991. Sedimentary Petrology, an introduction to the origin of sedimentary rocks. 2nd edition, Blackwell Scientific Publications, 260 p.

Urey, H.C., Lowenstam, H.A., Epstein S., McKinney C.R., 1951 Measurement of paleotemperature and temperature of the Upper Cretaceous of England, Denmark, and the southeastern United State. Bull Geol Soc Am 62, pp: 399-416.

Veizer, J., 1983. Trace elements and isotopes in sedimentary carbonates. In: Carbonates: Mineralogy and chemistry, Reviews in Mineralogy, 11 (Ed. by R. J. Reeder), Mineral Soc. America, Book Crafters, Chelsea, pp: 265-300.

Vieira, M.M., De Ros, F.L., 2006. Cementation patterns and genetic implications of Holocene beachrocks from northeastern Brazil. Sedimentary Geology 192, pp: 207-230.

Vollbrecht, R. and Meischner, D., 1993. Sea level and diagenesis: a case study on Pleistocene beaches, Whalebone Bay, Bermuda. Geologische Rundschau 82, pp: 248-262.

Wang, C.-H., Peng, T.-R., 1990. Oxygen and Carbon isotope records in shells of *Cyclotellina remies, Meretrix lusoria, and Pecten byoritsuensis*. Bull. Of Malacology, R.O.C. 15, pp: 49-58.

Wang, C.-H., Tsai, P.-S., 1993. The stable isotope records of *Corbicula subsulcata* from the Yuanshan shell mound: Paleo-environmental and Paleo-ecological implications. Journal of the Geological Society of China V 36 N° 1, pp: 25-34.

Wang, C.-H., Tsai, P.-S., Liu, T.-K., 1994. Paleo-environmental of the Tainan Formation, Southern Taiwan: Evidence from oxygen and carbon isotopic composition of molluscs. Proc. Natl. Sci. Counc. ROC(A) V 18 N° 2, pp: 151-157.

Wang, L., Sarnthein, M. 1999. Long-/short-term variations of monsoon climate and its tele-connection to global change. High resolution grain size records of siliciclates sediments from the South China Sea. In Reconstructing Ocean history: A window into the Future Ed. Abrantes and Mix, Kluwer Academic / Plenum Publisher, New York, 446 p.

Wang, L., Wang, P., 1990. Late Quaternary Paleoceanography of the south Chine Sea: Glacial-Interglacial contrasts in the enclosed basin. Paleoceanography V 5, pp: 77-90.

Webb, E.G., Jell, S.J., Baker, C.J., 1999. Cryptic intertidal microbialites in beachrock, Heron Island, Great Barrier Reef: implications for the origin of microcrystalline beachrock cement. Sedimentary Geology 126, pp: 317-334.

Wei, G., Deng, W., Yu, K., Li, X-h., Sun, W., Zhao, J-x., 2007. Sea surface temperature records in the northern South China Sea from mid-Holocene coral Sr/Ca ratios. Paleoceanography 22, PA 3206, doi: 10.1029/2006PA001270.

Weiner, S., Dove, P., 2003. An overview of Biomineralization Processes and the Problem of the Vital Effect, Cap 1. In Biomineralization, Reviews in Mineralogy & Geochemistry V. 54 Eds. Dove, P.M., Yoreo, J.J. & Weiner, S., Mineralogy Society of America Geochemical Society, 381 p.

Wefer, C., Berger, W.H., 1991. Isotope paleontology: growth and composition of extant calcareous species. Marine Geology 100, pp: 207-248.

Williams, D.F., Arthur, M.A., Jones, D.S., Healy-Williams, N., 1982. Seasonality and mean annual sea surface temperature from isotopic and sclerochronological records. Nature 296, pp: 432-434.

Winterholler, A.G., 2006. Beachrockvorkommen im Korallenarchipel der Malediven -ein topographisch-morphologischer Geneseansatz-, PhD. Thesis, von Mathematisch-Naturwissenschaftlichen Fakultät der Christian-Albrechts Universität zu Kiel. 112 p (in Germany).

Witbaard, R., Jenness. M.I., Van der Borg, K., Ganssen. G., 1994. Verification of annual growth increments an *A. islandica* L. from the North Sea by means of oxygen and Carbon isotopes. Neth. J. Sea Res. 33, pp: 91-101.

Woodroffe, C.D., Thom, B.G., Chappell, J., 1985. Development of widespread mangrove swamp in mid-Holocene times in northern Australia. Nature 317, pp: 711-713.
Woodroffe C.D., 1993. Late quaternary evolution of coastal and lowland riverine plains of Southeast Asia and Australia: an overview. Sedimentary Geology 83, pp: 163-175.

Woodroffe, S.A., Horton, P.B., 2005. Holocene sea-level changes in the Indo-Pacific. Journal of Asian Earth Science 25, pp: 29-43.

Wyrtki, K., 1961, Physical Oceanography of the Southeast Asian waters, Scripps Institution of Oceanography, La Jolla, 195 p.

Yafeng, S., Zhaozheng, K., Sumin, W., Lingyu, T., Fudao, W., Tandong, Y., Xitao, Z., Peiyuan, Z., Shaohua, S. 1993. Mid-Holocene climates and environments in China. Global and Planetary Changes 7, pp: 219-233.

Yin, W.W.-S., Huang, G., 2002. Middle Holocene higher sea-level indicators from the south chine coast. Marine Geology 182, p: 225-230.

Zhou, G.T., Zheng, Y.F., 2003. An experimental study of oxygen isotope fractionation between inorganically precipitated aragonite and water at low temperatures. Geochimica et Cosmochimica Acta 67(3), pp: 387-399.

Ziveri, P., Stoll, H., Probert, I., Klaas, C., Geisen, M., Ganssen, G., Young, J., 2003. Stable isotope ‚vital effects' in coccolith calcite. Earth and Planetary Science Letters 210, pp: 137-149.

Zong, Y., 2004. Mid-Holocene sea-level highstand along the Southeast Coast of China. Quaternary International 117, pp: 55-67.

9. Appendix

App. 9.1. Complete list of analysed samples evaluated during the work.

N°	Coordinates	Sediment-type	Fossils
VN 08110301	N10°56,578 // E108°17,987	Consolidate sand	Bivalve
VN 08110302	N10°54,981 // E108°17,658	Consolidate sand	
VN 09110302	N11°19,084 // E108°54,918	Beachridge	Coral and Bivalve
VN 09110303	"	"	Coral
VN 09110304	N11°20,007 // E108°52,447	Conglomerate	Oyster
VN 09110305	"	"	Snail
VN 09110306	N11°19,975 // E108°52,320	Beachrock	Coral
VN 11110301		Beach sandy	
VN 11110302	N11°19,434 // E108°50,260	Backshore	Sand, partly with Bivalve
VN 11110303	"	"	
VN 11110304	"	"	
VN 11110305	"	"	Bivalve
VN 11110306	N11°19,796 // E108°50,496	Beachridge (Top)	Bivalve and coral
VN 11110307	"	Beachridge (Mid)	Bivalve and coral
VN 11110308	"	Upperbeach	Sediment
VN 11110309	N11°19,803 // E108°50,550	Beachrock	Coral
VN 11110310	"	"	Coral
VN 11110311	N11°20,305 // E108°51,047	Washover	Gastropod
VN 11110312	"	Aeolinite	Sand (consolidated)
VN 13110302	N12°42,947 // E109°22,839	Paleo Lagoon	Oyster
VN 15110301	N11°34,173 // E109°07,717	Notch	Bivalve, corals
VN 15110302	"	"	
VN 15110303	"	Part of trunk	
VN 15110305	N11°34,098 // E109°07,725	Aeolinite	
VN 16110302	N11°39,149 // E109°11,107	"	
VN 16110303	N11°39,098 // E109°10,234	"	Coral
VN 04050501	N11°19,958 // E108°50,774	Beachrock	Coral
VN 04050502	"	"	Coral
VN 04050503	"	"	Bivalve
VN 04050504	"	"	Coral
VN 04050505	N11°20,058 // E108°51,422	Beachridge	Bivalve
VN 04050506	"	"	
VN 05050501	N11°19,801 // E108°50,495	Beachridge	Bivalve
VN 05050501 (A)			Coral
VN 05050502	"	"	Coral
VN 05050503	"	Aeolinite	Gastropod
VN 05050504	"	Aeolinite	
VN 05050505	"	Beachridge	Coral
VN 05050506	"	"	Bivalve
VN 05050507	N11°19,993 // E108°52,429	Beachrock	Coral
VN 05050508	"	"	Coral
VN 05050509	"	"	Bivalve
VN 06050501	N11°43,368 // E109°12,023	Evaporite	Bivalve
VN 06050502	N11°42,873 // E109°11,968	Taphonomic area	Coral
VN 06050503	"	"	Coral
VN 06050504	N11°24, 962 // E109°00,681	Platform reef	
VN 06050505	N11°24,946 // E109°00,622	Beachrock	Coral
VN 06050506	"	"	"
VN 06050507	"	"	Coral
VN 06050508	"	"	Coral
VN 07050501	N11°34,923 // E109°04,215	Beachridge	Bivalve
VN 07050502	"	"	
VN 07050502 (A)	"	"	
VN 07050503	"	"	Bivalve
VN 07050504	N11°28,120 // E109°00,925	Conglomerate	

App. 9.2. Petrographic thin sections from SE-Vietnam coast.

N°	Coordinates	Kind of sample	Used in this work
VN 08110301	N10°56,578 // E108°17,987	Consolidate sand	
VN 08110302	N10°54,981 // E108°17,658	Consolidate sand	
VN 09110304	N11°20,007 // E108°52,447	Conglomerate	
VN 11110310	"	Beachrock	*
VN 11110312	"	Aeolinite	
VN 15110301	N11°34,173 // E109°07,717	Notch	
VN 15110302	"	"	
VN 15110303	"	Part of trunk	
VN 15110305	N11°34,098 // E109°07,725	Aeolianite	
VN 16110302	N11°39,149 // E109°11,107	"	
VN 16110303	N11°39,098 // E109°10,234	"	
VN 04050501	N11°19,958 // E108°50,774	Beachrock	*
VN 04050502	"	"	*
VN 04050504	"	"	
VN 05050504	"	Aeolinite	
VN 06050501	N11°43,368 // E109°12,023	Evaporite	
VN 06050504	N11°24.962 // E109°00,681	Piece of Platform reef	
VN 06050505	N11°24,946 // E109°00,622	Beachrock	*
VN 06050507	"	"	*
VN 06050508	"	"	*

App. 9.3. Petrographic thin sections from SW-Madagascar coast.

N°	Coordinates	Kind of sample
MD 06120303	23°38.089S//43°39.089E	Beachrock
MD 07120301	23°40.267S//43°38.233E	"
MD 07120313	"	"
MD 10120301	23°10.053S//43°36.509E	"
MD 10120305	23°09.793S//43°36.478E	"
MD 10120307	"	"
MD 13110401	-	"
MD 14110404	-	"

App. 9.4. Fraction of aragonite in the carbonate material with AMS-radiocarbon and U/Th ages.

N°	Description	Identification of X-RD	% of Aragonite	Age ky BP	Kind of date
VN 08110301	Bivalve	MDV-1	90 %	-	-
VN 09110302	Bivalve	MDV-2	100 %	1760 ± 25 BP	AMS
VN 09110303	Coral	MDV-12	100 %	1470 ± 26 BP	U/Th
VN 09110304	Oyster	MDV-13	91 %	-	
VN 09110305	Snail	MDV-14	95 %	-	
VN 09110306	Coral	MDV-3	94 %	5420 ± 30 BP	AMS
VN 09110306	Coral	MDV-3	"	5490 ± 40 BP	U/Th
VN 11110302	Bivalve	MDV-15	99 %	2110 ± 25 BP	AMS
VN 11110305	Bivalve	MDV-16	100 %	-	
VN 11110306	Bivalve	MDV-4	100 %	5120 ± 55 BP	AMS
VN 11110307	Coral	MDV-17	99 %	5270 ± 40 BP	AMS
VN 11110307	Bivalve	MDV-17b	99 %	-	
VN 11110307	Gastropod	MDV-17c	100 %	-	
VN 11110307	Coral	MDV- 17d	99 %	-	
VN 11110309	Coral	MDV-18	96 %	-	
VN 11110310	Coral	MDV-5	97 %	3745 ± 30 BP	AMS
VN 11110311	Gastropod	MDV-6	99 %	2075 ± 30 BP	AMS
VN 11110312	Gastropod	MDV-19	24 %	-	
VN 13110302	Oyster	MDV-7	4 %	> 1954 A.D.	AMS
VN 13110302	Oyster	MDV-7b	66 %	-	
VN 15110301	Bivalve fragment	MDV-8	100 %	3215 ± 30 BP	AMS
VN 15110302	Bivalve fragment	MDV-9	*	3225 ± 30 BP	AMS
VN 16110303	Coral	MDV-10	96 %	3000 ± 28 BP	U/Th
VN 04050501	"	MDV-34	92%	3615 ± 25 BP	AMS
VN 04050502	"	MDV-35	100%	3325 ± 30 BP	AMS
VN 04050503	Bivalve	MDV 24	98 %	6160 ± 35 BP	AMS
VN 04050504	Coral	MDV-36	99%	6210 ± 35 BP	AMS
VN 04050505	Bivalve	MDV-30	19%	2165 ± 25 BP	AMS
VN 05050501	Bivalve	MDV-37	91%	4965 ± 30 BP	AMS
VN 05050501(A)	Coral	-	-	5010 ± 30 BP	AMS
VN 05050502(A)	Coral	MDV-42	99%	5185 ± 30 BP	AMS
VN 05050502(B)	Coral	MDV-43	99%	-	AMS
VN 05050503	Gastropod	MDV-33	98%	4680 ± 35 BP	AMS
VN 05050507	Coral	MDV-29	99%	6655 ± 40 BP	AMS
VN 05050509	Bivalve	MDV-38	95%	5650 ± 40 BP	AMS
VN 06050501	"	MDV-27	95%	-	
VN 06050502	Coral	MDV-39	99%	1260 ± 20 BP	AMS
VN 06050503	"	MDV-31	100%	1290 ± 25 BP	AMS
VN 06050505	"	MDV-32	99%	1005 ± 25 BP	AMS
VN 06050506	"	MDV-40	68%	-	
VN 06050507	"		*	1095 ± 35BP	AMS
VN 06050508	"	MDV-41	98%	1570 ± 25BP	AMS
VN 07050501	Bivalve	MDV-26	100%	4540 ± 30 BP	AMS
VN 07050503	"	MDV-28	74%	3685 ± 30 BP	AMS

* not analysed

App. 9.5. Isotope results in *Meretrix lyrata "C.*		
Distance of umbo	**δ^{18}O PDB‰**	**δ^{13}CPDB‰**
1	-3,80	-1,17
2	-3,86	-1,06
3	-3,78	-1,01
4	-3,84	-1,14
5	-4,07	-1,23
6	-3,93	-1,35
7	-4,01	-1,73
8	-4,10	-1,72
9	-4,64	-1,96
10	-4,45	-1,57
11	-4,09	-1,24
12	-4,86	-1,73
13	-3,78	-1,71
14	-3,96	-1,69
15	-3,21	-1,62
16	-2,93	-1,66
17	-2,66	-1,38
18	-2,98	-1,34
19	-3,19	-1,11
20	-3,50	-1,80
21	-3,16	-1,69
22	-3,68	-1,78
23	-4,00	-1,52
24	-4,04	-1,35
25	-3,96	-1,42
26	-4,79	-2,13
27	-5,17	-2,04
28	-3,83	-1,46
29	-3,52	-1,38
30	-3,37	-1,81
31	-3,03	-1,98
32	-3,26	-1,70
33	-3,33	-2,20
34	-3,39	-1,59
35	-3,31	-1,65
36	-3,41	-2,29
37	-3,95	-1,70
38	-3,68	-1,47
39	-4,03	-1,65
40	-4,18	-1,57
41	-4,28	-1,61
42	-3,95	-1,72
43	-4,54	-1,90
44	-3,65	-1,99
45	-2,98	-1,37
46	-3,20	-1,81
47	-2,66	-1,94
48	-2,51	-1,77
49	-2,76	-2,00
50	-3,06	-2,52
51	-2,91	-1,72
52	-3,62	-2,29

App. 9.6. Isotopic results in *Meretrix Lyrata "D"*.

Distance of umbo	$\delta^{18}O$ PDB‰	$\delta^{13}C$ PDB‰
1	-3,95	-1,59
2	-3,73	-1,61
3	-3,76	-1,68
4	-3,84	-2,42
5	-3,78	-1,64
6	-3,90	-1,26
7	-4,09	-1,59
8	-3,92	-2,12
9	-3,83	-1,56
10	-4,23	-1,96
11	-4,35	-2,19
12	-4,22	-2,09
13	-4,04	-1,58
14	-3,92	-1,57
15	-3,69	-1,71
16	-3,54	-1,46
17	-3,61	-2,00
18	-4,10	-1,66
19	-3,19	-0,75
20	-2,48	-1,01
21	-2,40	-0,74
22	-2,55	-0,88
23	-2,43	-1,41
24	-2,80	-0,62
25	-3,21	-1,27
26	-3,03	-1,31
27	-2,93	-1,67
28	-2,75	-1,36
29	-3,02	-1,35
29,5	-3,03	-1,49
30	-2,75	-1,20
30,5	-2,80	-1,00
31	-2,92	-1,19
31,5	-3,00	-1,57
32	-2,96	-1,36
32,5	-3,15	-1,52
33	-3,56	-2,16
33,5	-3,22	-1,65
34	-3,10	-2,37
34,5	-2,93	-1,68
35	-3,15	-2,12
35,5	-3,47	-2,48
36	-3,47	-1,48
36,5	-3,35	-1,85
37	-3,45	-1,91
37,5	-4,52	-1,84
38	-4,98	-2,16
38,5	-5,59	-3,46
39	-3,41	-1,70
39,5	-2,84	-1,45
40	-2,35	-1,77

App. 9.7. Isotopic results in *Meretrix lusoria.*

Distance of umbo	$\delta^{18}O$ PDB‰	$\delta^{13}C$ PDB‰
1	-2,34	1,27
2	-2,41	1,17
3	-2,55	1,40
4	-2,65	1,29
5	-2,69	1,35
6	-2,69	1,25
7	-3,35	-0,08
8	-2,85	0,31
9	-2,68	0,30
10	-2,25	0,38
11	-2,77	0,36
12	-3,05	0,14
13	-2,35	0,33
14	-2,13	0,36
15	-1,89	0,28
16	-2,15	0,32
17	-1,98	0,33
18	-1,94	0,56
19	-1,92	0,53
20	-2,15	0,42
21	-2,21	0,53
22	-2,45	0,48
23	-2,69	0,26
24	-2,39	0,31
25	-2,46	0,16
26	-2,55	0,37
27	-2,46	0,49
28	-1,95	0,64
29	-2,12	0,75
30	-2,37	0,79
31	-2,64	0,63
32	-2,17	0,81
33	-2,44	0,58
34	-2,62	0,71
35	-2,76	0,61
36	-3,13	0,26
37	-3,05	0,21
38	-2,96	0,39
39	-2,93	0,40
40	-3,05	0,29
41	-3,38	0,12
41,5	-2,38	0,41
42	-1,89	0,65
42,5	-2,21	0,55
43	-2,13	0,77
43,5	-1,98	0,92
44	-2,27	0,61
44,5	-2,30	0,45
45	-2,78	0,70
45,5	-2,30	0,48
46	-2,46	0,75
46,5	-2,11	1,06
47	-2,47	0,88
47,5	-2,79	0,32
48	-2,94	0,41
48,5	-2,69	0,50

49	-2,68	0,31
49,5	-2,48	0,35
50	-2,01	0,44
50,5	-2,63	0,05
51	-2,37	0,44
51,5	-2,73	0,61
52	-3,22	0,25
52,5	-3,07	0,31
53	-2,33	0,41
53,5	-2,10	0,48
54	-2,51	0,22
54,5	-2,81	-0,21
55	-2,09	0,31
55,5	-2,63	0,20

App. 9.8. Isotope results in *Spondylus sp.*

Distance of umbo	$\delta^{18}O$ PDB‰	δ13C PDB‰
1	-1,81	0,51
2	-1,96	1,02
3	-1,47	1,06
4	-1,44	0,28
5	-1,06	1,19
6	-1,28	1,73
7	-2,23	1,65
8	-2,43	1,60
9	-1,70	1,94
10	-1,62	1,83
11	-1,68	1,66
12	-1,67	1,59
13	-1,59	1,60
14	-1,69	1,51
15	-1,15	1,53
16	-1,05	1,35
17	-1,22	1,57
18	-1,41	1,13
19	-0,94	1,78
20	-0,49	1,85
21	-1,84	1,64
22	-1,85	1,86
23	-1,88	1,56
24	-1,81	1,49
25	-0,07	2,30
26	-0,91	1,46
27	-1,52	1,25
28	-1,59	1,40
29	-1,73	1,48
30	-1,00	1,18
31	-0,79	0,73
32	-0,68	0,85
33	-0,87	1,22
34	-0,86	1,13
35	-1,04	1,01
36	-1,60	0,32
37	-2,12	0,59
38	-1,91	0,67
39	-2,11	0,65
40	-1,55	0,66
41	-1,39	0,94
42	-2,12	0,84
43	-1,91	1,11
44	-1,68	1,23
45	-1,37	1,82
46	-0,94	2,09
47	-1,04	2,33
48	-0,99	2,33
49	-1,14	1,92
50	-1,93	1,84
51	-2,08	1,87
52	-1,94	1,91
53	-2,10	2,13
54	-1,69	1,78
55	-1,74	1,65

56	-1,81	1,47
57	-1,76	1,59
58	-1,78	1,42
59	-2,24	1,84
60	-2,17	1,75
61	-1,79	1,90
62	-1,61	1,72
63	-2,59	0,14
64	-1,65	1,14
65	-1,08	1,27
66	-0,69	2,01
67	-0,72	2,38
68	-1,23	1,77
69	-1,14	1,09
70	-1,53	1,17
71	-1,41	1,58
72	-1,15	2,52
73	-1,01	2,16
74	-1,93	1,79
75	-1,52	1,85
76	-1,25	2,23
77	-1,24	2,09
78	-1,66	1,83
79	-1,92	1,88
80	-2,42	1,65
81	-2,33	1,56
82	-2,56	1,54
83	-2,24	1,75
84	-2,20	1,29
85	-0,66	1,09
85,5	-0,91	1,03
86	-1,29	1,57
86,5	-1,07	1,29
87	-1,52	1,69
87,5	-2,45	0,78
88	-2,37	1,06
88,5	-2,11	1,34
89	-2,07	1,55
89,5	-2,24	1,43
90	-2,27	1,38
90,5	-2,01	0,86
91	-1,58	1,31
91,5	-1,34	1,34
92	-0,74	1,51
92,5	-0,94	1,64
93	-0,77	1,61
93,5	-1,20	0,93
94	-1,48	1,03
94,5	-1,10	1,18
95	-1,52	1,02
95,5	-1,59	1,06
96	-2,46	1,34
96,5	-2,12	1,01
97	-2,41	1,35
97,5	-2,30	1,64
98	-2,22	1,73
98,5	-2,58	0,90
99	-2,00	0,93
99,5	-1,02	1,61

100	-0,85	1,01
100,5	-0,47	1,05
101	-1,49	1,11
101,5	-1,67	1,23
102	-1,63	1,51
102,5	-1,45	1,59
103	-1,38	1,75
103,5	-2,24	1,74
104	-2,60	1,45
104,5	-1,42	1,77
105	-0,65	1,71
105,5	-1,13	0,76
106	-1,95	1,33
106,5	-2,42	1,78
107	-2,26	1,23
107,5	-1,44	1,29
108	-1,31	1,66
108,5	-1,77	0,79
109	-1,66	1,49
109,5	-2,17	1,55
110	-1,87	1,70

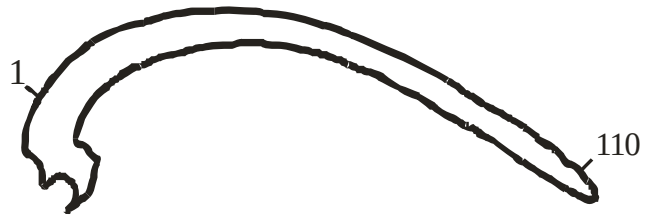

Curriculum

M. Oc. Maximiliano Michelli (Brasilian)

- Graduate in Biological Science, 1993-1998
  University of Caxias do Sul (UCS)-Brazil.

- Specialization in Oceanography, 1999-2000
  Oceanography Department
  Federal University of Pernambuco-Brazil

- Master in Oceanography, 2000-2002
  Oceanography Department
  Federal University of Pernambuco-Brazil

- Actual position:
  Ph.D. student in Geology and Paleontology since April of 2004.
  Christian Albrecht University of Kiel/Germany - Geosciences Institute
  Superviser: Prof. Dr. Karl Stattegger